Tajuk penyelidikan

VOT 72008

THE CATALYTIC COMBUSTION FOR NATURAL GAS

PEMBAKARAN SECARA PEMANGKINAN BAGI GAS ASLI

Nama-nama penyelidik

PROF. DR. WAN AZELEE WAN ABU BAKAR
(KETUA PENYELIDIK)
DR. NOR AZIAH BUANG

RESEARCH VOT NO:
72008

Nama Fakulti/Institut/ Pusat/Jabatan

Jabatan Kimia
Fakulti Sains
Universiti Teknologi Malaysia

Tahun diserahkan

2003

ACKNOWLEDGEMENTS

First of all, deepest gratitude goes to Allah for His providence and blessings.

The chief researcher and group would like to thank the RMC for the fund that makes this project a reality.

We also like to thank CAT group members for their diligent work in making this project a success.

Sincere gratitudes also go to all those who have helped directly or indirectly in this research, Assoc. Prof. Dr. Mohd. Ambar Yarmo (UKM), Mrs. Mariam Hassan, Mr. Mokhtar Abu Bakar, Mr. Mohd. Nazri Zainal, Mr. Kadir Abd. Rahman, Mr. Ibrahim, Mr. Jaafar Raji (Department of Physics), Mrs. Sariah Pin, Mr. Zainal Abidin Abbas and Mr. Jefri (Faculty of Mechanical).

Finally, to those who are involved directly or indirectly in this project, thank you.

ABSTRACT

Noble metals such as Pt, Rh and Pd have been widely used as catalyst for the catalytic combustion(oxidation) of methane. They can be used either with or without a support but supported catalysts are favored for the combustion. The disadvantages of noble metals in catalytic combustion application are i) limited supply, ii) high price, iii) high volatility and iv) ease of combustion. As such a viable alternative material should be invented which can overcome all the weakness possess by the noble metals and which can give much better performance of catalytic combustion of methane. In this research all possible catalyst based on metal oxides were prepared using various preparation techniques. The catalytic activity was determined using fixed-bed micro reactor whereby the temperature for 100 % conversion of methane was determined. The main selection of the catalysts used are high physical and chemical stability, cheap, high availability and local mineral resources. The combustion of methane over various catalysts that has been studied were metal oxides or mixed metal oxides such as Mn/SnO_2, Sn/Ln_2O_3 (Ln = La, Pr, Nd, Sm, Gd), Sn/ZrO_2, Cu/SnO_2, Sn/CeO_2 and Cu/ZrO_2. The catalytic combustion of the prepared catalysts in this research, in general, are accomplished at high temperature i.e. above 500^oC. The XRD analysis showed that the prepared catalysts have some degree of amorphous properties which might serve as the active sites. The XPS results showed that the surface of the catalysts are enriched with oxygen and the atoms distribution are more homogeneous upon ageing, with a fair amount of dopants on the surface. The TG/DTG analysis showed the complete elimination of water and residual species at 300 ^oC for all catalysts. DTA analysis agrees with TG/DTG whereby the complete removal of surface water and foreign species occurred below 300 ^oC. FTIR analysis showed that the existence of hydroxyl group occurred at 400 ^oC which indicated that there is a need for a certain amount of water for good catalytic reaction. Nitrogen adsorption analysis showed that the catalyst consists of a mixture of micro- and mesopores with non-uniform slit shaped pores. Different calcination temperatures will result in a different shape of pores. The SEM micrograph on the best catalyst showed that the catalyst has evenly distributed particle size at the range of 11-32 μm.

ABSTRAK

Logam nobel seprti Pt, Rh dan Pd telah diguna secara meluas bagi pembakaran(pengoksidaan) bermangkin bagi metana. Ianya boleh berupa berpenyokong atau tidak tetapi dalam keadaan berpenyokong adalah lebih baik. Kelemahan jenis logam nobel ialah i) bekalan terhad, ii) harga mahal, iii) meruap dan iv) mudah terbakar. Justeru itu suatu bahan alternatif perlu dicipta bagi mengatasi faktor tersebut dan dapat memperbaiki pencapaian pembakaran bermangkin metana. Dalam kajian ini, berbagai mangkin berdasarkan logam oksida disediakan menggunakan berbagai teknik penyediaan. Aktiviti pemangkinan ditentukan menggunakan reaktor mikro padatan tetap dimana suhu 100% pertukan metana dicerap. Pemilihan utama bagi mangkin berdasarkan kepada sifat fizik dan kimia yang stabil, murah, mudah didapati dan sumber asli tempatan. Pembakaran bermangkin metana menggunakan mangkin seperti Mn/SnO_2, Sn/Ln_2O_3 (Ln = La, Pr, Nd, Sm, Gd), Sn/ZrO_2, Cu/SnO_2, Sn/CeO_2 and Cu/ZrO_2. Secara umumnya, aktiviti pemangkinan metana yang dicerap berlaku pada suhu tinggi iaitu melebihi 500 ^oC. Analisis XRD menunjukkan mangkin mempunyai sedikit sifat amorfus berkemungkinan bertindak sebagai fasa aktif mangkin. Keputusan analisis XPS menunjukkan bahawa selepas proses penuaan, permukaan mangkin telah diperkaya dengan oksigen dan taburan atom adalah lebih homogen dengan jumlah bahan pendop yang seragam. Analisis TG/DTG menunjukkan penyingkiran lengkap air dan bahan residu pada 300 ^oC bagi semua mangkin. Analisis DTA menyokong keputusan TG/DTG. Analisis FTIR menunjukkan kewujudan kumpulan hidroksil pada 400 ^oC dan kehadiran sedikit air adalah perlu untuk aktiviti pemangkinan yang baik. Analisis penjerapan gas nitrogen menunjukkan bahawa mangkin terbaik mempunyai liang mikro dan meso dengan bentuk celahan yang tidak sekata. Suhu pengkalsinan yang berbeza juga dikenalpasti menghasilkan bentuk liang yang berbeza. Analisis SEM menunjukkan mangkin terbaik mempunyai saiz partikel yang sekata pada julat 11-32 μm.

KANDUNGAN

CHAPTER 1

1.0 Introduction -Catalytic combustion of methane

The production of energy by the combustion of methane and natural gas is well established [1]. Overall, the reaction may be represented by the equation

$$CH_4 + 2O_2 = CO_2 + 2H_2O \qquad H_{298} = -802.7 \text{ kJ/mol}$$

This overall equation is, however, a gross simplification with the actual reaction mechanism involving very many free radical chain reactions. Gas-phase combustion can only occur within given flammability limits, and the temperatures produced during combustion can rise to above ca. 1600 ^{o}C, where the direct combination of nitrogen and oxygen to unwanted nitrogen oxides could occur.

Catalytic combustion offers an alternative means of producing energy. A wide range of concentrations of hydrocarbon can be oxidized over a suitable catalyst, and it is possible to work outside the flammability limits of fuel. Reaction conditions can usually be controlled more precisely, with reaction temperatures being maintained below 1600^{o}C. This may be important both to minimize the production of nitrogen oxides and also to avoid thermal sintering of the catalyst. The catalytic combustion of methane is somewhat more complicated, as a result the fact that it is necessary to initiate oxidation at quite a high temperature. Once the reaction starts, subsequent oxidation is rapid and the heat release is considerable. As a result, it is more difficult to control temperature below the desired maximum.

With natural gas, it is somewhat easier to control temperature, since the presence of overall amounts of higher hydrocarbons allows initiation of oxidation at lower temperatures. Thus, for example, the light-off temperature of methane at an air: fuel ratio of 5.3 is 368^{o}C; for ethane, the corresponding value is 242^{o}C. Once the higher hydrocarbon starts to oxidize, the heat liberated is sufficient to heat up the system and to initiate the oxidation of methane. Obviously, this depends on the fact that there is sufficient higher hydrocarbon to supply the heat required. The main focus of this article is on the chemistry of methane, but it is useful to remember that the use of natural gas can introduce some change.

The combustion of methane can produce carbon dioxide or carbon monoxide, depending on the air: methane ratio:

$CH_4 + 2O_2 = CO_2 + 2H_2O$ (1.1)

$CH_4 + 3/2\ O_2 = CO + 2H_2O$ (1.2)

Other reactions may also be involved to a greater or less extent. These could include steam reforming (1.3) and (1.4) and the water shift (1.5) reactions:

$CH_4 + 2O_2 = CO + 3H_2$ (1.3)

$2H_2 + O_2 = 2H_2O$ (1.4)

$CO + H_2O = CO_2 + H_2$ (1.5)

It is shown that the most effective catalysts are based on precious metals and over such systems, steam reforming becomes important at temperature in excess of 550^{o}C-well within the range of catalytic combustion. The equilibrium of the water gas shift reaction has been well studied. Values of the equilibrium constants have been listed over a range operational conditions but the approach to equilibrium depends on the catalyst in use. Generally, higher temperatures favor the formation of carbon monoxide. Thus, it is necessary to consider the possibility of reactions other than (1.1) and (1.2).

The general pattern of catalytic combustion of hydrocarbons is well established (Figure 1). As temperature is increased, oxidation is initiated at a temperature that depends on the hydrocarbon and the catalyst.

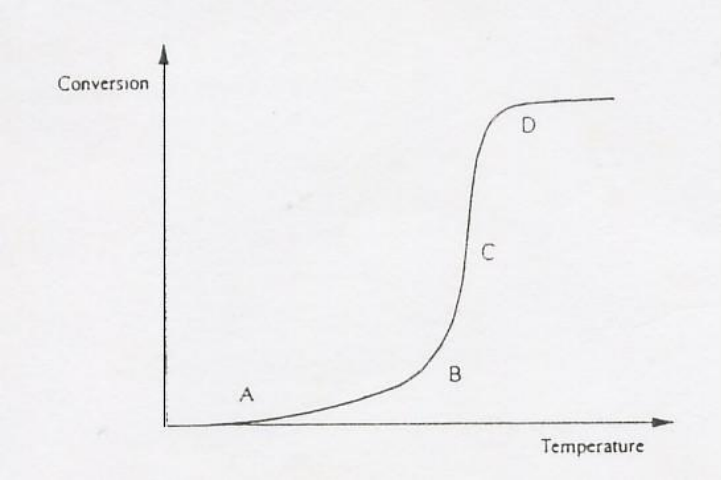

Figure. 1: Conversion versus temperature in catalytic combustion.

A further increase in temperature leads to an exponential increase in rate (area B in Figure 1) to the point where heat generated by combustion is much greater than heat supplied. The reaction becomes mass transfer controlled (area C) until the reactants are depleted (area D in Figure 1).

One important factor in the catalytic combustion of hydrocarbons is 'light-off'. This can be defined in various ways but refers to the temperature at which mass transfer control becomes rate controlling. Because of the shape of the curve (Figure 1), the definition of light-off temperatures at which conversion reaches 10%, 20% or 50% makes little difference. It is also seen that the kinetics of catalytic combustion are only relevant to parts A and B of Figure 1. Once light-off occurs, mass and heat transfer are the important parameters. The geometry of the catalytic combustor together with the porosity of the catalyst/support have much more effect in this region.

The reaction rapidly approaches complete conversion of one or both reactants (Figure 1), and the heat generated from the combustion results in a significant increase in catalyst temperature. Thus, the stability of catalyst at high temperatures is also considerable interest. It is possible to design devices in which efficient heat transfer is used to minimize temperature rise (e.g. the catalytic boiler) but particular attention must be paid in all cases to the temperature stability of materials. Thus, it is clear that considerations of catalytic combustion must include the chemical reactivity of the catalyst and the hydrocarbon (areas A and B), mass and heat transfer effects (area C) and maximum temperatures reached (relevant to area D). In some cases, further complexity may result from initiation of homogeneous combustion by overheating the catalyst. The present article considers mass and heat transfer effects only briefly, but relevant references are provided. Rather, attention is focused on the oxidation of methane on various catalysts in the presence of supports.

Finally, the performance of catalyst with respect to deactivation and sintering is examined.

1.1 Catalysts and catalytic oxidation

Metal oxides and noble metals such as Pt, Rh and Pd have been used as catalyst for the catalytic oxidation of methane. Noble metal catalysts show higher activity than metal oxide catalyst. They can used either with or without a support but supported catalysts are favoured for the oxidation. One particular advantage of supported metal catalysts is that the metal is dispersed over a greater surface area of the support and shows different activity from the unsupported metals due to interactions of the metal with the support. The support also reduces thermal degradation.

The application of noble metals other than Pt and Pd in catalytic combustion is limited practically because of their high volatility, ease of oxidation and limited supply. Palladium and platinum have been the most widely used catalyst for the catalytic oxidation of methane.

The oxidation of methane over various catalysts has been studied by many researchers. Some of the previous results are presented in Table 1. the oxidation of methane has been studied using catalysts based on both noble metals and metals oxide such as Co_3O_4, Co_3O_4/alumina, $ZnCrO_4$, $CuCrO_4$, $PbCrO_4$, Cr_2O_3/alumina, CuO/alumina and CeO_2/alumina. The Co_3O_4 catalyst was the most active metal oxide catalyst, but the activity was much less than Pd/alumina catalyst (Table 1). Various perovskite-type oxides have also been tested for the catalytic oxidation of methane. The highest activity metal oxide catalyst was $La_{0.6}Sr_{0.4}MnO_3$, which showed similar activity to Pt/alumina catalyst at a conversion level below 80%. However, unlike the Pt/alumina catalyst, the increase temperature was significantly suppressed at high conversion levels.

During the catalytic oxidation of methane, it was observed that some carbon was deposited on the catalysts. This carbon has almost no effect on the activity of the catalysts, and it was found that the rate of methane oxidation was independent of the deposition of carbon on Pd catalysts. Is was reported that the deposition of carbon on Pt catalyst first reduced activity but that this recovered in 15 min.

1.2 The effect of feed ratio.

The feed ratio ($[O_2]/[CH_4]$) has a strong effect on the total oxidation of methane to CO_2. Under oxygen-rich conditions, methane is oxidized to carbon dioxide over Pt and Pd supported on alumina. However, under oxygen-deficient conditions, the formation of carbon monoxide was observed over Pt/Al_2O_3, Pd/Al_2O_3 and Rh/Al_2O_3 catalysts and the selectivity to carbon monoxide was dependent on temperature. Under oxygen-deficient conditions, the conversion of methane to CO_2 and water increased with increasing temperature up to full consumption of oxygen. At this point, the formation of CO was observed while the partial pressure of CO_2 remained almost constant. As the temperature kept increasing, the selectivity to CO increased and Co became the main product under low $[O_2]/[CH_4]$ ratios. This is good agreement with the results of Trimm and Lam, who observed the formation of Co at high temperatures.

Since CO is produced from the oxidation of methane under oxygen-deficient conditions, methane oxidation over Pt/Al_2O_3, Pd/Al_2O_3 and Rh/Al_2O_3 catalysts was studied in the

characteristics of methane conversion with CO-free feed were similar to those observed with the feed containing CO. Under O_2-deficient conditions, similarities in methane oxidation with and without CO were observed for the whole range of conversions. The oxidation began at comparable temperatures foe each noble metals and as the temperature increased, the methane conversion increased. Passing through the light-off temperatures, similar asymptotic methane conversion levels (about 90%) were achieved above 550^{o}C. It was therefore suggested that the methane conversion characteristics are independent of the presence of CO in the feed.

1.3 The effect of precious metal loading on the support

The effect of Pt and Pd loading on the support on the oxidation of methane was investigated [1]. For conversions of methane less than 10% (kinetic controlled region: area B in Fig. 1), the oxidation rate of methane increased with an increase in Pt loading over the range of 0.1-2.0 wt%. Similarly, an increase in Pd or Pt loading (2.7-10 wt%) on γ-Al_2O_3 increased the overall rate of methane oxidation. However, although the increase in the overall rate of methane oxidation was observed, the activity per unit metal surface area decreased with an increase in loading [2]. Pd/TiO_2 catalysts also showed the same trend.

The effect of Pt loading on methane oxidation was investigated over the range 0.027-100 wt% . Below 1.4 wt% of Pt loading, the oxidation rate was almost constant, while above 1.4 wt%, the rate increase in Pt loading to reach a maximum at about 5 wt%. Above 10 wt% the reaction rate decreased significantly. Similar results have been observed by various authors [3-5].

1.4 Structure sensitivity

It was observed that methane oxidation over platinum and palladium was structure-sensitive reaction and this structure sensitivity was caused by the different reactivity of adsorbed oxygen on the surfaces of platinum and palladium. For platinum, two types of platinum particles on the support exist. One is completely dispersed platinum and the other is in the form of crystallites of platinum. In the former case, platinum is oxidized to PtO_2, whereas in the latter system, oxygen is absorbed on the crystallites to provide highly reactive adsorbed oxygen. The crystallites of platinum (large particles) are therefore more active than dispersed platinum (small particles).

A similar explanation was proposed for Pd-based catalyst. When palladium is oxidized with an excess of O_2, oxidation decreased the particle sizes of palladium. Therefore, the oxidation of small crystallites of palladium produced PdO dispersed on the support, while the oxidation of large crystallites produced PdO dispersed on small crystallites of palladium. The Pd oxides on small crystallites of palladium are more active than Pd oxides on the support. Therefore, the large crystallites of palladium are more active than the small crystallites of palladium.

In contrast to this result, there was no clear effect of particle sizes of the supported palladium catalysts on the activity of catalyst for methane oxidation, once the rates were measured in terms of specific rate constants.

1.5 The effect of pretreatment conditions.

The activity of the catalyst was found to be significantly dependent on gases used for catalyst pretreatment. The effect of pretreatment on the activity of Pt and Pd catalysts was studied with H_2, He and O_2. Pretreatment with H_2 increased the activity of catalysts whereas O_2 decreased the activity. Reactant gases were also used for the pretreatment of catalyst.

Catalysts which were reduced under hydrogen are called state I and catalysts pretreated with O_2/CH_4 mixtures (conversion level = 100 %) after reduction with hydrogen, are called state II. For Pd/Al_2O_3 catalysts. The oxidation of methane over state II catalysts started at a much lower temperature and the light-off temperatures were significantly lower). The conversions of methane over Pd/Al_2O_3 catalysts (states I and II) are represented as function of temperature in Figure 2. For the Pd/SiO_2 catalyst, the activities of state II catalysts were found to be slightly more active than state I catalysts (methane conversion of 5-100%) while the activities and dispersion of states I and II Pd/SiO_2 were observed to be similar to those for state II Pd/Al_2O_3 [22].

Several explanations for an increase in activity of the Pd catalysts with the two methods of pretreatment were proposed. It was suggested that the increase in activity was based on the reconstruction of palladium oxide crystallites. The increase in the catalytic activity was proposed to result from the changes in the reactivity of absorbed oxygen, caused by a change in noble metal particle sizes. An increase in metal particle size could also result in a decrease in the heat of oxygen chemisorption as was observed on large particles. This suggestion is similar to the explanation of structure sensitivity by Haruta et al. [3]. For Pt catalysts, state II Pt/Al_2O_3 catalysts were slightly more active than the freshly reduced state I Pt/Al_2O_3 catalysts at temperatures

between 300-500^{o}C (methane conversion <30%). Above 550^{o}C (up to 100% conversion), both catalysts showed the same activity. Pretreatment with reactant mixtures (O_2-CH_4-carrier gas) leads to catalysts more active than these pretreated with H_2.

1.6 The effect of water

Since water is produced during the catalytic oxidation of methane, there is a need to study the influence of water on the catalytic behavior. When a catalyst was treated in 18% steam-nitrogen for6.5 h at 750^{o}C, the products of oxidation of methane under O_2-deficient conditions were changed. The selectivity to CO_2 decreased markedly and formaldehyde was produced. Carbon monoxide became a main product and was not oxidized over this catalyst over the temperature range 415-630^{o}C. In contrast to this result, heating supported palladium catalysts under wet (saturated with water vapor at room temperatures) did not affect the activity. The concentration of water for both studies is quite different, so that the discrepancy in the studies could be caused by the different experimental conditions.

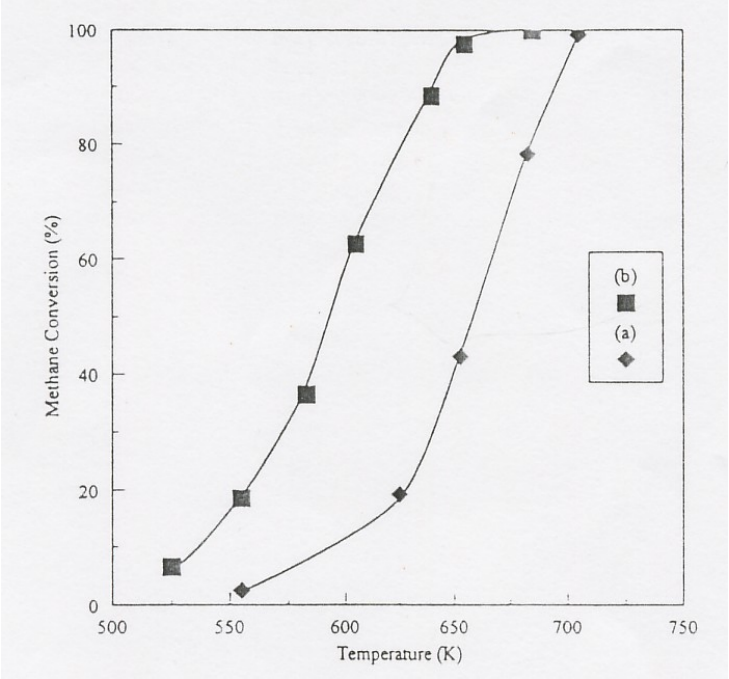

Figure 1: Methane conversion on Pd /Al_2O_3 catalyst [12] (N_2-O_2-1% CH4, O_2/CH_4 = 4): (a) state I catalyst reduced with hydrogen; (b) state II catalyst pretreated with reactant mixture after reduction.

The effect of addition of water to reactant mixtures on the oxidation of methane was studied over Pd/Al_2O_3 catalyst under sub-stoichiometric oxygen conditions. The selectivity of CO_2 increased with the presence of water. Additionally, when water and methane were the only reactants (1.4 and 7 vol % H_2O/CH_4), methane was converted to CO and CO_2 at 500-600^oC. These results were explained on the basis of the steam reforming reaction and the water gas shift reaction.

steam reforming reaction: $CH_4 + H_2O = CO + H_2 \quad \triangle H_{298} = 206.1$ kJ/mol (1.6)

water gas shift reaction: $CO + H_2O = CO_2 + H_2 \quad \triangle H_{298} = -41.2$ kJ/mol (1.7)

Both these reactions are thermodynamically possible over the temperature range 400-600^oC. The conversion of methane without O_2 in the feed was due to the steam reforming reaction and the CO produced was then converted to CO_2 via the water gas shift reaction.

In conclusion, the treatment of catalyst with the gases containing steam either has no effect on the activity or decreases the selectivity of CO_2, depending on the fraction of water. However, the presence of water in the reaction feed increases the formation of CO_2. Palladium catalysts have been shown to be the most active catalysts. The oxidation of methane has been studied over Pt, Rh and Pd catalysts supported on Al_2O_3. At 500^oC, methane conversion was about 80% for Pd/Al_2O_3 while at the same temperature, Pt/Al_2O_3 and Rh/Al_2O_3 catalysts were much less active (methane conversions less than 25%). The methane oxidation activity decreases in the order $Pd/Al_2O_3 > Rh/Al_2O_3 > Pt/Al_2O_3$ [13,23].

1.7 Supports

Noble metals are usually dispersed on a support in order to increase cost efficiency. In addition to dispersing the metal, the support acts to stabilize thermally the catalyst and in some cases may be involved in the catalytic reaction. For catalytic combustion where high throughputs are desired, the catalyst is often suspended in a washcoat and on a substrate. Both compounds have several roles to play.

Several types of substrates may be used; these include pellets, wires, tubes, fibre pads and monoliths. Monoliths are mainly used for catalytic combustors in order to obtain high geometric areas of the catalyst and low pressure drop through the system. The choice of monolith material is made on the basis of physical and chemical properties such as surface area, porosity, thermal stability, thermal conductivity, reactivity with reactants or products, chemical stability and catalytic activity.

Special metal alloys or ceramics are usually used for fabrication of substrates, depending on the required operating temperature. Metal alloys, which are made of iron, chrome and aluminium, provide excellent mechanical properties and a thinner cell wall, but their thermal stability is not as high as ceramics Therefore, ceramics have been used far more than metal alloys in the past. The most common high-temperature ceramics are based on alumina which is relatively inexpensive and reasonably resistant to thermal shock. The alumina is taken with other materials such as silica and chromium. Mullite ($3Al_2O_3.SiO_2$) and cordierite ($2MgO.5SiO_2.2Al_2O_3$) are the most frequently used substrates. One good candidate for substrates is zirconia since the oxide can be used at the highest temperature (2110^oC) among the ceramics and shows excellent inertness to most metals. For catalytic combustion, a high surface area is required. Hence, there is a need to increase the low surface areas of the monoliths structure. This can be achieved by covering the substrates with a porous layer of ceramic material, which is called a washcoat. The washcoat is coated on the substrates to provide a high surface area.

The thermal expansion coefficient of the washcoat should be similar to that of the substrate, since a large difference may result in washcoat-substrate separation. Furthermore, the surface area of washcoat should not be changed under operating conditions since a decrease in the surface area (e.g. caused by sintering) can result in pore closure and encapsulation of active catalytic sites. The most commonly used washcoat material is γ-Al_2O_3, the surface area of which is quite high. However, above 1000^oC, the high surface area γ-Al_2O_3 changed to relatively low surface area χ-Al_2O_3. The surface area of washcoat decreases from ca. 300 to ca. 5 m^2/g because of this phase change.

For the catalytic combustion of methane, the support plays an important part in determining the activity and long-term stability of the catalysts. To investigate the effect of support on the activity of catalysts, methane oxidation over Pd and Pt catalysts supported on various metal oxides has been studied [6,7]. The oxidation of methane was carried out over Pt catalysts on Al_2O_3, SiO_2-Al_2O_3, and SiO_2 [14]. It was found that the activity of catalysts decreased in the order: Pt/SiO_2-Al_2O_3 > Pt/ Al_2O_3 > Pt/SiO_2 (Table 1). The dispersion of Pt on supports was found to be proportional to the activity of catalysts. However, for palladium catalysts reduced with hydrogen, Pd/SiO_2 catalyst was more active than Pd/Al_2O_3 catalyst. For γ-Al_2O_3, TiO_2 and ThO_2 supports, the activities of both Pt and Pd catalysts are presented in Table 1 and decrease in the order: γ-Al_2O_3 > TiO_2 > ThO_2.

Table 1: Studies of the catalytic oxidation of methane.

Catalyst/support	Temperature (^oC)	$[O_2]/[CH_4]$ ratio	Pretreatment of catalyst	CH_4 conversion	Reaction rate (mol/g cat min)
Co_3O_4	450	O_2 rich	-	-	0.78
0.5% Pd/Al_2O_3	450	O_2 rich	-	-	22.5
0.5% Pd/Al_2O_3	450	O_2 rich	-	-	1.02
Pd	290-480	2	Reduced with H_2 at 480 ^oC	5-80%	-
0.155% Pd/Al_2O_3	275-475	4	Heated to 500 ^oC in He	up to 80%	-
0.153% Rh/Al_2O_3	350-500	4	containing 1% O_2	up to 25%	-
0.22% Pt/Al_2O_3	300-500	4		up to 10%	-
0.2% Pt/SiO_2	450	2	Reduced with H_2 at 300 ^oC	-	$1.6x10^{-5}$
0.2% Pt/Al_2O_3	450	2		-	$2.3x10^{-5}$
0.2% Pt/SiO_2-Al_2O_3	450	2		-	$7.4x10^{-5}$
2.7% Pt/γ-Al_2O_3	410	0.45	Heated to 500 ^oC in He or H_2	-	0.296
2.7% Pd/γ-Al_2O_3	410	0.45		-	0.35
2.7% Pt/TiO_2	410	0.45		-	0.22
2.7% Pd/TiO_2	410	0.45		-	0.269
3.0% Pt/ThO_2	410	0.45		-	0.076
3.0% Pd/ThO_2	410	0.45		-	0.09
1.93% Pd/Al_2O_3 (I)	310-600	4	I: reduced with H_2 at 600^oC	445 ^oC : 50%	-
1.93% Pd/Al_2O_3 (II)	310-600	4	II: pretreated with O_2/CH_4 at 600 ^oC	375 ^oC : 50%	-
Pd/γ-Al_2O_3	289-432	1% CH_4/air	Calcined at 600 ^oC	2.4-74.0%	-
Pd/SiO_2	290-422	1% CH_4/air		0.3-22.4%	-
1.95% Pt/Al_2O_3 (I)	280-600	4	I: reduced with H_2 at 600^oC	0-100%	-
1.95% Pt/Al_2O_3 (II)	280-600	4	II: pretreated with O_2/CH_4 at	0-100%	-

			600 ^{o}C		
1.95% Pd/Al_2O_3 (I)	400	4	I: reduced with H_2 at 600^{o}C	-	8.58
1.95% Pd/Al_2O_3 (II)	400	4	II: pretreated with O_2/CH_4 at 600 ^{o}C	-	41.6
0.16% Pd/Al_2O_3	250-700	5	Calcined with air at 500 ^{o}C	up to 100%	-
0.14% Rh/Al_2O_3	370-700	5		up to about 80%	-
0.2% Pt/Al_2O_3	400-700	5		up to about 80%	-
2.18% Pd/Al_2O_3 (I)	275-430	4	I: reduced with H_2 at 600^{o}C	2-100%	-
2.18% Pd/Al_2O_3 (II)	250-415	4	II: pretreated with O_2/CH_4 at 600 ^{o}C	6-100%	-
2.18% Pd/Al_2O_3 (II[a])	315-555	4	II[a]: pretreated with O_2/CH_4 at 600 ^{o}C	4-100%	-

I: Catalyst which was freshly reduced with hydrogen

II: Catalyst which was preheated with reactant mixture after reduction with hydrogen

[a] Feed mixture containing 100 ppm H_2S

It was found that the support material had a strong effect on determining the life of the catalyst. The oxidation of methane was studied over Pt catalysts supported on porous and non-porous alumina fibre. The activity of Pt/Al_2O_3 (porous) catalyst was constant for at least 100 h, while the oxidation of methane over Pt/Al_2O_3 (non-porous) gave a variation in products after only approximately 40 h with a constant rate of methane consumption. CO was formed from the oxidation of methane over an aged (40h use) Pt/Al_2O_3 (non-porous) although, with fresh Pt/Al_2O_3 (non-porous), CO_2 was the only product of oxidation of methane. Active alumina-supported catalysts were found to last longer than silica-supported catalysts. These results were explained on the basis that reconstruction of silica-supported catalysts under reaction conditions was easier, hence causing activation to last for less time than with alumina-supported catalysts.

1.8 The kinetics and mechanism of methane catalytic combustion

The kinetics of the catalytic oxidation of methane are important for the initial stages (kinetically controlled regime) of reaction where operating temperatures are lower than the light-off temperature. Where temperatures and conversions are high, mass and heat transfer become important. The kinetics of the oxidation of methane have been investigated extensively over supported and unsupported noble metal catalysts [8]. Some of the previous studies are summarized in Table 2.

Table 2: Kinetics for catalytic oxidation of methane

Catalyst/support	Temperature (^oC)	$[O_2]/[CH_4]$ ratio	Experimental method	Activation energy (kJ/mol)	Reaction order		C
					$[CH_4]$	$[O_2]$	o
Pd/Al_2O_3	260-440	excess O_2	Microcalorimetric technique	<290^{o}C: 138	1.0	-	-
				>290^{o}C: 51.8	1.0	-	
Pt/Al_2O_3	400-500			199	1.0	-	
Pd	295	0.37	Pulse flow reactor	94.5	0.5	0	1
Pd wire	350-500	0.1-0.7	Continuous flow reactor	71.1	0.8	0.1	<
Rh wire	450-550	0.1-0.7		100	0.6	0	
Pt wire	475-550	0.25-1		87.8	1.0	-0.6	
Pd/Al_2O_3	400	0.25	Continuous flow reactor	71.1	0.7	0	
Rh/Al_2O_3	500	0.25		92.0	0.45	0.05	
Pt/Al_2O_3	500	0.25		100	1.2	-0.5	
Pt/Al_2O_3	<540	0.5-1.7	Continuous flow reactor	188	1.0	0.75	-
(porous)	>540	0.5-1.7		83.8	1.0	1.0	
Pt/Al_2O_3	<550	0.3-2.0	Continuous flow reactor	167	1.0	1.0	
(non-porous)	>550	0.3-2.0		75.2	1.0	1.0	
2 wt% Pt/Al_2O_3	450	0.5	Continuous flow reactor	123	0.9	0	<

$Pt/\gamma\text{-}Al_2O_3$	350-450	0.02-0.4	Recirculation batch reactor	Pt loading: <5 wt%: 147 5-30 wt%: 115	1.0	0	-

For the catalytic oxidation of methane on Pd/alumina, apparent activation energies changed from 139 kJ/mol at low temperatures (290'C) to 52 kJ/mol at high temperatures (> 290'C). In contrast, the apparent energies of activation for supported rhodium, iridium and platinum were constant over the temperature range 260-440^{o}C. Since this change (87 kJ/mol) in activation energy was similar to the heat of formation of Pd oxide (85 kJ/mol at 300'C), it was suggested that adsorbed 0_2 involved in the reaction above 300'C was similar to the O_2 involved in the reaction to form Pd oxide.

The kinetics of methane oxidation over Pd, Rh and Pt catalysts (unsupported and supported on Al_2O_3) have been investigated. The rate of methane oxidation over Pd and Rh catalysts (supported and unsupported) was found to be 0.45-0.8 order in CH_4 concentration and almost independent of oxygen, with an apparent activation energy of 71-1000 kJ/mol. However, the kinetics of the methane oxidation over supported and unsupported Pt catalysts showed a significantly different effect of oxygen on reaction rate, in that oxidation over Pt catalysts was inhibited by oxygen. These results were explained by the observation that, under O_2-rich conditions, the surfaces of Pd and Rh catalysts were covered with 0_2 (as expected from thermodynamic considerations) and thus the oxidation of methane was independent of 0_2 concentration. However, platinum has a relatively high ionization potential compared in Pd and Rh and the oxide is of lower stability. Therefore, the oxygen coverage on Pt is expected to be less than on Pd and Rh, to be significantly dependent on the $0_2/CH_4$ ratio, and to depend on the ease of chemisorption and reaction of CH_4. Unlike the studies carried out with a considerable excess of 0_2, the oxidation rates determined under 0_2-deficient conditions were thus strongly dependent on oxygen concentration.

Although methane is the simplest hydrocarbon, the mechanistic pathways of oxidation over noble metals have not been clearly identified. Oxygen adsorption is faster than methane adsorption and the noble metal surface is first covered with 0_2. Subsequent chemisorption of CH_4 onto the

catalyst surface occurs. However, at lower temperatures or $[O_2]/[CH_4]$ ratios, oxygen adsorption on noble metals might not be completed, enabling methane to compete with oxygen for adsorption sites. Thus for example, methane is adsorbed on two different types of adsorption sites on Pd/Al_2O_3 at 280^oC. One site is a site for which there is no competition and, as a result, is completely covered with oxygen. The site is suggested to still be able to adsorb methane without competing with oxygen. The other site is a "competition" site, where the empty adsorption sites could provide competitive adsorption of methane or oxygen. The surface coverage of both reactants is interdependent.

The chemisorption of methane onto noble metals is dissociative, and methyl or methylene radicals are produced by removing hydrogen atoms from CH_4. The adsorbed radicals subsequently react with adsorbed oxygen to produce CO_2 and H_2O or chemisorbed formaldehyde. This chemisorbed formaldehyde is either desorbed as HCHO or dissociated to adsorbed CO and adsorbed H atoms. Adsorbed CO and H atoms are either desorbed as CO and H_2 or reacted with adsorbed 0_2 to produce CO_2 and H_2O, depending on the composition of the reactant mixture [30]. A possible mechanism for methane oxidation is represented in Figure 3.

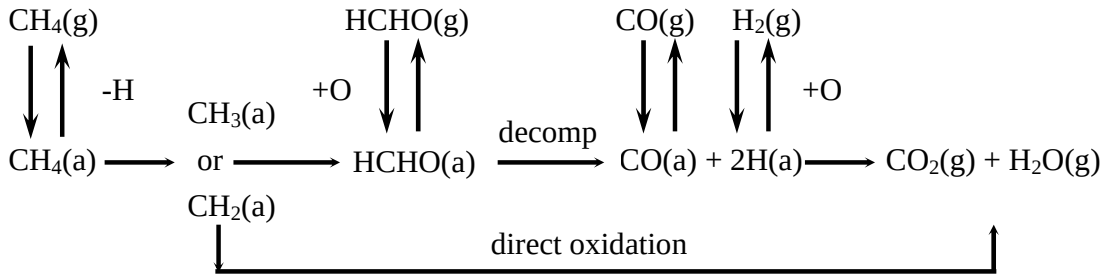

Figure 3 : Proposed mechanism for methane oxidation. (a) adsorbed, (b) gas phase.

Only a trace amount of formaldehyde was detected in the reaction products of methane oxidation. It was therefore suggested that the decomposition of adsorbed formaldehyde intermediate to CO(a) and H(b) is much faster than desorption to HCHO(g). One further complication arises from the fact that, in the catalytic combustion of methane, both heterogeneous and homogeneous reactions have to be recognized. At low temperatures (kinetically controlled region), the heterogeneous reactions are dominant and the homogeneous reaction rates are

unimportant. At high temperatures, the homogeneous reactions become more important. Several models have been proposed for such systems.

Groppi [9] have developed a two-dimensional model for the combustion of CO in an adiabatic laminar reactor. Three variations of the model (the homogeneous case, the heterogeneous case and the heterogeneous-homogeneous case) were investigated. Comparison between these three cases indicated that, below 377^{o}C, the reaction could be represented by heterogeneous reactions, whereas, at temperatures higher than 877^{o}C, the reactor behavior approached that of the homogeneous system. Between 377^{o}C and 877^{o}C, both reactions were needed in modeling. Groppi has also developed a two-dimensional model for the steady-state combustion of propane to include axial and radial convection and diffusion of mass, momentum and energy. Homogeneous and heterogeneous reactions were considered. The model involved complete two-dimensional steady laminar flow equations. Heat transfer characteristics were included using an experimentally measured wall temperature. Trends of predicted concentrations by the model were in good agreement with experimental results, but the magnitudes of predicted and experimental concentrations were often different.

In this work, we report data concerning the catalytic performance of various metal oxide catalysts comprise of non-noble metals in the form of powder or supported system for the combustion of methane. Furthermore, in order to give insights into the nature of the active sites, we also report data obtained using several characterization techniques.

1.9 Objective

The objectives of this research work are described as follows;

i) To synthesize non-noble mixed metal oxide catalysts which posses excellent catalytic combustion properties for natural gas utilizing various preparation techniques,

ii) To execute screening and testing activities for all the prepared catalysts using simulated natural gas,

iii) To characterize the selected excellent catalysts identified from the testing, using various analytical techniques.

1.10 Scope

The main transition metals and the lanthanide metals will be employed. The mixing chemical compositions will be done according to previous works. Sol-gel, impregnation and coprecipitation methods will be used directly or with some modifications. Testing of the prepared catalysts will be accomplished using fixed bed microreactor using simulated mixed natural gas which comprises of 1% methane and 99% nitrogen. Elucidation of physical properties of the catalysts will be done using various instruments available in Malaysia

References

1. Oh, S and Siewert, R, "Methane oxidation over metal oxide noble catalyst as related by controlling natural gas vehicle exhaust emission", Am. Chem. Soc., 1992.
2. Machita, M and Arai, H, "Catalytic Properties of BaMA111O19 for catalytic combustion", Journal of Catalysis, 120, 377-386, 1989.
3. Haruta, M and Ueda, A, "Low-temperature catalytic combustion over supported gold", Catalyst Technology, Japan, 1996.
4. Machita, M and Sato, A, "Catalytic properties and structure modification hexaaluminate microcrystals for combustion catalyst", Catalysis Today, 3-4, 26, 1995.
5. Berg, M and Jaras, S, "Stable magnesium oxide catalyst for catalytic combustion of methane", Catalysis Today, 3-4, 26, 1995.
6. Tatsumi, I and Sumi, H, "Pd-ion exchanged silicoaluminophosphate(SAPO) for low temperature combustion of methane", Catalyst Technology, Japan, 1996.
7. Poirier, M and Couture, L, "Ruthenium catalysts for the catalytic combustion of natural gas", Catalyst Technology, Japan, 1996.
8. Mc Carty, J.G, "Kinetic of PdO combustion catalyst" Catalysis Today, 26, 238-239, 1995.
9. Groppi, G and Forzatti, P, "Modelling of catalytic combustion for gas turbine application", 16(49), Elsevier, 1993.

CHAPTER 2

THE CHARACTERISATION OF CHROMIUM(VI)-PROMOTED TIN(IV) OXIDE CATALYSTS

Wan Azelee Wan Abu Bakar*, Nor Aziah Buang and Philip G. Harrison**

Department of Chemistry, Faculty of Science, Universiti Teknologi Malaysia, Skudai, Locked Bag 791, 80990 Johor Bahru, Johor, Malaysia.**Department of Chemistry, University of Nottingham, University Park, Nottingham NG7 2RD, U.K.

Abstract

The nature of Cr(VI)/Sn catalysts has been investigated by a number of techniques including photon correlation spectroscopy, gas adsorption, powder X-ray diffraction, mid infrared, Raman, and thermogravimetric and differential thermal analysis. Chromium(VI) oxide causes deaggregation of aqueous tin(IV) oxide colloidal sols and of which, the particle size depending on the sol concentration and the chromium:tin ratio. The surface adsorbed species formed on tin(IV) oxide gel particles are chromium(VI) oxyanions of the types CrO_4^{2-}, $Cr_2O_7^{2-}$ and $Cr_3O_{10}^{2-}$, which disappear on calcination. Prior to calcination the materials are microporous, but significant changes in specific surface area, pore volume and pore size occur at temperature >673 K. After calcination at temperatures of 873 K and above, the materials are essentially non-porous solids. Loss of adsorbed water and the condensation of surface hydroxyl groups can be followed by mid and near infrared as well as TGA/DTA. Powder X-ray diffraction confirm the formation of Cr_2O_3 on calcination at 1273 K.

Keywords: Catalyst, photon correlation spectroscopy, gas adsorption, powder X-ray diffraction.

* Corresponding author

Abstrak

Sifat fizik sampel mangkin Cr(VI)/Sn telah dikaji menggunakan pelbagai teknik analisis seperti spektroskopi korelasi foton, penjerapan gas, pembelauan sinar-x, inframerah pertengahan, Raman dan analisis gravimetri termal dan termal pembeza. Oksida kromium telah menyebabkan pendeagregasian sol oksida timah(VI) dan saiz zarah sampel bergantung kepada kepekatan sol dan nisbah kromium:timah. Spesies permukaan terjerap yang terbentuk dipermukaan gel oksida

timah(VI) adalah berupa oksianion kromium(VI) daripada jenis CrO_4^{2-}, $Cr_2O_7^{2-}$ dan $Cr_3O_{10}^{2-}$, dan akan hilang apabila pengkalsian dilakukan. Sampel sebelum dikalsinkan mempunyai liang mikro tetapi perubahan yang jelas terhadap luas permukaan, isipadu liang dan saiz liang berlaku apabila sampel dikalsinkan melebihi suhu 673 K. Pengkalsinan pada $\geq$ 873 K menghasilkan sampel mangkin yang tak berliang. Kehilangan air terjerap dan kondensasi kumpulan hidroksi permukaan boleh diikuti melalui teknik inframerah pertengahan dan gravimetri termal dan termal pembeza. Pembelauan sinar-x mengesahkan pembentukan spesies Cr_2O_3 dalam sampel mangkin apabila dikalsinkan pada suhu 1273 K.

Introduction

The control of noxious emission resulting from either the combustion of fossil fuels or from other industrial activities is one of the most immediate and compelling problems faced by nearly every country in the world. The levels of pollutants from automobiles, carbon monoxide (CO), hydrocarbons (HC's), and nitrogen oxides (NO_x), are the subject of ever increasingly stringent legislation controlling the maximum permitted levels of emissions of each substance [1,2]. Platinum group catalysts currently represent the state-of the-art in internal combustion engine emission technology. The driving force for the development of non-platinum exhaust emission catalysts is the price, strategic importance and low availability of the platinum group metals. Tin oxide-based materials have been known for a long time to have good activity towards the CO/ O_2 and CO/NO reactions [4-10]. Our recent data [3] have demonstrated that Cr/SnO_2 and $Cu/Cr/SnO_2$ catalysts exhibit three-way activity, which is comparable to conventional noble metal catalysts. These data show that the performance of these catalysts is similar to the $Pt/Rh/Al_2O_3$ catalyst for CO and HC oxidation.

In spite of this very promising observed activity, however, we have not been able as yet to investigate either the constitution of these catalyst materials, the chemistry involved in their preparation, or the surface speciation/reaction mechanisms of the involved species in the catalytic processes. The nature of these materials is unclear and even simple questions such as the oxidation state of chromium in the active catalyst remains unanswered. In this study we report initial data concerning both the physical and chemical nature of the material, including aggregation behaviour of primary particles, pore texture and surface area, phase identification, particle size, defect structure and change induced by calcination.

Experimental

Photon correlation spectroscopy data were obtained using a Malvern 3700 system equipped with a type K7025 correlator, gas adsorption isotherms were obtained using a custom made apparatus, X-ray diffraction data using a Phillips PW 1710 diffractometer (Cu K_α radiation λ = 1.54060 Å), mid and near infra-red spectra were obtained using Nicolet 20SXC and Perkin-Elmer Lambda 9 UV-VIS-NIR spectrometers, respectively, Raman spectra were recorded using a Perkin-Elmer 2000 NIR FT-Raman spectrometer equipped with a Nd^{3+}-YAG laser, thermogravimetric analysis and differential thermal analysis were obtained using a Stanton-Redcroft Model STA 1000/1500 instrument. Elemental analysis data for tin and chromium were obtained by atomic absorption.

Preparation of Cr(VI)/SnO_2 Catalysts

To a suspension of tin(IV) oxide gel (2.5 g) in triply distilled water (25 cm^3) was added a solution of chromium(VI) oxide (1 M) also dissolved in triply distilled water in CrO_3/SnO_2 molar ratios of 0.01, 0.05, 0.1, 0.5 and 1. Each set of mixtures was stirred at room temperature or under reflux for 24 h. The resulting yellowish mixture solution was filtered and the yellowish precipitate was dried in air at 60 ^oC for 24 h. At this point the precipitate was of a yellow powdery appearance. This was then washed with triply distilled water until no more yellow solution of chromium(VI) could be washed out. The resultant yellowish precipitates were then dried in air at 60 ^oC for 24 h. Target and observed Cr:Sn atomic ratio data are listed in Table 1. Materials which were treated for 0.5 h and 3 h gave very low loading of chromium(VI) and it was found that the loading is dependent not only on the concentration of the aqueous CrO_3 solution, but also on the washing regime employed.

Table 1. Analytical data and preparative treatment conditions for CrO_3/SnO_2 catalysts.

"Target" CrO_3/SnO_2 molar ratio	Treatment conditions	Observed Cr:Sn ratio
0.01	Stir at RT reflux	0.008 0.007

0.05	Stir at RT reflux	0.011 0.041
0.10	Stir at RT reflux	0.020 0.048
0.50	Stir at RT reflux	0.054 0.031
1.00	Stir at RT reflux	0.132 0.130

Results and Discussion

Photon Correlation Spectroscopy

Stable colloidal sols of SnO_2 can be readily made using choline as the stabilisation agent, and the effect on aggregation in this colloidal sol due to the presence of Cr(VI) can be assessed by photon correlation spectroscopy which allows rapid *in situ* sizing. Previous studies have shown that the average particle size in choline-stabilised SnO_2 sols increases with increase in concentration [11]. A plot of average particle size versus the Cr(VI): SnO_2 ratio is shown in Figure 1(a) from which it can be seen that the particle size is strongly and linearly dependent on the quantity of Cr(VI) dopant added over the concentration range studied. The effect of addition of Cr(VI) to the choline-stabilised tin sol is to significantly reduce the particle size, and the smallest particle size (217 nm) is exhibited at the lower ratio of Cr(VI):Sn (Table 2). At higher ratios the particle size increases steadily, reaching a value similar to that observed for the choline-stabilised tin sol alone (*ca*. 520 nm) at a Cr:Sn ratio of 0.025. Above this value further addition of Cr(VI) results in destabilisation of the sol and precipitation occurs.

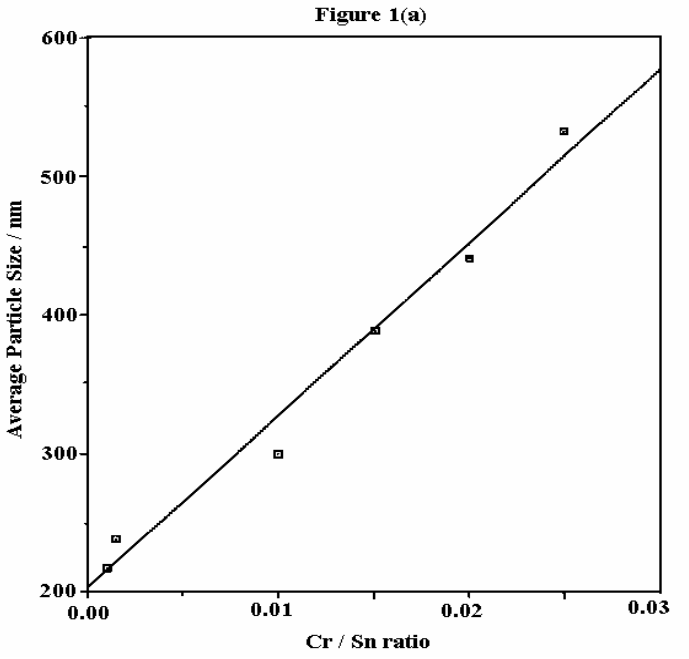

Figure 1(a) The plot of average particle size versus the Cr:Sn ratio in the chromium (VI): tin sol. The straight line in this figure represent the least-squares best fit (particle size = 202.5 + 12389 [Cr/Sn ratio], $R^2 = 0.981$).

Table 2.The effect of dopant on the average particle size (nm) derived from PCS Analysis.

Cr(VI)/Sn Ratio[a]	Average Particle Size of Cr(VI):Sn Sol
0	522
0.0010	217
0.0015	238
0.0100	300
0.0150	388
0.0200	440
0.0250[b]	530

(a) The concentration of SnO_2 in the sol was constant at 0.7201 Molar.

(b) Cr(VI) dopant destabilised tin sol at a ratio greater than 0.025.

A plot of average particle size versus Cr(VI) concentration shows that, after the dramatic decrease in particle size following the addition of a very small amount of Cr(VI), there is little effect on the particle size up to a concentration of *ca*. 0.05 M. However, at higher concentrations the particle size increases rapidly (Figure 1(b).

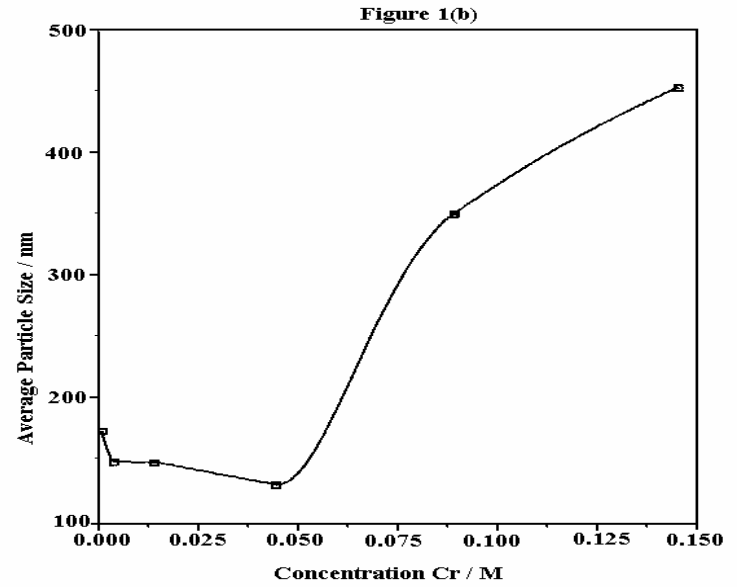

Figure 1(b) The plot of average particle size versus the Cr:Sn ratio in the concentrations of chromium (VI).

Gas Adsorption data for Cr(VI)/SnO_2

Nitrogen adsorption data for Cr(VI)/SnO_2 (Cr(VI):Sn ratio 0.132:1) at calcination temperatures from room temperature to 1273 K is shown in Table 3. Corresponding BET isotherm is shown in Figure 2. Freshly prepared Cr(VI)/SnO_2 exhibits similar microporous properties to SnO_2 gel itself. However, on calcination, it becomes coarsely mesoporous at 837 K, and at 1273 K becomes non-porous. At room temperature, the isotherm is characteristic of adsorption on a microporous solid of Type I according to the BET classification [12]. At 873 K the adsorption isotherm is typical of Type V behaviour with coarse mesoporous texture, but at 1273 K, the isotherm is that of a non-porous solid of Type III. Both isotherm of Type V and III are associated with weak adsorbent-adsorbate interactions. This weakness of the adsorbent-adsorbate forces cause the uptake at low relative pressure to be small but once a molecule has become adsorbed, the adsorbent-adsorbate forces promote the adsorption of further molecule by a cooperative process.

The process rationalises the convexity of isotherms to the pressure axis at higher relative pressure [13].

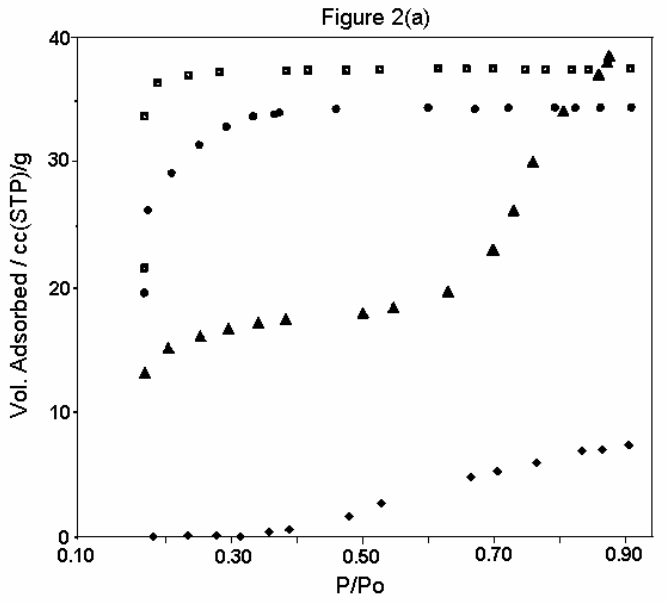

Figure 2: Nitrogen adsorption isotherms after calcination at temperature of 333K (■) , 573K (●), 873K (▲)and 1273K (◆)

The microporous properties in the Cr(VI)/SnO_2 catalyst materials are close to the lower limit of mesoporous range since the C value is fairly small. This indicates that the sample has only a low microporosity. From the BET isotherm, there is little doubt that the micropore filling process is responsible for the initial shape of the isotherm at low P/P_o at room temperature. The fairly high adsorption affinity, reflected by a steep uptake at low P/P_o, and the fairly high C value obtained, is a direct result of enhanced gas-solid interactions brought about by the close proximity of the gas molecules to pore walls in micropores [13].

Compared to SnO_2 gel which has specific surface area (SSA) of *ca.* 185 $m^2\ g^{-1}$ decreasing to *ca.* 40 $m^2\ g^{-1}$ after calcination at 1273 K, the Cr(VI)/SnO_2 catalyst exhibits a much smaller SSA at room temperature (114 $m^2\ g^{-1}$), which is reduced by a relatively small amount to 96 $m^2\ g^{-1}$on calcination at 573 K. However, after calcination at 1273 K the SSA is almost zero. This change is in accordance with the transformation of the micro-particulate structure of the dried gel into a continuous dense oxide structure during the treatment, which results in progressive pore elimination. It has been shown that the surface properties of this type of oxide material change dramatically upon calcination at temperature >573 K. This behaviour arises because densification

at higher temperature eliminates most of the accessible pore surface, and changes the fairly highly porous structure to a dense and non-porous structure. However, the Cr(VI)/SnO_2 catalyst still seem to possess some external surface even after calcination at 1273 K as demonstrated by the existence of small broad peak ca. 3400 cm^{-1} (ν(OH)) from i.r. analysis (see later) due to hydroxyl species trapped in deep pores.

It is interesting to note that, although the surface area decreases dramatically with increasing temperature, there is only a small change in average pore size below 573 K compared to that above 573 K. When the Cr(VI)/SnO_2 gel is calcined up to 573 K agglomeration occurs and the pore volume decreases in proportion to the decrease in surface area whilst the pores which remain do not change much in size. It appears that portions of the gel agglomerate completely to a dense solid while the remainder undergoes little or no change. This behaviour is similar to that of silica gel [14]. However, above 573 K, the pore volume is increased whilst the surface area decreases and the pore diameter increases. At 1273 K, the pore diameter is further increased, but the pore volume is now severely reduced.

Comparing the data in Table 3, it is clear that calcination at 873 K and 1273 K induces a large structural change in this type of catalyst. This is reflected by a large reduction in surface area and pore volume and a large increase in mean pore size. The small C value indicate that the sample calcined at 1273 K has lost its microporosity and has become a completely non-porous solid.

It has to be pointed out that a total elimination of surface Sn-OH and/or Cr-OH groups does not necessarily imply a total elimination of pores throughout the entire gel structure. Mid-ir and NIR results (see later) show that both the internal SnOH and/or CrOH groups have been found to exist in the sample even after calcination at 1273 K, a result of hydroxyl species trapped in deep pores (pores with closed necks).

Table 3. Nitrogen adsorption data calculated by the BET methods for Cr(VI)/SnO_2 (0.132:1) catalyst.

Calcination	BET Method				
Temp/K	V_m (cc/g)	A_{BET} (m^2/g)	C	V_p (cc/g)	d (Å)

333	26	114	167	0.057	18
573	22	96	425	0.053	19
873	13	58	16	0.059	40
1273	0.1	0.4	6	0.011	42

V_m = monolayer capacity; A_{BET} = specific area derived from BET plot; C = BET constant, V_p = pore volume; d= mean pore diameter.

X-Ray Diffraction of Cr(VI)/SnO_2 catalyst material

Representative powder X-ray diffraction patterns obtained for Cr(VI)/SnO_2 catalyst material calcined at various temperatures are shown in Figures 3(a) and 3(b), together with diffractograms of different CrO_3 loading after calcination at 1273 K (Figure 3(c)). Prior to calcination, all ratios of Cr(VI)/SnO_2 materials studied exhibit diffractograms comprising the four characteristic very broad bands due to very small particulate SnO_2. No bands are observed due to other constituents indicating that they are amorphous in nature. On heating there is a distinct sharpening and increase in the intensity of the peaks indicating an increasing crystallinity of the SnO_2 phase, and no other phases are observed even after heating at 873 K. For samples with loading of Cr $\leq$0.048:1, no crystalline phase containing Cr could be observed, even after calcination, presumably due to the relatively low level of chromium in this materials (Figure 3(b)). As such it is unlikely that any crystalline mixed phase would be detected. Particle size measurements deduced from line broadening show that the particle size increases relatively little until *ca*. 1173 K when a very sharp increase takes place (Figure 4 and Table 4).

However, after calcination of the Cr(VI)/SnO_2 (0.054:1) material at 1273 K (Figure 3(a)), peaks characteristic of crystalline Cr_2O_3 appears. The highest intensity peak at a d-value of d = 2.6650 Å of Cr_2O_3 is masked by the second most intense peak of SnO_2 at d =2.6440 Å. The second highest intensity peak of Cr_2O_3 is observed at d = 2.4791 Å (lit. [15] d-values for Cr_2O_3: 3.6310, 2.6650, 2.4800, 2.1752, 1.8152, 1.6754, 1.4649, 1.4316 Å). The third highest intensity peak of Cr_2O_3, d = 1.6724 Å, is again masked by SnO_2.

At higher chromium loading (*eg*. 1:0.13), the chromium-containing phase becomes more pronounced with the peaks at d = 2.6650, 2.4791 and 3.6304 Å of Cr_2O_3 are now clearly observable beside the peaks at d = 2.1765, 1.8159 and 1.4638 Å. It is apparent that at chromium

loading of 0.0542 and above, phase separation of Cr_2O_3 in Cr(VI)/SnO_2 catalyst materials is quite facile (Figure 3(c)

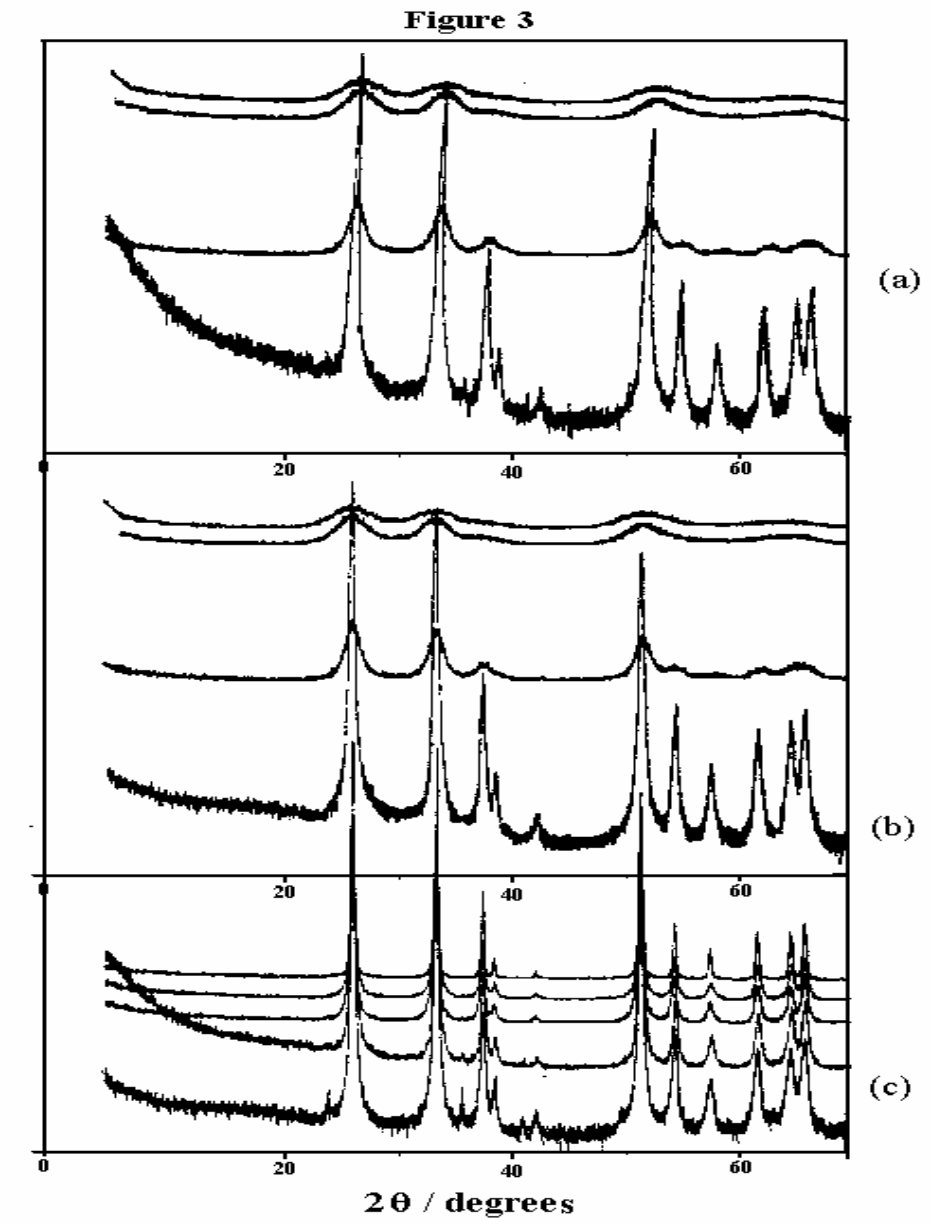

Figure 3 The X-ray diffraction patterns of Cr(VI)/SnO_2 catalysts of Cr:Sn ratio (a) 0.054:1 and (b) 0.048:1 after calcination at temperature of 333 (top), 573, 873 and 1273 K(bottom) and (c) catalysts with increasing chromium loadings after calcination at 1273 K (neat SnO_2 is shown as the top trace, with Cr:Sn ratios of 0.01, 0.048, 0.05 and 0.132 (bottom))

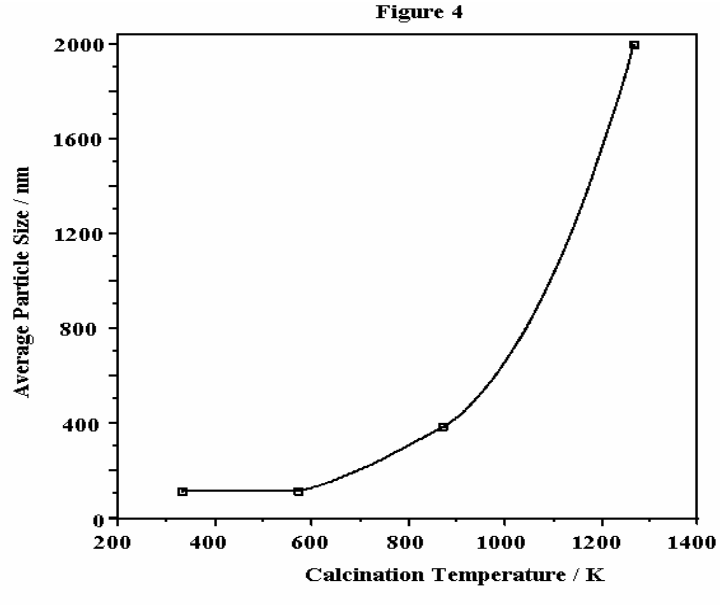

Figure 4 The plot of average particle size versus temperature, derived from X-ray diffraction for Cr(VI)/SnO_2 (0.132:1) oxide catalyst.

Table 4. Average particle size (Å) of Cr(VI)/SnO_2 materials calculated from X- Ray diffraction peak widths.

Sample/Cr:Sn Ratio	Phase	Calcination temperature/K			
		333	573	873	1273
1:0.011[a]	SnO_2	117	119	371	2076
1:0.048[a]	SnO_2	117	119	343	4082
1:0.054	SnO_2	117	-	372	1361
	Cr_2O_3	-	-	-	627
1:0.132	SnO_2	117	119	392	2040
	Cr_2O_3	-	-	-	1393

(a) Cr_2O_3 not observed

Density Measurements

The density of the Cr(VI)/SnO_2 (0.132:1) material, measured using a conventional Weld pycnometer, increases with calcination temperature (Table 5). This distinct increase in density

appears to be due the formation of the crystalline phase of cassiterite (density 6.95 g cm^{-3} [17]), generated in the structure as shown by X-ray diffraction.

Increase in calcination temperature results in an increase in the density of the material and also in an increase of the average particle size of the sample. When comparing the average particle size from X-ray diffraction line broadening with the corresponding sizes obtained by nitrogen adsorption method (Table 5), it is obvious that the difference in size obtained by the two techniques is larger at higher calcination temperature. This phenomenon arise mainly due to the low sensitivity of the line broadening technique to large crystallite sizes. Similar behaviour has also been observed previously [18,19] in the studies of $Ag/\alpha\text{-}Al_2O_3$ catalysts. Another quite reasonable explanation for high values obtained from XRD calculations is due to the method of specimen preparation for XRD analysis in which the material is subjected to prolonged grinding. This grinding process subject the material to excessive mechanical stress, and the local energy produced could quite possibly cause a sintering effect thereby producing larger particles. The opposite effect is the case for the calcined material where the mechanical forces causes the large sintered particles to fracture giving misleading size values in the XRD calculation. As such both techniques offer qualitative information.

Table 5: Comparison of the average particle size (D) obtained from powder X-ray diffraction and nitrogen adsorption methods for the $Cr(VI)/SnO_2$ (0.132:1) catalyst.

Temp. (K)	Density (g cm^{-3})	$D_{X\text{-}ray}$a (Å)	D_{NA}a (Å)
333	4.15	117	115
873	5.42	382	187
1273	5.95	1361	1008

[a] $D_{X\text{-}ray}$a and D_{NA}a = average particle size derived from X-ray diffraction and nitrogen adsorption methods, respectively, calculated using equation [16] $d = 6/\mu A_s$, where μ = density; A_s = specific area (derived from BET).

Thermal Analysis of the Cr(VI)/SnO_2 (0.132:1) material

Representative TGA and DTA plots for the Cr(VI)/SnO_2 (0.132:1) material are shown in Figure 5. The TGA thermogram (Figure 5 (a)) shows two stages of mass loss. The small continual mass loss of *ca.*11 % between room temperature and 423 K is attributed to the loss of physisorbed water from surface [20]. The second mass loss commencing at 423 K and continuing up to 823 K is attributed to the condensation of adjacent hydroxyl groups on the SnO_2 particle surface, contributing another 6 % of mass loss. The mass loss is completed at *ca.* 823 K, and the overall mass loss is 17 %.

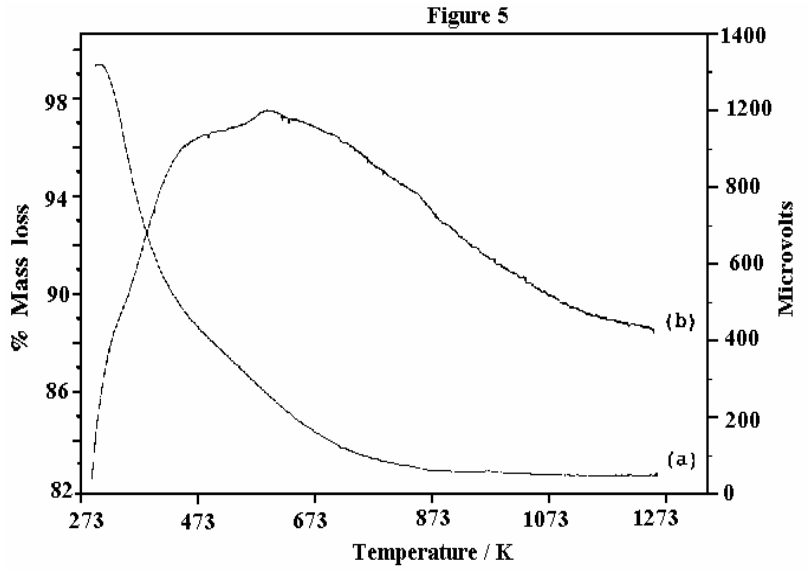

Figure 5: The thermogram of Cr(VI)/SnO_2 (0.132:1) oxide material for (a) thermogravimetric analysis and (b) differential thermal analysis.

The first event in DTA thermal analysis (Figure 5(b)) is the shoulder type of endotherm at *ca*. 373 K that is assigned to the dehydration process. This is followed by a major event, a large broad exotherm enveloped between *ca.* 433 K and 873 K, which is attributed to the condensation of hydroxyl groups bonded to the surface. A small broad distinct exotherm centred at *ca.* 573 K is attributed to crystallisation rearrangement, which is in a good agreement with XRD diffractogram and infrared analysis.

Mid-infrared analysis of the Cr(VI)/SnO_2 (0.132:1) material

Representative infrared spectra for the Cr(VI)/SnO_2 (0.132:1) material before calcination and after calcination at various temperatures up to 1273 K are illustrated in Figure 6. The freshly prepared gel material exhibits an intense, very broad hydroxyl stretching envelope ranging from *ca.* 3600 to 2500 cm^{-1}, with a maximum at *ca.* 3437 cm^{-1}, which shifts to higher wavenumber on increasing heat treatment, due largely to adsorbed molecular water. The corresponding water deformation mode is centred at *ca.* 1640 cm^{-1}.

The band at *ca.* 1245 cm^{-1} and 1160 cm^{-1} are assigned to hydroxyl deformation modes of surface hydroxyl groups. These bands are lost after calcination at calcination temperatures of ≥873 K. The bands at *ca.* 942, 893 and 822(sh) cm^{-1} are assigned as Cr-O stretching modes of surface chromate species. These bands reduce in intensity on calcination but are still observable at 1273 K. The powder X-ray diffraction analysis shows the formation of Cr_2O_3 in this material at a calcination temperature of 1273 K, and it appears that the chromate (VI) species are transformed into Cr_2O_3 on calcination.

Figure 6(a)

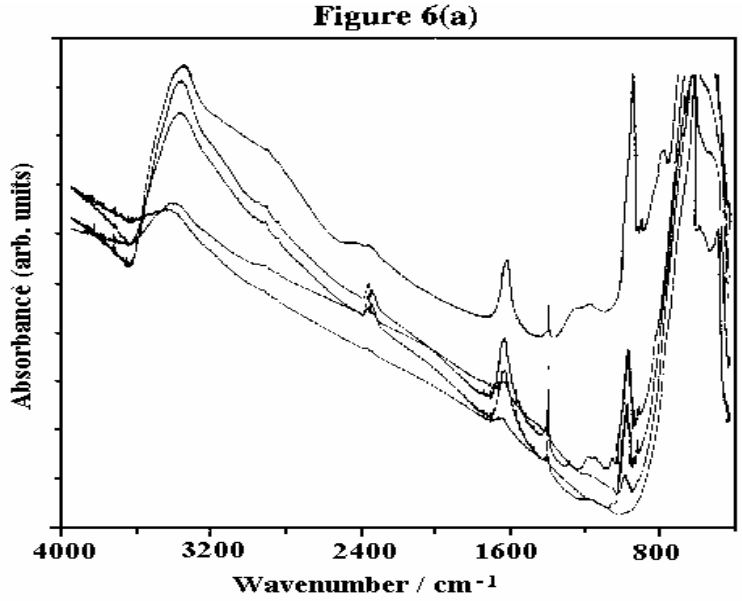

Figure 6(a) The mid-infrared spectra of Cr(VI)/SnO_2 oxide catalyst in the range of 4000-400 cm^{-1} after calcination at the temperatures of 333 (top), 573, 873, 1073 and 1273 K (bottom).

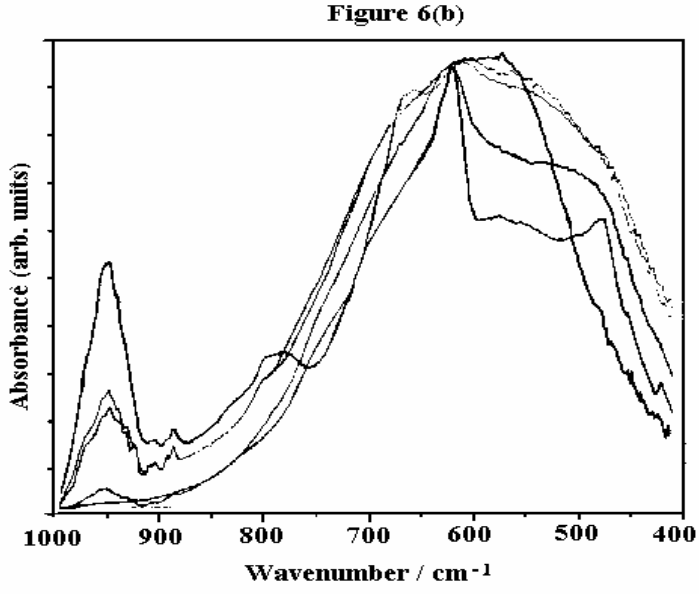

Figure 6(b) The mid-infrared spectra of Cr(VI)/SnO_2 oxide catalyst in the range of 1000-400 cm^{-1} after calcination at the temperatures of 333 (top), 573, 873, 1073 and 1273 K (bottom).

The intense broad band at *ca*. 1160 cm^{-1} observed at ambient temperature, increases in intensity and sharpens as the temperature of treatment is increases and is assigned as the antisymmetric Sn-O-Sn stretching modes of the surface-bridging oxide formed by condensation of adjacent surface hydroxyl groups. This Sn-O-Sn band shift to higher wavenumber as the temperature of calcination increases denoting the strengthening of Sn-O bond as a result of condensation of OH-group. At 1273 K this peak reaches a maximum at *ca.* 620 cm^{-1} compared with values of ν_{as}(SnOSn) for $Me_3SnOSnMe_3$ [21] which occurs at 737 cm^{-1} and for SnO_2 [20] which occurs at 770 cm^{-1}. The weak broad band observed at *ca*. 620 cm^{-1} is assigned to the symmetric Sn-O-Sn stretching mode [20,22] (Figure 6(b)).

FT-Raman spectra of Cr(VI)/SnO_2 materials

Raman spectra in the range 750-1050 620 cm^{-1} (ν(Cr-O) region) of four Cr(VI)/SnO_2 catalysts ((0.011:1), (0.048:1), (0.054:1), and (0.132:1)) (Figure 7) have been recorded at a low laser intensity of ~100 mV cm^{-2} , in order not to induce any alterations on the surface. All four spectra are similar in form exhibiting two principle maximum together with several shoulders. However, the position of the peaks maximum shifts with Cr:Sn ratios.

For the lowest chromium loading, two broad weak band at *ca*. 887 and 942 cm^{-1} are observed; the former indicates the presence of adsorbed CrO_4^{2-} ion whilst the latter indicates the presence of $Cr_2O_7^{2-}$ anion (Table 6). Other bands due to these species are present as shoulder features, and it is also probable that the shoulder at high wavenumber is due to a small amount $Cr_3O_{10}^{2-}$ anion. The vibration bands assigned for SnO_2 in this material only exhibits two large broad bands at *ca.* 632 and 475 cm^{-1}.

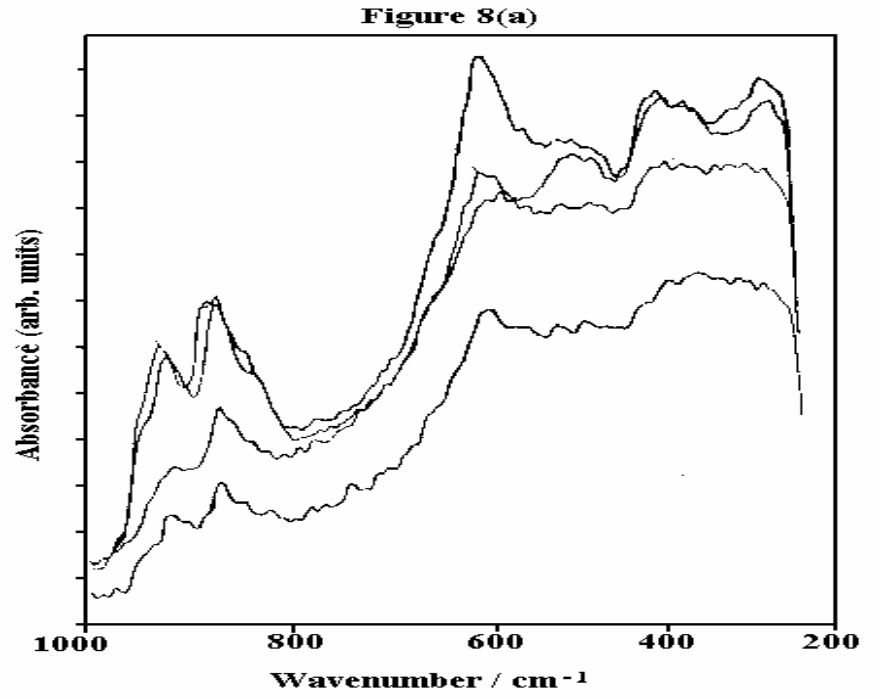

Figure 7(a) The FT-Raman spectra of freshly prepared Cr(VI)/SnO_2 oxide material at ratio of 0.011:1 (bottom), 0.048:1, 0.321:1 and 0.054:1 (top).

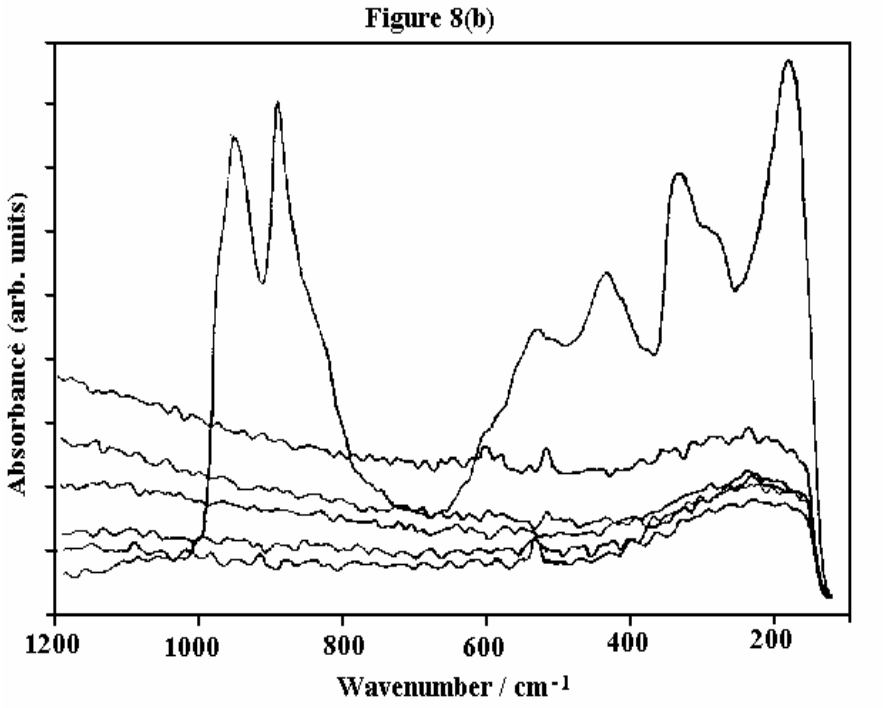

Figure 7(b) The FT-Raman spectra of Cr(VI)/SnO_2 oxide material at ratio of 0.011:1 (bottom), 0.048:1, 0.321:1 and 0.054:1 (top) after calnination at temperature of 333 (top), 1273, 1073, 873, 673 and 573 K (bottom).

As the chromium loading is increased, the maxima shift to 886 and 942, 884 and 943 and 883, 895 and 949 cm^{-1} for Cr loadings 0.048:1, 0.052:1 and 0.132:1, respectively. In all cases, pronounced shoulder features are present both to higher and lower wavenumber. The observed shift to higher wavenumber is readily rationalised by an increased concentration of adsorbed $Cr_2O_7^{2-}$ and adsorbed $Cr_3O_{10}^{2-}$ anions in these catalysts. However, the adsorbed CrO_4^{2-} ions could also be present but only in small amounts.

Table 6. Assignment of FT-Raman bands for chromate anions (cm^{-1}) [23-26]

CrO_4^{2-}	$Cr_2O_7^{2-}$	$Cr_3O_{10}^{2-}$	$Cr_4O_{13}^{2-}$	Assignment
		987	987	$\nu_{as}(CrO_2)$
		956	963	$\nu_s(CrO_2)$
886	942			$\nu_{as}(CrO_4)/(CrO_3)$
848	904	904	902	$\nu_s(CrO_4)/(CrO_3)$
		844	842	$\nu_{as}(Cr'OCr'')$

At higher loading of chromium 0.052:1 and 0.132:1, besides exhibiting the two maximum vibrational bands of CrO_4^{2-} and $Cr_2O_7^{2-}$ anions, and the strong shoulder features (*ca.* 973 and 981 cm^{-1}) of $Cr_3O_{10}^{2-}$ anions, the pair of bands at 846 and 853 cm^{-1} {ν_{as}(Cr-O-Cr)} and at 973 and 980 cm^{-1} {ν_{as}(CrO_2 and {ν_{as}(CrO_3)}, respectively, have become clearly resolved indicative of trimeric and tetranuclear oxochromium anions [24,27-29]. However, we cannot exclude other higher polychromate species at high Cr:Sn ratios.

Another interesting feature to note is that, as the ratios of chromium loading is increased, the intensity of SnO_2 bands is reduced indicating the increased covered of the SnO_2 surface by adsorbed chromate ions.

When all these catalyst materials were calcined at 573 K, all the bands attributed to surface chromium disappear totally. The band at *ca.* 632 and 475 cm^{-1} which is assigned to SnO_2 can still be observed but at much reduced intensity. However, after calcination at 873 K, this band is absent. This phenomenon can be explained in terms of incorporation of the oxochromium species into the tin oxide lattice structure causing the SnO_2 band to become inactive. Furthermore, it should be noted that, it is difficult to take FT-Raman spectra from calcined samples of these material.

It is also interesting to point out that for the higher chromium loadings (above a loading of 0.052:1) after calcination at 1273 K, the band at 550 cm^{-1} which is assigned to the metal-oxygen vibration of distorted octahedrally coordinated chromium(III) atoms [29] in crystalline Cr_2O_3, start to appear. This Cr_2O_3 formation can also be observed from the XRD diffractogram (see above), but only after the catalyst has undergoes calcination at 1273 K. This discrepancy between Raman and XRD data for the detection of Cr_2O_3 is due to the fact that crystallites must be larger than 40 Å to be detected by XRD, whilst Raman spectroscopy has excellent sensitivity to much smaller metal oxide crystallites. Thus, both the Raman and XRD data reveal that Cr_2O_3 is formed in the material at higher calcination temperatures. The reason why the band at *ca.* 550 cm^{-1} is not observable for the sample of chromium loading below 0.052:1 even after heat treatment at 1273 K is probably due to the very low chromium loading which give rise to highly dispersed, amorphous Cr_2O_3.

Conclusions

Both physical and chemical properties of chromium(VI)-doped tin(IV) oxide catalyst materials were determined by various techniques of analysis. PCS data show that the addition of

aqueous chromium(VI) oxide causes deaggregation of the colloidal sol particulate relative to tin(IV) oxide sols, the particle size depending on the sol concentration and the chromium:tin ratio. FT-Raman spectra show that the surface adsorbed species formed on the particulate tin(IV) oxide are chromium(VI) oxyanions of the types CrO_4^{2-}, $Cr_2O_7^{2-}$ and $Cr_3O_{10}^{2-}$. However, these oxochromium species disappear on calcination at 573 K. Nitrogen adsorption data show that the most significant changes in specific surface area, pore volume and pore sizes occur at temperature >673 K, at which point the mesopores are substantially reduced. Calcination at temperatures of 873K and above, the mean pore diameter increases greatly indicating the existence of non-porous solids. Infrared spectra for the materials before calcination, exhibit intense bands due to surface hydroxyl groups and adsorbed molecular water which decreases on calcination. However, the band due to ν(SnOSn) increases on calcination due to the condensation of adjacent surface hydroxyl groups. TGA and DTA data support the infrared data as events due to dehydration and surface hydroxyl groups condensation are observed. Powder X-ray diffraction and electron microscopy analyses confirm the formation of Cr_2O_3 on calcination at 1273K.

Acknowledgements:- We thank to Malaysian Government for the award of grants IRPA Vot 72008, UPP(UTM) Vot 71051 and 71160.

REFERENCES

1. For the EC see EC Directives Dir. 88/76/EEC, December 1987, Dir. 88/436/EEC, 16 June 1988, and Dir. 89/458/EEC, 18 July 1989.
2. EC Communication COM (89) 662, 2nd February 1990.
3. P.G Harrison and P.J. Harris, U.S. Patent 4 908 192, 1990; U.S. Patent 5 051 393, 1991.
4. M.J. Fuller and M.E. Warwick, *J.Catalysis*, 1973, **29**, 441.
5. M.J. Fuller and M.E. Warwick, *J.Catalysis*, 1974, **34**, 445.
6. G.C. Bond, L.R. Molloy and M.J. Fuller, *J Chem. Soc., Chem. Commun*., 1975, 796.
7. G. Croft and M.J. Fuller, *Nature*, 1977, **269**, 585.
8. M.J. Fuller and M.E. Warwick, *J.Catalysis*, 1976, **42**, 418.
9. M.J. Fuller and M.E. Warwick, Chem. *Ind.* (London), 1976, 787.
10. F. Solymosi and J. Kiss, *J. Catalysis*, 1978, **54**, 42.

11. P.G. Harrison and W. Azelee, *J. Sol-Gel Sci. Technology*, 1994, 813.
12. X. Li, Ph.D Thesis, Brunel University, 1991.
13. S. Brunauer, L.S. Deming, W.S Deming and E. Teller, *J. Amer. Chem. Soc*. 1940, **62**, 1723.
14. S.J. Gregg and K.S.W. Sing, *Adsorption, Surface Area and Porosity, 2nd Edition*, Academic Press, London, p.249, 1982.
15. Powder Diffraction File, Inorganic Phases, International Centre for Diffraction Data, American Society of Testing Material, 1991, 1.
16. S.J. Gregg and K.S.W. Sing, *Adsorption, Surface Area and Porosity, 2nd Edition*, Academic Press, London, p.26, 1982.
17. V. Yu Gavrilov and G.A Zenkovets, *J. Catalysis*, in communication, 1994.
18. D.E. Arohmayer, G.L. Geoffrey and M.A. Vannice, *Appl. Catal*., 1983, **7**, 189.
19. A. Gavriilidis, B. Sinno and A. Varma, *J. Catalysis*, 1993, **139**, 41.
20. P.G. Harrison and A. Guest, *J. Chem. Soc., Faraday Trans. 1*, 1987, **83**, 3383.
21. H. Kriegsman, H. Hoffman and H. Geissler, *Z. Anorg. Allg. Chem*., 1965, **341**, 24.
22. P.G. Harrison, C.C. Perry, D.A. Creaser and X. Li, *Eurogel '91*, 1992, 175.
23. F. Gonzales-Vilchez and W.P. Griffith, *J. Chem. Soc., Dalton Trans*., 1972, 1417.
24. M.A. Vuurman, Ph.D Thesis, Univ. of Amsterdam, 1992.
25. G. Michel and R.Machiroux, *J. Raman Spectr*., 1983, **14**, 22.
26. G. Michel and R.Machiroux, *J. Raman Spectr*., 1986, **17**, 79.
27. F.D. Hardcastle and I.E. Wachs, *J. Mol. Catal*., 1989, **46**, 173.
28. U. Scharf, H. Schneider, A. Baiker and A. Wokaun, *J. Catal*., 1994, **145**, 464.
29. G. Michel and R. Cahay, *J. Raman Spectr*., 1986, **17**, 4.

CHAPTER 3

THE INVESTIGATION OF THE ACTIVE SITE OF Co(II)-DOPED MnO CATALYST USING X-RAY DIFFRACTION TECHNIQUE

Wan Azelee Wan Abu Bakar, Mohd Yusof Othman and Norzila Saat.

Department of Chemistry, Faculty of Science, Universiti Teknologi Malaysia, 81310 UTM Skudai, Johor Bahru, Malaysia.

ABSTRACT

Catalytic activity study of Co(II)-doped MnO catalyst sample at various loading ratios of dopant and calcination temperatures illustrate that the sample with atomic loading ratio of 0.05:1 and treated at 400^{o}C give the lowest temperature of 100% conversion of CO and C_3H_8 toxic gases. X-ray diffraction analysis reveals that the prerequisite amount of Mn^{3+} species in the form of Mn_2O_3 and in the mixture of spinnel compound of Mn_3O_4 provide the active sites for an excellent oxidation reaction of the toxic gases. Meanwhile, the evolution of Mn^{2+} species in the form of MnO tremedously deactivates the catalytic performance of the catalyst system.

ABSTRAK

Kajian aktiviti pemangkinan terhadap sampel mangkin Co(II)-dop MnO pada pelbagai nisbah muatan pendop dan pelbagai suhu pengkalsinan menunjukkan bahawa nisbah sampel 0.05:1 pada suhu pengkalsinan 400^{o}C memberikan 100% pengoksidaan lengkap CO dan C_3H_8 pada suhu terendah. Analisis XRD menunjukkan jumlah tertentu spesies Mn^{3+} dalam bentuk Mn_2O_3 dan dalam campuran sebatian spinel, Mn_3O_4, berperanan menyediakan tapak aktif bagi tindak balas pengoksidaan gas toksik secara berkesan. Sebaliknya, kewujudan spesies Mn^{2+} dalam bentuk MnO, menurunkan aktiviti pemangkinan bagi sistem mangkin tersebut.

Keywords: Catalyst, X-Ray Diffraction(XRD), Catalytic Activity

* To whom correspondence should be addressed.

INTRODUCTION

Among the major pollutants originating from automotive and industrial activities are gases such as CO, hydrocarbons and NO_x. By using catalytic converter these components can be treated to non toxic gases such as CO_2, H_2O and N_2 [1]. The current catalytic converter consists of the noble metals that are very expensive and nearly exhausted. The viable usage of non noble metal oxides as catalyst in catalytic converter has attracted researchers to explore in this area due to low price, high availability and strategic

importance. The studies of catalyst materials such as tin (IV) oxide, cerium (IV) oxide and zirconium (IV) oxide had been progressively conducted and showed a promising catalytic behaviour[2-4]. In addition, manganese oxide based catalyst also showed a good catalytic activity. Copper-manganese mixed oxides and in particular, amorphous hopcalite "$CuMn_2O_4$", are powerful oxidation catalyst. It is known that these materials can catalyze the oxidation of CO to CO_2 at 65^oC and at higher temperature 300-500^oC promoted the combustion of several organic compounds including hydrocarbons, halide and nitrogen containing compounds [5]. As such detail studies has to be carried out to investigate what's structure contribute to the enhancement towards CO and hydrocarbon oxidation in manganese based oxide catalyst system.

EXPERIMENTAL

Preparation of Sample

Catalyst was prepared by sol-gel modification method. The appropriate quantities of $Mn(NO_3)_2.6H_2O$ was stirred for 30 minutes with a minimum amount of triply distilled water (t.d.w). The specific quantities of $Co(CH_3OO)_2.6H_2O$ was dissolved in minimum amount of t.d.w. This solution was added slowly into the $Mn(NO_3)_2.6H_2O$ solution and left stirred for another 30 minutes. The resulting reddish purple solution was poured into an evaporating dish and left dry at 60^oC for 24 hours. Then the sample was calcined at 400, 600, 800 and 1000^oC in muffle furnace for 17 hours at a slow heat ramp of 10^oC/min. The calcined samples were ground into fine powder using a mortar and characterised with X-Ray Diffraction technique.

X-Ray Diffraction (XRD) Analysis

Samples were analysed by the XRD spectrometer which was performed on Philip PW 1730/10 using Cu-Kα radiation. The 2θ angular region from 10-70 ^{o} was scanned with step size 0.020 ^{o} and time per step 0.400 seconds. The XRD diffractogram pattern of the samples were interpreted using the Powder Diffraction File (PDF)[6].

RESULTS AND DISCUSSION

Catalytic Activity Study

The study shows that the sample with the atomic ratio of 0.05:1 after calcination at 400^oC illustrated an excellent catalytic activity (Table 1) towards C_3H_8 and CO oxidation with T_{100} (C_3H_8) = 280^oC and T_{100} (CO) = 90^oC. The light-off temperature, T_{Lo}, for all samples occurred around 50^oC. The additional loading of dopant into Co(II)/MnO system higher than 0.05 seems to deteriorate the reactivity of the catalyst systems. Furthermore, the pretreatment temperature of the catalyst system, higher than 400^oC has

deactivated the catalytic performance as such required higher temperature for the complete oxidation reaction to occur.

Table 1: The catalytic activity data for propane conversion over Co(II) doped MnO catalyst material.

Sample/Pretreatment Temperature (^oC)	T_{100} (C_3H_8) (^oC)	T_{100} (CO)(^oC)
Co(II)-doped MnO (0.005:1)		
300	475	250
400	330	130
600	435	200
800	455	255
1000	500	290
Co(II) doped MnO (0.05:1)		
300	470	240
400	280	90
600	420	200
800	450	250
1000	500	295
Co(II) doped MnO (0.1:1)		
300	450	245
400	340	120
600	410	220
800	460	255
1000	510	300
Co(II) doped MnO (0.5:1)		
300	420	260
400	380	130
600	410	230
800	450	270
1000	510	310
Commercial catalyst, Pt/Al_2O_3	380	200

T_{100} = temperature for complete oxidation reaction

XRD analysis

The diffractogram data obtained from the XRD analysis were tabulated in Table 2. The phase changes for Co(II)-doped MnO catalysts with an excellent catalytic activity with the ratios of 0.05:1 at various calcination temperatures were obtained and studied. The assignment of peaks were accomplished by comparing the 2θ value of materials studied with the 2θ value of phases from the Powder Diffractogram File[6].

Table 2: Peaks position (2θ) in the XRD pattern of Co(II) doped MnO (0.05:1) catalyst system.

Temperature (^{o}C)	2θ (^{o})	Assignment
400	32.33	Mn_2O_3(c)
	32.90	Mn_3O_4(t)
	36.38	Mn_3O_4(t)
	45.10	Mn_2O_3(c)
	56.12	Mn_2O_3(c)
	59.85	Mn_3O_4(t)
600	31.33	Mn_3O_4(t)
	32.33	Mn_2O_3(c)
	32.90	Mn_3O_4(t)
	36.38	Mn_3O_4(t)
	45.10	Mn_2O_3(c)
	57.98	Mn_3O_4(t)
	59.88	Mn_3O_4(t)
800	27.84	MnO(c)
	31.33	Mn_3O_4(t)
	32.90	Mn_3O_4(t)
	36.38	Mn_3O_4(t)
	57.95	Mn_3O_4(t)
	59.88	Mn_3O_4(t)
1000	27.84	MnO(c)
	31.33	Mn_3O_4(t)
	32.80	MnO(c)
	32.90	Mn_3O_4(t)
	36.38	Mn_3O_4(t)
	57.96	Mn_3O_4(t)

	59.88	Mn_3O_4(t

t: tetrahedron, c: cubic

For the Co(II)-doped MnO (0.05:1) catalyst calcined at 400°C, the observable phases were due to based material, comprises of Mn_3O_4 in tetrahedron structure and Mn_2O_3 with cubic phase. The few highest dominant peaks due to Mn_3O_4 with tetrahedron structure occurred at 2θ of value = 32.90, 36.38 and 59.85° [PDF[6] 2θ value = 32.89, 36.38, 59.90°]. Whilst the peaks for Mn_2O_3 species in cubic phase were observed at 2θ value = 32.33, 45.10 and 56.12° [PDF[6] 2θ value = 32.34, 45.14, 56.10°]. On calcination at 600°C, the peaks due to Mn_2O_3 were observed only at 2θ value = 32.33 and 45.10°. Furthermore, the intensity of these peaks are reduced denoting the decreasing of Mn_2O_3 species in Co(II)/MnO catalyst system. In contratry, the peaks arise from Mn_3O_4 become more observable and increase in intensity. Two new peaks due to Mn_3O_4 appeared at 2θ value = 31.33 and 57.98° [PDF[6] 2θ value = 31.35, 57.98°]. Further increased of temperature at 800°C revealed profound phase changes whereby the phase due to Mn_2O_3 was disappeared. In addition, a single peak which was resemblance to MnO species was detected at 2θ value = 27.84° [PDF[6] 2θ value = 27.85°], besides the dominance peaks due to Mn_3O_4 with tetrahedron in structure. Further calcination at 1000°C, reconfirm the existence of MnO phase with cubic structure in which an additional of one new peak evolved at 2θ value = 32.80 ° [PDF[6] 2θ value = 27.85, 32.80°]. The peaks due to Mn_3O_4 phase in cubic form , still dominant.

No significant peaks which can be assigned to species due to Co in the Co(II)/MnO(0.05:1) catalyst system. This is predicted since the composition of dopant is very small and undectable by XRD. However, it's presence could be recognised using XPS spectroscopy technique.

CONCLUSION

The study reveals that sample of Co(II)-doped MnO (0.05:1) calcined at 400°C showed the optimum catalytic activity towards complete oxidation of carbon monoxide and propane conversion. The structural studies using XRD for this sample shows that prerequisite existence mixture of Mn_3O_4 (tetrahedron) and Mn_2O_3 (cubic) species in Co(II)/MnO catalyst system are necessary in order to provide an optimum active site for the oxidation reaction.

ACKNOWLEDGEMENTS

We thank the Research and Development Unit of UTM, (Vot no. 71051 and 71160), Ministry of Science and Environment, Malaysia (IRPA Vot no. 72008) and UTM Scholarship to support NS study.

REFERENCES

1. Y.J. Mergler, A.Van Aaslt, J.Van Delft and B.E.Nieuwenhugs(1996), *J. of Catal*, **161**, 310-318.
2. W.A.W.A. Bakar, P.G.Harrison and N.A.Buang(1997), "Investigation of Oxidation States and Catalytic Activity of Cu(II) dan Cr(VI)-doped ZrO_2 Environmental Catalysts" , Proceeding of Malaysian Chemical Congress'97.
3. W.A.W.A.Bakar(1995), "*Non-noble Metal Environmental Catalysts: Synthesis, Characterisation dan Catalytic Activity"*, P.*h*.D Thesis, University of Nottingham, United Kingdom.
4. Nor Aziah Buang(2000), 'Zirconia Based Catalysts for Environmental Emission Control: Synthesis, Characterisation and Catalytic Activity", Ph.D Thesis, Universiti Teknologi Malaysia.
5. P.Porta, G.Moretti, M.Musicanti and A. Nardella (1991), "Characterization of Copper-Manganese Mixed Oxide", *Catalysis Today*, **9**, 211-218.
6. Power Diffraction File(1991), Inorganic Phases, International Centre for Diffraction Data, American Society of Testing Material.

CHAPTER 4

Catalytic and Structural Studies of Co(II)-Doped MnO Catalysts For Air Pollution Control

Norazila Saat, Wan Azelee Wan Abu Bakar and Mohd.Yusuf Othman*
Department of Chemistry, Faculty of Science
Universiti Teknologi Malaysia, Locked Bag 791
80990 Johor Bahru, Johor, Malaysia

ABSTRACT

Investigation on catalytic activity of Co(III)-doped MnO catalyst at various ratios and temperatures were carried out. The testing of these samples calcined at 400 ^{o}C gave better results compared to those calcined at 300 and 600 ^{o}C. The present of water , hydroxyl and other surface species were the factors that contribute to the low catalytic property of the sample. Gas adsorption analysis for all samples illustrated the isotherm obtained are of type III with hysteresis loop suggesting the present of mixture porosity of macropore and mesopore. XRD analysis revealed the formation of cobalt oxide phase after calcination at 600 ^{o}C whereby deactivated the catalytic activity of the catalysts.

Keywords: TGA/DTG, XRD, Gas Adsorption, Catalytic Activity
* To whom correspondence should be addressed.

INTRODUCTION

Among the major pollutants originating from automotive exhaust gases are CO, hydrocarbons and NO_x. By using a three way catalyst converter (TWC) these components can be treated to non toxic substances such as CO_2, H_2O and N_2. The current TWC consists of the noble metals catalyst that are very expensive and nearly exhausted. The viable usage of non noble metal oxides as catalytic converter has attracted researchers to explore in this area due to low cost, low availability and strategic importance. The catalytic converter usually consists of the transition metals whereby they are noted for their redox behaviour and in most cases their ability to exist in more than one stable oxidation state. The studies of catalysts such as tin (IV) oxide, cerium (IV) oxide and zirconium (IV) oxide had been progressively conducted and showed a promising catalytic behaviour. Furthermore manganese oxide based catalyst also showed a good catalytic activity. Copper-manganese mixed oxides and in particular, amorphous hopcalite, "$CuMn_2O_4$" , are powerful oxidation catalyst. It is known that these materials can catalyze the oxidation of CO to CO_2 at 65 ^{o}C and at higher temperature 300-500 ^{o}C promoted the combustion of several organic compounds including hydrocarbons, halide and nitrogen containing compounds [1]. Manganese oxides such as Mn_2O_3, Mn_3O_4 and MnO_2 can decomposed N_2O but Mn_2O_3 is better for catalytic NO decomposition [2]. As such detail studies has to be conducted to investigate what's contributr to the enhancement towards CO, hydrocarbon oxidation and Nox reduction

in manganese based oxide catalyst system. In this paper the discussion was limited to metal oxide catalysts which consist of Co(II) oxide doped MnO as based material to elucidate their structural and catalytic activity properties.

EXPERIMENTAL

Preparation of Sample

Catalysts were prepared by impregnation method. The appropriate quantities of $Mn(NO_3)_2.6H_2O$ was stirred for 30 minutes with a minimum amount of triply distilled water (t.d.w). The specific quantities of $Co(CH_3OO)_2.6H_2O$ was dissolved in minimum amount of t.d.w. This solution was added slowly into the $Mn(NO_3)_2.6H_2O$ solution and left stirred for another 30 minutes. The resulting reddish purple solution was poured into an evaporating dish and left dry at 60 ^oC for 24 hours. Then the samples were calcined at 300, 400, 600, 800 and 1000 ^oC in muffle furnace for 17 hours at a slow heat ramp of 10 ^oC/min. The calcined samples were ground into fine powder using a mortar and characterised with thermogravimetric/differential thermogravimetric, nitrogen gas adsorption and X-Ray Diffraction analytical techniques.

Thermogravimetric/Differential Thermogravimetric Analysis (TGA/DTG)

The mass loss of samples during heat treatment was monitored with a Mettler JCII Processor. During the analysis, the temperature was scanned from room temperature up to 1000 ^oC at a rate of 20 ^oC/min.

Gas Adsorption Analysis

The specific surface area and porosity measurements were carried out on a micromeritic ASAP 2010 instrument using the N_2 gas adsorption technique. Samples were vacuumed at 120 ^oC to eliminate all the gases and moistures.

X-Ray Diffraction (XRD) Analysis

Samples were analysed by the XRD spectrometer which was performed on Philip PW 1730/10 using Cu-Kα radiation. The 2θ angular region from 10-70 ^{o} was scanned. The XRD diffractogram pattern of the samples were interpreted using the Powder Diffraction File (PDF)[3].

Catalytic Activity Studies

The catalytic studies were perfomed using a fixed bed microreactor. The sample (0.5 g) was packed in a pyrex glass tube and located in the reactor furnace. Sample was activated by in-situ heat treating in the microreactor furnace at 300 ^oC for 2 hours under a flow of air (21 % O_2 + 79 % N_2). The sample was allowed to cool to room temperature under the flow of air. Propane gas was flowed to observe the conversion of propane to CO_2 and H_2O and CO gas was flowed to observe the conversion of CO to CO_2 . A stretching mode of propane, CO and CO_2 were monitored by FTIR at regions of 3040-2840, 2244-2044 and 2379-2259 cm^{-1} respectively. The samples were tested with both 3 % of propane (3 % C_3H_8, 20.32 % O_2 and 76.48 % N_2) and 3 % CO (3 % CO, 20.37 % O_2 and 76.63 % N_2) under the stoichiometri condition with a flow rate of 97 and 100 mL/min respectively. The results of conversion

of propane and CO were compared with the commercial catalysts, Pt/Al_2O_3 and $CuMn_2O_4$ (hopcalite) with 100 % conversion, $T_{100}(C_3H_8)$= 380 °C and $T_{100}(C_3H_8)$=420 °C and $T_{100}(CO)$= 200 °C and $T_{100}(CO)$=65 °C respectively.

RESULTS AND DISCUSSION

Catalytic Activity Study

Both samples with atomic ratio of 0.05:1 and 0.5:1 after calcination at 400 °C showed a good catalytic activity compared to 300 and 600 °C (Table 1, Figure1-4). The Co(II)-doped MnO (0.05:1) catalyst system calcined at 300 and 600 °C both gave 100 % conversion of propane, T_{100}= 470 and 420 °C with both light-off temperature, T_{Lo} >100 °C. Meanwhile calcination at 400 °C, $T_{100}(C_3H_8)$= 280 °C showed an excellent catalytic activity compared to both commercial catalysts with T_{Lo} < 100 °C (Figure 1). Further increasing of dopant to 0.5 and calcined at temperature 300 and 400 °C, gave T_{Lo} ~ 100 °C with T_{100}= 420 and 380 °C respectively. Thereby sample were calcined at 400 °C gave a better catalytic activity compared to commercial catalysts, but on the other hand, at temperature of 600 °C obtained the reduction of catalytic activity was observed even though the T_{Lo} occur at much lower temperature (Figure 2).

Meanwhile for the oxidation catalytic of CO, the Co(II)-doped MnO (0.05:1) catalyst system calcined at 300 and 600 °C both gave T_{100}= 240 and 200 °C with both light-off temperature, T_{Lo} >100 °C. The calcination at 400 °C gave a much better catalytic activity compared to commercial catalyst, Pt/Al_2O_3 with T_{100}= 90 °C and the T_{Lo} occur at room temperature (Figure 3). Further increasing of dopant to 0.5, decreased the catalytic activity whereby the deactivation took place in all calcination temperatures. The calcination at 400 °C gave T_{100}= 130 °C with T_{Lo} at room temperature. Calcined samples at 300 and 600 °C gave $T_{100}(CO)$= 260 and 200 °C respectively with both light-off temperature, T_{Lo} > 100 °C.

Table 1: The catalyctic activity data for propane conversion over Co(II) doped MnO catalyst material.

Sample	**T_{100} (C_3H_8) / °C**	**T_{100} (CO) / °C**
Commercial catalysts		
Pt/Al_2O_3	380	200
$CuMn_2O_4$(hopcalite)	420	65
Co(II) doped MnO (0.05:1)		
300 °C	470	240
400 °C	280	90
600 °C	420	200
Co(II) doped MnO (0.5:1)		
300 °C	420	260
400 °C	380	130
600 °C	420	200

TGA/DTG ANALYSIS

Figure 5 and 6 show the thermograms of Co(II)-doped MnO which indicate a remarkable mass loss during the heat treatment up to 1000 ^{o}C. The thermogram of Co(II)-doped MnO (0.05:1) show a mass loss of ca. 14.3 % at 177-273 ^{o}C, 2.0 % at 500-540 ^{o}C and 1.8 % at 773-818 ^{o}C (Figure 5). A sharp mass loss in range of 177-273 ^{o}C refers to surface molecular water from the materials. At 500-540 ^{o}C mass loss due to the surface hydroxyl condensation process and the decomposition of residual nitrates from based materials. Then mass loss at 773-818 ^{o}C is due to completion of the surface hydroxyl condensation process. For 0.5 loading of Co(II), mass loss ca. 5.5 % occurred at 204-277 ^{o}C (Figure 6). This may be due to combination of surface hydroxyl condensation and the completion of dehydration processes. Furthermore, the mass loss at >477 ^{o}C is assigned to the interaction between Mn and Co. Meanwhile, the mass loss at 327-627 ^{o}C corresponds to the formation and the growth of crystalline phase of the materials[4]. The whole deduction was accomplished based on Cu(II)-doped ZrO_2 (0.3:1) material[6] which showed almost similar features of thermogram.

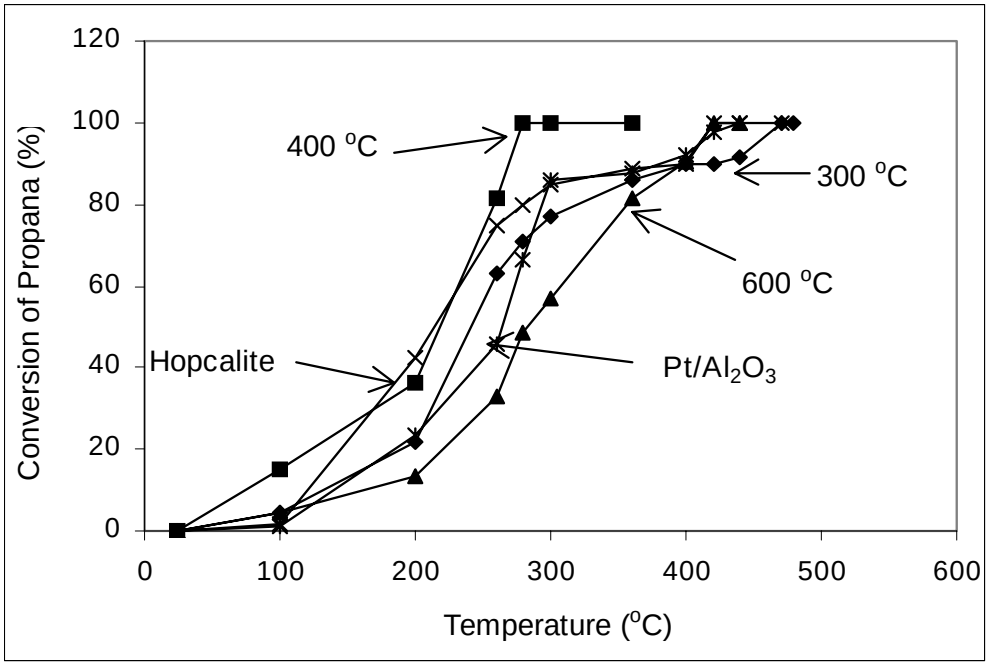

Figure 1: Conversion of propane by Co(II)-doped MnO (0.05:1) at various temperatures

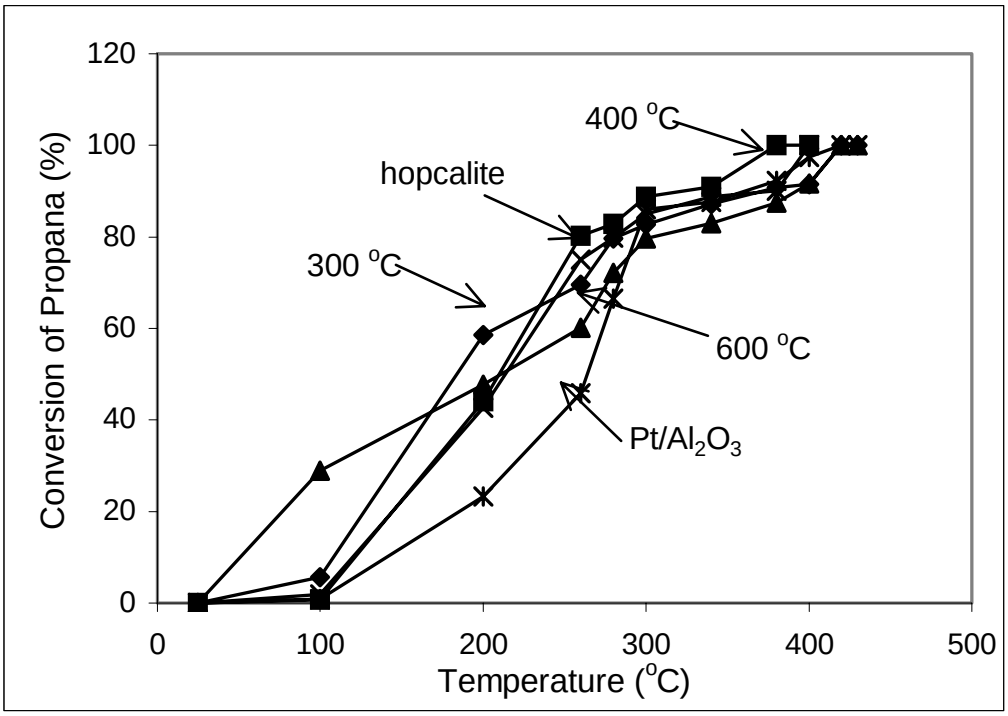

Figure 2 : Conversion of propane by Co(II)-doped MnO (0.5:1) at various temperatures

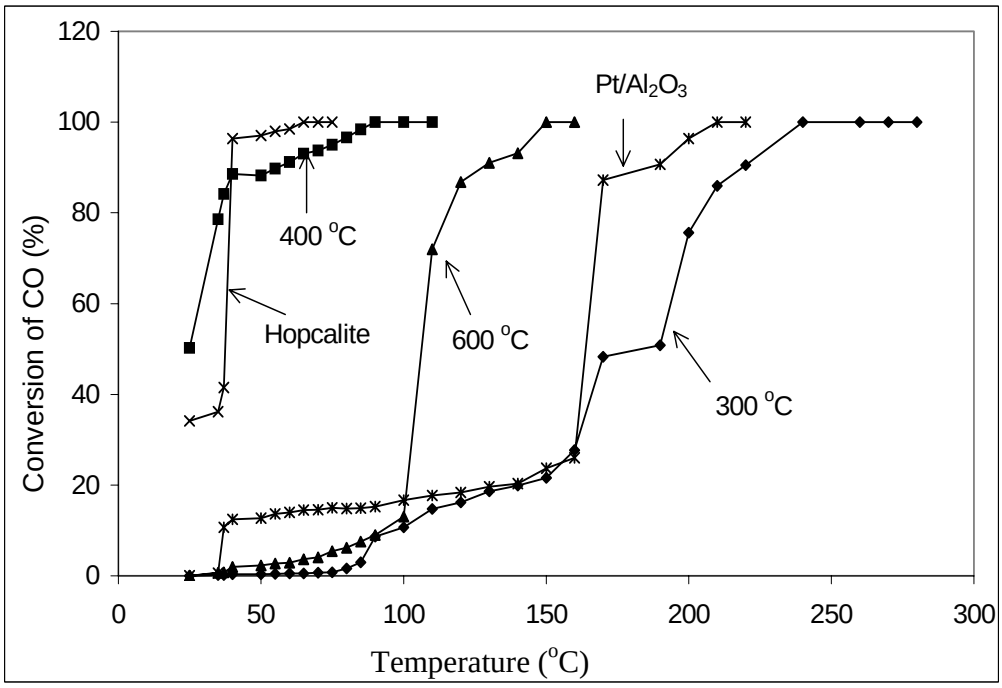

Figure 3: Conversion of CO by Co(II)-doped MnO (0.05:1) at various temperatures

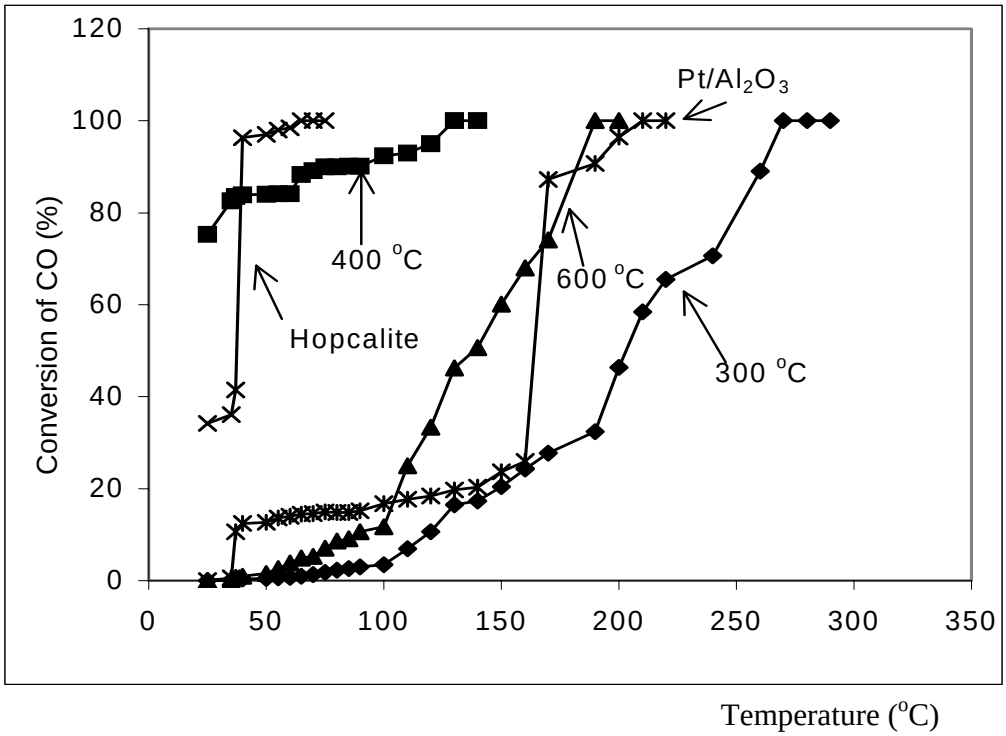

Figure 4: Conversion of CO by Co(II)-doped MnO (0.5:1) at various temperatures

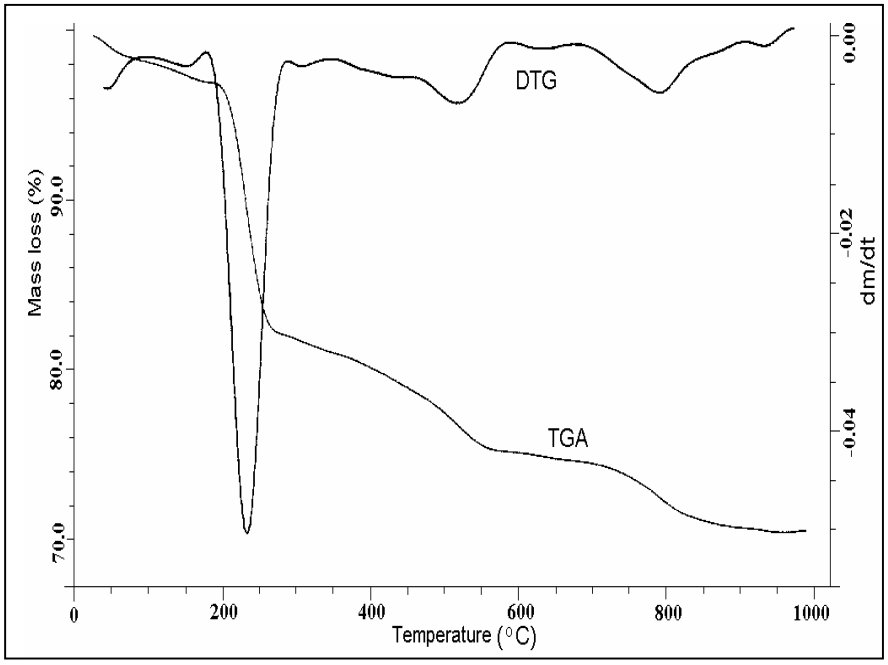

Figure 5: TGA and DTG thermogram of Co(II)-doped MnO (0.05:1) at temperature of 60 °C

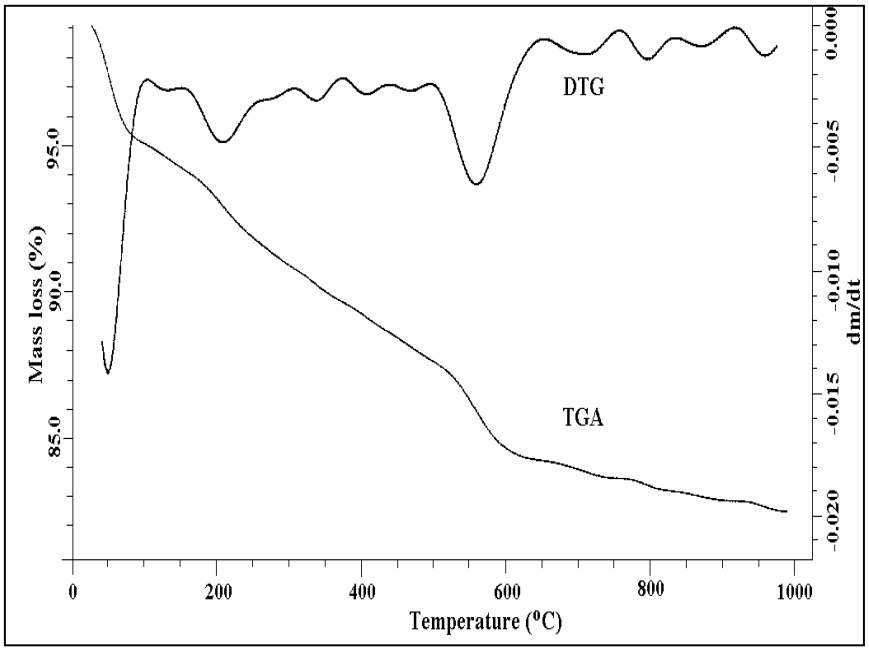

Figure 6: TGA and DTG thermogram of Co(II)-doped MnO (0.5:1) at temperature of 60 °C

XRD ANALYSIS

The diffractogram data obtained from the XRD analysis were tabulated in Table 2 and 3. The phase changes for Cu(II) doped MnO catalysts with ratios 0.05:1 and 0.5:1 at various calcination temperatures were obtained by comparing the 2θ value of materials studied with the 2θ value of phases from the Powder Diffractogram File.

For the Co(II) doped MnO (0.05:1) catalyst calcined at 400 ^{o}C, the phase was due to based materials, MnO_2 with tetragonal structure at 2θ value = 24.00, 37.38, and 56.76 ^{o} or at d value = 3.70, 2.40 and 1.62 Å [PDF[3] d value = 3.71, 2.41 and 1.63 Å]. A cubic structure formed at 600 ^{o}C was due to $MnCo_2O_4$ and Mn_2O_3. The peaks of Mn_2O_3 were observed at 2θ value = 33.21, 36.09 and 63.65 ^{o} or at d value = 2.69, 2.48 and 1.46 Å [PDF[3] d value = 2.67, 2.42 and 1.57 Å] and the peaks of $MnCo_2O_4$ were obtained at at 2θ value = 30.63, 35.55 and 57.98 ^{o} or at d value = 2.91, 2.62 and 1.58 Å [PDF[3] d value = 2.95, 2.62 and 1.60 Å]. Further increased of temperature at 800 ^{o}C revealed no profound phase changes for both metals oxide except an additional of 2 peaks due to $MnCo_2O_4$ occurred at 2θ value = 38.46 and 57.95 ^{o} or at d value = 2.33 and 1.59 Å [PDF[3] d value = 2.32 and 1.60 Å]. The calcination at 1000 ^{o}C showed the existence of MnO phase with cubic structure at 2θ value = 30.62, 32.81 and 36.08 ^{o} or at d value = 2.91, 2.73 and 2.49 Å [PDF[3] d value = 3.01, 2.69 and 2.43 Å] besides the peaks due to $MnCo_2O_4$ phase in cubic form (Table 2).

For the Co(II) doped MnO (0.5:1) catalyst, phase changes occured at 600 ^{o}C whereby the peaks were identified as MnO with orthorhombic structure at 2θ value = 33.18, 36.33 and 60.90 ^{o} or at d value = 2.69, 2.45 and 1.58 Å [PDF[3] d value = 2.64, 2.40 and 1.60 Å]. Meanwhile, for the peaks at 2θ value = 29.52, 48.05 and 65.50 ^{o} or at d value = 3.02, 1.89 and 1.42 Å was assigned to Co_3O_4 phase [PDF[3] d value = 2.95, 1.87 and 1.43 Å]. Further increased of temperatures at 800 ^{o}C, new phase was observed at 2θ value = 33.13, 36.60 and 60.89 ^{o} or at d value = 2.70, 2.45 and 1.52 Å due to Mn_2O_3 phase with orthorhombic structure [PDF[3] d value = 2.64, 2.44 and 1.55 Å] beside the peaks due to Co_3O_4 phase. A significant change of phases was observed after calcination temperature of 1000 ^{o}C due to cubic phase of CoO at 2θ value = 29.52, 39.33 and 69.27 ^{o} or at d value = 3.02, 2.28 and 1.35 Å [PDF[3] d value = 2.99, 2.25 and 1.37 Å] and orthorhombic phase of MnO_2 at 2θ value = 33.18, 36.33 and 39.08 ^{o} or at d value = 2.99, 2.25 and 2.30 Å [PDF[3] d value = 2.65, 2.45 and 2.34 Å](Table 3).

In principle, XRD analysis give an information of phase changes and structure transformation of the sample. Furthermore at high calcination temperature, the diffractograms pattern of each materials showed narrow peaks with higher intensity which indicate the formation of crystalline properties in the materials[5]. The catalytic activity reduced when the cobalt oxide peaks were observed in the diffractogram. This phenomenon was probably due to the incorporation of cobalt oxide in the bulk lattice structure of MnO and this reduced the efficiency of gas adsorption . Consequently, the active site will reduce and caused the deactivation of catalytic activity. The Cu(II)-doped SnO_2 and Cr(VI)-doped SnO_2 catalysts[5] showed a same result which exhibited the deactivation of activity when the formation of CuO and Cr_2O_3 were clearly observed in XRD diffractogram. The EPR and ESEEM analyses revealed the incorporation of CuO atom in SnO_2 lattice [6].

Table 2: Peaks position (2θ) in the XRD pattern of Co(II) doped MnO (0.05:1) catalyst system.

Temperature / ^{o}C	2θ	Assignment
400	24.00	MnO_2(t)
	37.38	MnO_2(t)
	56.72	MnO_2(t)
600	30.63	$MnCo_2O_4$(c)
	33.21	Mn_2O_3(c)
	35.55	$MnCo_2O_4$(c)
	36.09	Mn_2O_3(c)
	57.98	$MnCo_2O_4$(c)
	63.63	Mn_2O_3(c)
800	30.67	$MnCo_2O_4$(c)
	33.15	Mn_2O_3(c)
	36.15	Mn_2O_3(c)
	38.46	$MnCo_2O_4$(c)
	57.95	$MnCo_2O_4$(c)
	63.70	Mn_2O_3(c)
1000	30.62	MnO(c)
	32.81	MnO(c)
	36.08	MnO(c)
	57.86	$MnCo_2O_4$(c)
	63.77	$MnCo_2O_4$(c)

t: tetragonal, o: orthorhombic, c: cubic

Table 3: Peaks position (2θ) in the XRD pattern of Co(II) doped MnO (0.5:1) catalyst system.

Temperature / ^{o}C	2θ	Assignment
600	29.52	Co_3O_4(c)
	33.18	MnO(o)
	36.33	MnO(o)
	48.05	Co_3O_4(c)
	60.90	MnO(o)
	65.50	Co_3O_4(c)
800	29.57	Co_3O_4(c)
	33.18	Mn_2O_3(o)
	36.60	Mn_2O_3(o)

	60.89	Mn_2O_3(o)
	65.43	Co_3O_4(c)
1000	29.52	CoO(c)
	38.18	MnO_2(o)
	36.63	MnO_2(o)
	39.08	MnO_2(o)
	39.33	CoO(c)
	69.27	CoO(c)

t: tetragonal, o: orthorhombic, c: cubic

GAS ADSORPTION

Assessment of Porosity

A non porous silica, TK-800 was used as a reference for the BET and α_s method. The results obtained was given in Table 4. All isotherms showed similar characteristic features of adsorption of Type III isotherm with hysteresis loop (Figure 7). This is assigned to the existence of mixture of nonporous and mesoporous properties [7]. Hysteresis loop is of Type B which indicate the presence of slit pore shaped [7-8]. Mostly the adsorption was interrupted by the present of surface molecules such as surface hydroxyl (^-OH) and nitrate (NO_3^-) from the preparation process especially at calcination temperature $\leq 300^oC$.

To support the porosity results, the α_s plots were used. All the α_s plots (Figure 8) at various temperature exhibit upward deviation from the linearity which implies the presence of mixture of macroporous and mesoporous properties in the materials. At a temperature of 400 and 600 ^oC, the isotherms showed a higher monolayer coverage uptake gradient at 0.0-0.3 relative pressure. This may suggest the increasing of microporous properties at that temperature.

Assessment of Surface Area

In this work , Co(II)-doped MnO (0.05:1) material calcined at 300 ^oC has a high specific surface area, A_{BET} = 41.135 m^2/g. After calcination at 400 and 600 ^oC, the materials showed decreasing of A_{BET} value ,12.680 and 9.957 m^2/g respectively. A pattern of the A_{BET} value for ratio (0.5:1) is different. At temperature 300 ^oC, the A_{BET} value is 39.118 m^2/g and increased to 56.875 m^2/g at 400 ^oC. However, as the temperature increase to 600 ^oC, the A_{BET} value of sample decrease drastically to 10.282 m^2/g. The increasing of A_{BET} values is probably due to the complete elimination of the surface molecules from the materials.

Although the Co(II)-doped MnO (0.05:1) material calcined at 300 ^oC has a high specific surface area, A_{BET} 39.118 m^2/g, it does not give a good catalytic activity. This may be explained due to the fact that at this temperature, not all the surface molecular water from the surface material has been eliminated. The decrease of A_{BET} value probably due to the occurrence of agglomeration process whereby the primary particle was transformed to secondary particle. This phenomenon will effect the growth of particle size. Generally, materials with high A_{BET} contributes

more active sites for catalytic activities. Therefore, in this research samples calcined at 400 ^{o}C showed the highest surface area and are suitable to be used as catalyst for carbon monoxide and hydrocarbon gas treatment.

Assessment of Pore Diameter and Pore Volume Surface Area

Table 4 show the significant changes of pore volume, V_p and pore diameter, d for Co(II)-doped MnO materials. For Co(II) doped MnO(0.05:1) material, when the calcination temperature is increased, the A_{BET} value , V_p and d also increased. Meanwhile for Co(II) doped MnO(0.5:1) materials, the A_{BET} value is directly proportional with V_p but d value is increased with the increasing of the calcination temperature.

Table 4: Data of the N_2 adsorption analysis using the BET method

(i) Co(II) doped MnO(0.05:1)

Temperature (^{o}C)	V_m (cc/g)	A_{BET} (m^2/g)	C	V_p (cc/g)	d (nm)
300	9.449	41.135	102.319	0.115	12.119
400	2.913	12.680	85.821	0.029	10.404
600	2.287	9.957	80.865	0.017	7.694

(ii) Co(II) doped MnO(0.5:1)

Temperature (^{o}C)	V_m (cc/g)	A_{BET} (m^2/g)	C	V_p (cc/g)	d (nm)
300	8.986	39.118	84.377	0.072	7.966
400	13.065	56.875	92.234	0.139	10.491
600	2.362	10.282	73.400	0.027	13.431

V_m= mono layer volume, A_{BET} = surface area, C = BET constant, V_p= pore volume, d = pore diameter

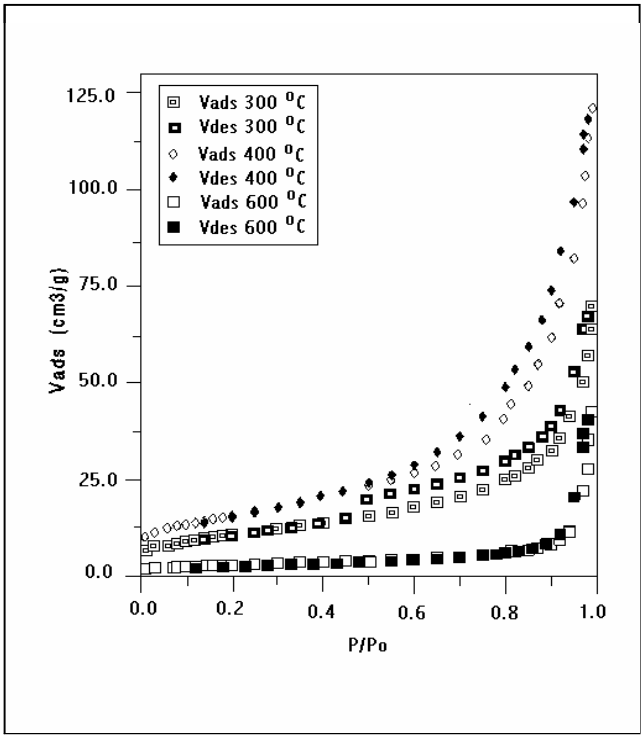

V_{ads} = volume of adsorption; V_{des} = volume of desorption

Figure 7 : Isotherms of the Co(II)-doped MnO (0.05:1) calcined at various temperatures

(a)

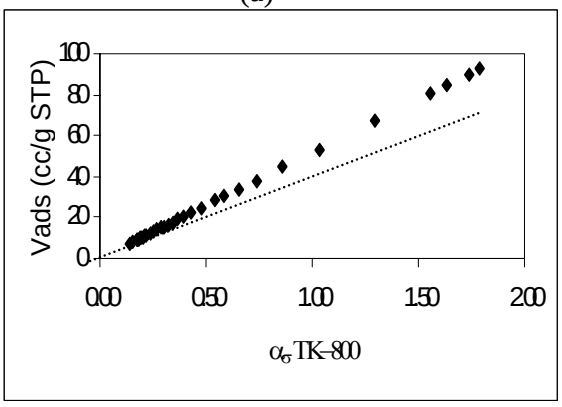

(b)

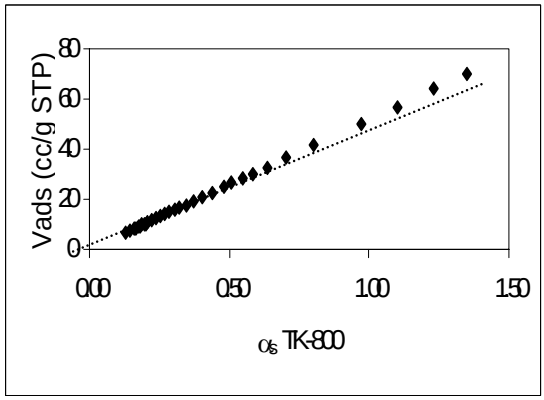

i) Co(II)-dop MnO (0.05:1) 300 °C

i) Co(II)-dop MnO (0.5:1) 300 °C

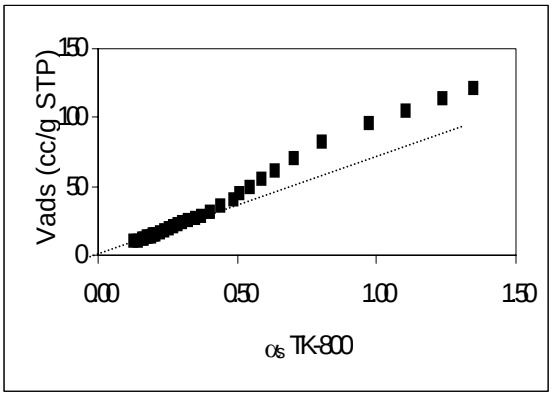

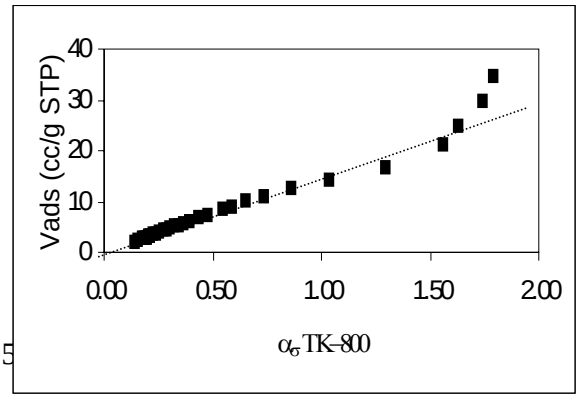

ii) Co(II)-dop MnO (0.05:1) 400 ^{o}C

iii) Co(II)-dop MnO (0.05:1) 600 ^{o}C

ii) Co(II)-dop MnO (0.5:1) 400 ^{o}C

iii) Co(II)-dop MnO (0.5:1) 600 ^{o}C **Figure 8**: α_s

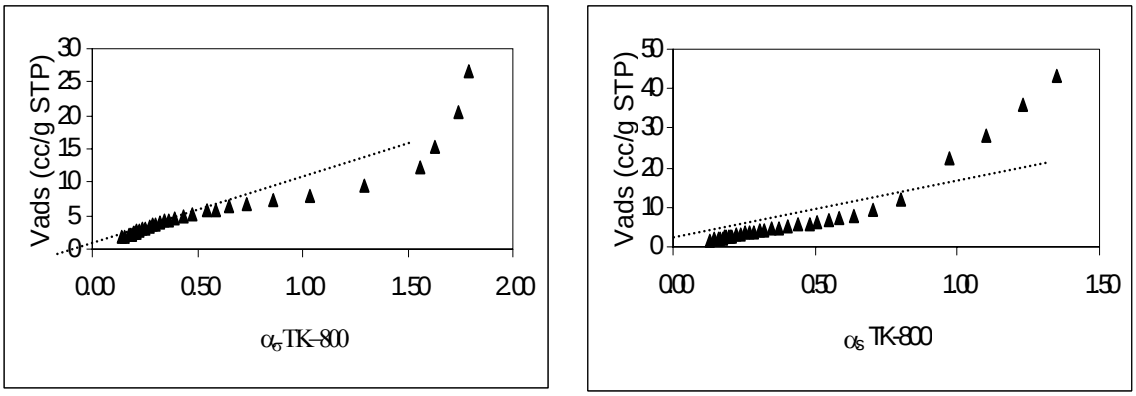

plot of the Co(II)-doped MnO catalyst system calcined at various temperatures with atomic ratio (a) 0.05:1 and (b) 0.5:1

CONCLUSION

Samples calcined at 400 ^{o}C showed the optimum catalytic activity towards hydrocarbon conversion. The structural study of the materials show that at this temperature, samples possess high specific surface area which contribute more active sites and enhance the catalytic activity. In addition, XRD analysis for the atomic ratio of 0.05:1, showed the existence of MnO_2 phase with tetragonal structure. However, with higher percentage addition of dopant, the material become more amorphous in nature as such this phenomenon will deactivate the catalytic activity of the catalyst sample eventhough there was an increased of specific surface area value. Overall, the performance of this type of catalyst with atomic ratio of 0.05:1 calcined at 400^{o}C give an excellent oxidation of hydrocarbon and showed a comparable oxidation of carbon monoxide compared to the commercial catalysts. As such this catalyst system is a potential catalyst for the treatment of polluted air due to these gases.

ACKNOWLEDGEMENTS

We thank the Research and Development Unit (UPP) (Vot no. 71051 and 71160), IRPA Vot 72008 and UTM Scholarship to support NS study.

REFERENCES

1. Y.J. Mergler, A.Van Aaslt, J.Van Delft and B.E.Nieuwenhugs, 1996, "Promoted Pt Catalysts for Automobile Pollution Control: Characterization of Pt/SiO_2 , $Pt/CoO_x/ SiO_2$ and $Pt/MnO_x/ SiO_2$ Catalysts", *J. of Catal*, **161**, 310-318.
2. W.A.W.A. Bakar, P.G.Harrison and N.A.Buang, "Investigation of Oxidation States and Catalytic Activity of Cu(II) dan Cr(VI)-doped ZrO_2 Environmental Catalysts" , Proceeding of Malaysian Chemical Congress, Nov 97.

3. Power Diffraction File, 1991, Inorganic Phases, International Centre for Diffraction Data, American Society of Testing Material.
4. G.F.Liptrort, 1975. Inorganic Chemistry Throught Experiment , Mills and Boon Ltd: London, pg. 158-159.
5. I. Baba, 1994. Kimia Tak Organik: Konsep dan Struktur, Dewan Bahasa dan Pustaka : Kuala Lumpur, pg. 228.
6. W.A.W.A.Bakar, 1995. "*Non-noble Metal Environmental Catalysts: Synthesis, Characterisation dan Catalytic Activity*", P.*h*.D Thesis, University of Nottingham, United Kingdom.
7. N.A.Buang, W.A.W. A.Bakar and P.G.Harrison, 1998, "Structural and Pore Texture Analyses on ZrO_2 and Cu (II) – Doped ZrO_2 Catalysts", *J. of Malaysian Anal. Sci*., in press.
8. P.Porta, G.Moretti, M.Musicanti and A. Nardella, 1991, "Characterization of Copper-Manganese Mixed Oxide", *Catalysis Today*, **9**, 211-218.
9. W.A.W.A.Bakar, N.A.Buang and P.G.Harrrison, "Beberapa Bahan Oksida yang Noble Berasaskan Zirkonia: Sintesis dan Pencirian", Dec 1996, Proceeding of SKOTO IV, Universiti Kebangsaan Malaysia.

CHAPTER 5

Catalytic, Surface and Structural Evaluation of Co(II)-Doped MnO Catalysts For Environmental Pollution Control

Wan Azelee Wan Abu Bakar *, Mohd.Yusuf Othman and Norazila Saat

Department of Chemistry, Faculty of Science

Universiti Teknologi Malaysia

Locked Bag 791, 80990 Johor Bahru

Johor, Malaysia

Abstract

Studies on catalytic activity of Co(II)-doped MnO catalyst at various ratios and temperatures illustrated that the samples with atomic ratio of (0.05:1) and calcined at 400^{o}C gave better conversion of toxic gases, CO and C_3H_8, compared to other atomic ratio compositions and calcination temperatures. Pore texture analysis of these samples displayed the isotherm of Type III with hysteresis loop suggesting the present of mixture porosity of macropore and mesopore. Furthermore, XRD analysis revealed that after calcination above 400^{o}C, the peak due to cobalt oxide phase was observed suggesting some incorporation of cobalt oxide particles in the lattice structure of MnO. Meanwhile, the XPS analysis conclude the existence of active surface species of Mn^{2+} and/or Mn^{3+}, and Co^{2+} and/or Co^{3+} which contribute to the enhancement of the catalytic performance of the catalyst sample.

Keywords: X-Ray Diffraction(XRD), X-Ray Photoelectron Spectroscopy(XPS), Gas Adsorption, Catalytic Activity

Introduction

Among the major pollutants originating from automotive and industrial activities are gases such as CO, hydrocarbons and NO_x. By using catalytic converter these components can be treated to non toxic gases such as CO_2, H_2O and N_2 [1]. The current catalytic converter consists of the noble metals that are very expensive and nearly exhausted. The viable usage of non noble metal oxides as catalyst in catalytic converter has attracted researchers to explore in this area due to low price, high availability and strategic importance. The catalytic converter usually consists of the transition metals whereby they are noted for their redox behaviour and in most cases their ability to exist in more than one stable oxidation state[2-4]. The studies of catalyst materials such as tin (IV) oxide, cerium (IV) oxide and zirconium (IV) oxide had been progressively conducted and showed a promising catalytic behaviour[5-6]. In addition, manganese oxide

based catalyst also showed a good catalytic activity. Copper-manganese mixed oxides and in particular, amorphous hopcalite "$CuMn_2O_4$", are powerful oxidation catalyst. It is known that these materials can catalyze the oxidation of CO to CO_2 at 65^oC and at higher temperature 300-500^oC promoted the combustion of several organic compounds including hydrocarbons, halide and nitrogen containing compounds [7]. Manganese oxides such as Mn_2O_3, Mn_3O_4 and MnO_2 can decomposed N_2O but Mn_2O_3 is better for catalytic NO decomposition [8]. As such detail studies has to be carried out to investigate what's contribute to the enhancement towards CO, hydrocarbon oxidation and NOx reduction in manganese based oxide catalyst system. In this paper the discussion was limited to metal oxide catalysts which consist of Co(II) oxide doped MnO as based material to elucidate it's surface, structure and catalytic activity properties.

Experimental

Preparation of Sample

Catalyst was prepared by impregnation method. The appropriate quantities of $Mn(NO_3)_2.6H_2O$ was stirred for 30 minutes with a minimum amount of triply distilled water (t.d.w). The specific quantities of $Co(CH_3OO)_2.6H_2O$ was dissolved in minimum amount of t.d.w. This solution was added slowly into the $Mn(NO_3)_2.6H_2O$ solution and left stirred for another 30 minutes. The resulting reddish purple solution was poured into an evaporating dish and left dry at 60^oC for 24 hours. Then the sample was calcined at 300, 400, 600, 800 and 1000^oC in muffle furnace for 17 hours at a slow heat ramp of 10^oC/min. The calcined samples were ground into fine powder using a mortar and characterised with, nitrogen gas adsorption, X-Ray Diffraction and photoelectron X-ray spectroscopy techniques.

Gas Adsorption Analysis

The specific surface area and porosity measurements were carried out on a micromeritic ASAP 2010 instrument using the N_2 gas adsorption technique. Samples were vacuumed at 120^oC to eliminate all the gases and moistures.

X-Ray Diffraction (XRD) Analysis

Samples were analysed by the XRD spectrometer which was performed on Philip PW 1730/10 using Cu-Kα radiation. The 2θ angular region from 10-70 ^{o} was scanned. The XRD diffractogram pattern of the samples were interpreted using the Powder Diffraction File (PDF)[9].

Photoelectron X-ray Specroscopy Analysis

The XPS studies were performed using a Kratos Instrument type XSAM HS surface analysis spectrometer with MgKα X-ray source(1253.6eV) and a spectrum was taken at 10mA current and 14 kV

energy source. The spectrometer was calibrated using clean Ag plate assuming binding energy of the Ag ($3d_{5/2}$) line to be at 368.25 eV. The C (1s) peak of carbon at 284.5 eV was used as a second reference. The samples were mounted onto a standard holder stub by using double sided adhesive tape. Survey scan in the range of 10 to 1100 eV were recorded at a pass energy of 160 eV with a step size of 1 eV $step^{-1}$ and a sweep time at 300 second $sweep^{-1}$. Narrow scan (20 eV pass energy, 0.1 eV $step^{-1}$ and sweep time at 59.898 second $sweep^{-1}$) was obtained for the elemental analysis regions. The pressure in the sample analysis chamber (SAC) during the scan was approximately 5 x 10^{-9} or less. All core-level spectra were deconvoluted into Gaussian component peaks using soft-ware called Vision, provided by Kratos Instruments.

Catalytic Activity Studies

The catalytic studies were perfomed using a fixed bed microreactor. The sample (0.5 g) was packed in a pyrex glass tube and located in the reactor furnace. Sample was activated by in-situ heat treating in the microreactor furnace at 300^{o}C for 2 hours under a flow of air (21 % O_2 + 79 % N_2). The sample was allowed to cool to room temperature under the flow of air. Propane gas was flowed to observe the conversion of C_3H_8 to CO_2 and H_2O, and CO gas was flowed to observe the conversion of CO to CO_2 . A stretching mode of C_3H_8, CO and CO_2 were monitored by FTIR at regions of 3040-2840, 2244-2044 and 2379-2259 cm^{-1} respectively. The samples were tested with both 3 % of C_3H_8 (3 % C_3H_8, 20.32 % O_2 and 76.48 % N_2) and 5 % CO (5 % CO, 20.00 % O_2 and 75.00 % N_2) under the rich condition with a flow rate of 97 and 100 mL/min respectively. The results of conversion of C_3H_8 and CO were compared with the commercial catalysts, Pt/Al_2O_3 and $CuMn_2O_4$ (hopcalite) with 100 % conversion, $T_{100}(C_3H_8)$= 380^{o}C and 420^{o}C and T_{100}(CO)= 200^{o}C and 65^{o}C respectively.

Results and Discussion

Catalytic Activity Study

Both samples with atomic ratio of 0.05:1 and 0.5:1 after calcination at 400^{o}C showed a good catalytic activity compared to 300 and 600^{o}C (Table 1, Figure1-4). The Co(II)-doped MnO (0.05:1) catalyst material calcined at 300 and 600^{o}C both gave 100 % conversion of propane, T_{100}= 470 and 420^{o}C with both light-off temperature, T_{Lo} >100^{o}C. Meanwhile calcination at 400^{o}C, $T_{100}(C_3H_8)$= 280^{o}C showed an excellent catalytic activity compared to both commercial catalysts with T_{Lo} < 100^{o}C (Figure 1). Further increased of dopant to 0.5 and calcined at temperature 300 and 400^{o}C, gave T_{Lo} ~ 100^{o}C with $T_{100}(C_3H_8)$= 420 and 380^{o}C respectively. Hence, samples that were calcined at 400^{o}C gave a better catalytic activity compared to commercial catalysts. Furthermore, samples calcined at 600^{o}C illustrated the deactivation in catalytic activity eventhough the T_{Lo} occur at much lower temperature (Figure 2).

Meanwhile, for the catalytic oxidation of CO, the Co(II)-doped MnO (0.05:1) catalyst material calcined at 300 and 600^{o}C both gave T_{100}= 240 and 200^{o}C with both light-off temperature, T_{Lo} >100 ^{o}C. However, sample calcined at 400^{o}C gave much better catalytic activity compared to commercial catalyst, Pt/Al_2O_3 with T_{100}= 90^{o}C and the T_{Lo} occur at room temperature (Figure 3). Further increased of dopant to 0.5, decreased the catalytic activity whereby deactivation took place in all calcination temperatures. The calcination at 400^{o}C gave T_{100}= 130^{o}C with T_{Lo} at room temperature. Calcined samples at 300 and 600^{o}C gave T_{100}(CO) = 260 and 200^{o}C respectively with both light-off temperature, T_{Lo} > 100^{o}C.

Table 1: The catalytic activity data for propane conversion over Co(II) doped MnO catalyst material.

Sample	**T_{100} (C_3H_8) (^{o}C)**	**T_{100} (CO)(^{o}C)**
Commercial catalysts		
Pt/Al_2O_3	380	200
$CuMn_2O_4$(hopcalite)	420	65
Co(II) doped MnO (0.05:1)		
300 ^{o}C	470	240
400 ^{o}C	280	90
600 ^{o}C	420	200
Co(II) doped MnO (0.5:1)		
300 ^{o}C	420	260
400 ^{o}C	380	130
600 ^{o}C	420	200

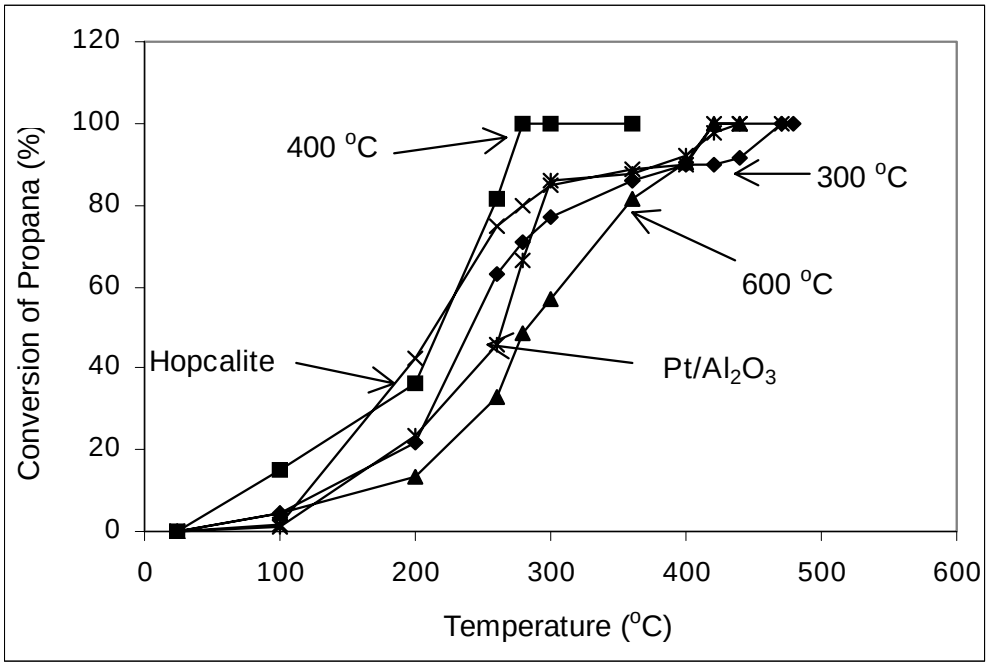

Figure 1: Conversion of propane by Co(II)-doped MnO (0.05:1) at various temperatures

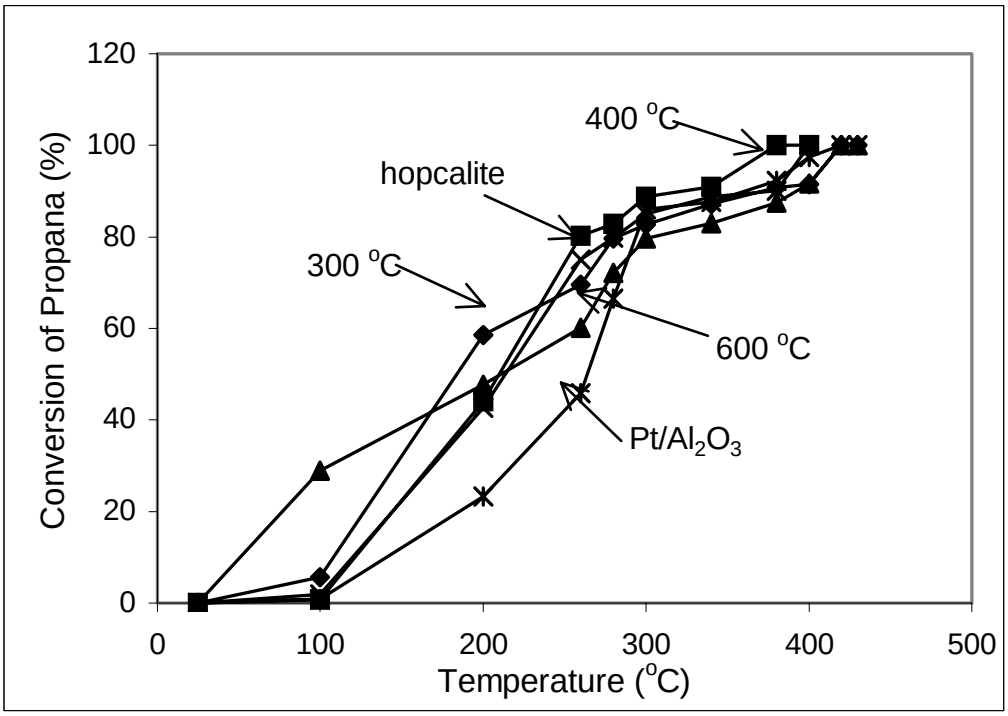

Figure 2 : Conversion of propane by Co(II)-doped MnO (0.5:1) at various temperatures

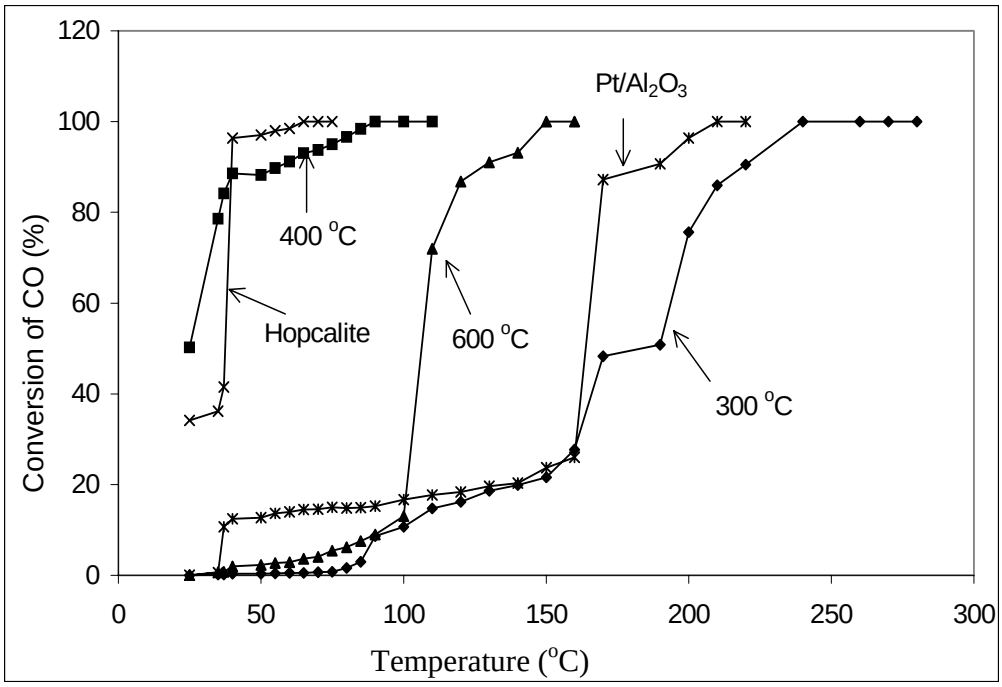

Figure 3: Conversion of CO by Co(II)-doped MnO (0.05:1) at various temperatures

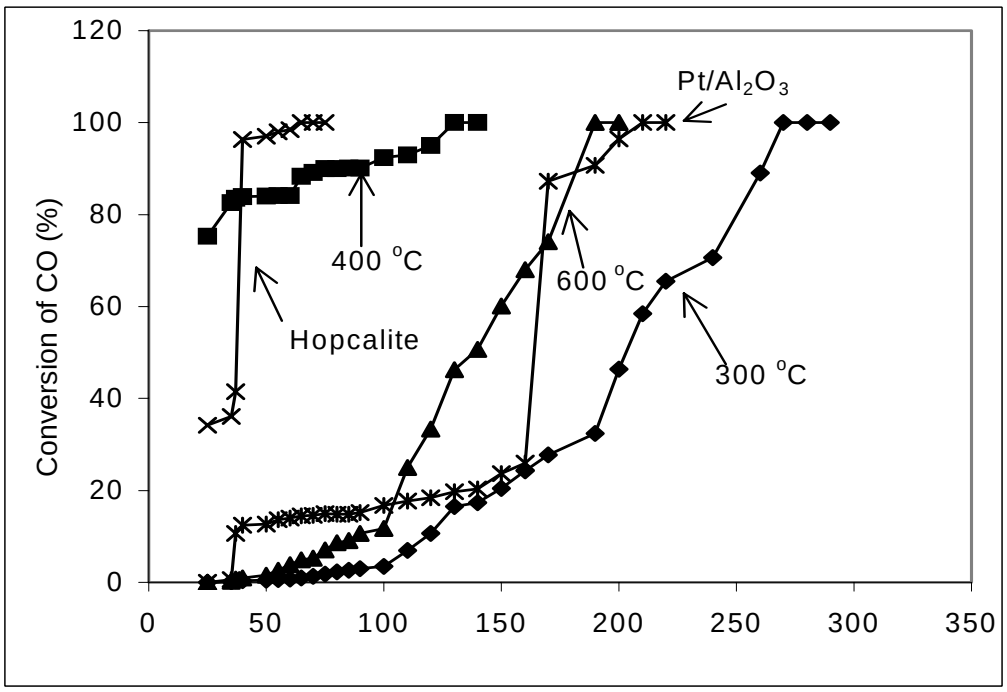

Figure 4: Conversion of CO by Co(II)-doped MnO (0.5:1) at various temperatures

XRD analysis

The diffractogram data obtained from the XRD analysis were tabulated in Table 2 and 3. The phase changes for Co(II) doped MnO catalysts with ratios 0.05:1 and 0.5:1 at various calcination temperatures were obtained by comparing the 2θ value of materials studied with the 2θ value of phases from the Powder Diffractogram File.

For the Co(II) doped MnO (0.05:1) catalyst calcined at 400^{o}C, the phase was due to based materials, MnO with orthorhombic in structure at the highest peak of 2θ value = 36.33^o or at d value = 2.45 Å [PDF[9] d value = 1.47 Å]. In addition, two other peaks at 2θ value = 36.09 and 63.65^o or at d value = 2.48 and 1.46 Å were assigned to Mn_2O_3 in cubic structure [PDF[9] d value = 2.42 and 1.46 Å]. On calcination at 600^{o}C, the peaks due to Mn_2O_3 were observed at 2θ value = 33.21 and 63.65^o or at d value = 2.69 and 1.46 Å [PDF[9] d value = 2.67 and 1.47 Å], the peaks of $MnCo_2O_4$ were obtained at at 2θ value = 30.63, 35.55 and 57.98^o or at d value = 2.91, 2.62 and 1.58 Å [PDF[9] d value = 2.95, 2.62 and 1.60 Å] and a peak due to MnO was observed at 2θ value of 36.08^o. Further increased of temperatures at 800^{o}C revealed no profound phase changes for both metals oxide except two additional peaks due to $MnCo_2O_4$ occurred at 2θ value = 38.46 and 57.95^o or at d value = 2.33 and 1.59 Å [PDF[9] d value = 2.32 and 1.60 Å]. The calcination at 1000^{o}C showed the existence of MnO phase with cubic structure at 2θ value = 30.62, 32.81 and 36.08^o or at d value = 2.91, 2.73 and 2.49 Å [PDF[9] d value = 3.01, 2.69 and 2.43 Å](Table 2), beside the peaks due to $MnCo_2O_4$ phase in cubic form.

Temperature (^{o}C)

For the Co(II)-doped MnO (0.5:1) catalyst, phase changes occurred at 600^{o}C whereby the peaks were identified as MnO with orthorhombic structure at 2θ value = 33.18, 36.33 and 60.90^o or at d value = 2.69, 2.45 and 1.58 Å [PDF[9] d value = 2.64, 2.40 and 1.60 Å]. Meanwhile, for the peaks at 2θ value = 29.52, 48.05 and 65.50^o or at d value = 3.02, 1.89 and 1.42 Å was assigned to Co_3O_4 phase [PDF[9] d value = 2.95, 1.87 and 1.43 Å]. Further increased of temperatures at 800^{o}C, new phase was observed at 2θ value = 33.13, 36.60 and 60.89^o or at d value = 2.70, 2.45 and 1.52 Å due to Mn_2O_3 phase with orthorhombic structure [PDF[9] d value = 2.64, 2.40 and 1.50 Å], beside the peaks due to Co_3O_4 phase. A profound changes of phases was observed after calcination temperature of 1000 ^{o}C due to cubic phase of CoO at 2θ value = 29.52, 39.33 and 69.27^o or at d value = 3.02, 2.28 and 1.35 Å [PDF[9] d value = 2.99, 2.25 and 1.37 Å] and orthorhombic phase of MnO_2 phase with orthorhombic structure was observed at 2θ value = 33.18, 36.33 and 39.08^o or at d value = 2.69, 2.45 and 2.30 Å [PDF[9] d value = 2.65, 2.45 and 2.34 Å](Table 3).

In principle, XRD analysis give an information of phase changes and structure transformation of the sample. Furthermore at high calcination temperature, the diffractograms pattern of each materials showed narrow peaks with higher intensity which indicate the increase of crystalline properties in the materials[10]. The catalytic activity was reduced when the cobalt oxide peaks were observed in the diffractogram. This phenomenon was probably due to the incorporation of cobalt particle in the bulk lattice structure of MnO and thus reduced the efficiency of gas adsorption on the catalyst surface. Consequently, the active site will reduce and caused the deactivation of catalytic activity. The Cu(II)-doped SnO_2 and Cr(VI)-doped SnO_2 catalysts[5] showed similar result which exhibited the deactivation of activity when the formation of CuO and Cr_2O_3 were clearly observed in XRD diffractogram. The EPR and ESEEM analyses revealed the incorporation of Cu atom in SnO_2 lattice [10].

Table 2: Peaks position (2θ) in the XRD pattern of Co(II) doped MnO (0.05:1) catalyst system.

Temperature (^oC)	2θ (^{o})	Assignment
400	36.08	MnO(o)
	36.15	Mn_2O_3(c)
	63.72	Mn_2O_3(c)
600	30.63	$MnCo_2O_4$(c)
	33.21	Mn_2O_3(c)
	35.55	$MnCo_2O_4$(c)
	36.08	MnO(o)
	57.98	$MnCo_2O_4$(c)
	63.63	Mn_2O_3(c)
800	30.67	$MnCo_2O_4$(c)
	33.15	Mn_2O_3(c)
	36.15	Mn_2O_3(c)
	38.46	$MnCo_2O_4$(c)
	57.95	$MnCo_2O_4$(c)

	63.70	Mn_2O_3(c)
1000	30.62	MnO(c)
	32.81	MnO(c)
	36.08	MnO(c)
	57.86	$MnCo_2O_4$(c)
	63.77	$MnCo_2O_4$(c)

o: orthorhombic, c: cubic

Table 3: Peaks position (2θ) in the XRD pattern of Co(II) doped MnO (0.5:1) catalyst system.

Temperature(^{o}C)	2θ(^{o})	Assignment
600	29.52	Co_3O_4(c)
	33.18	MnO(o)
	36.33	MnO(o)
	48.05	Co_3O_4(c)
	60.90	MnO(o)
	65.50	Co_3O_4(c)
800	29.57	Co_3O_4(c)
	33.18	Mn_2O_3(o)
	36.60	Mn_2O_3(o)
	60.89	Mn_2O_3(o)
	65.43	Co_3O_4(c)
1000	29.52	CoO(c)
	38.18	MnO_2(o)
	36.63	MnO_2(o)
	39.08	MnO_2(o)
	39.33	CoO(c)
	69.27	CoO(c)

o: orthorhombic, c: cubic

Gas adsorption

A non porous silica, TK-800 was used as a reference for the BET and α_s method. The results obtained was given in Table 4. All isotherms showed similar characteristic features of adsorption of Type III isotherm with hysteresis loop (Figure 7). This is assigned to the existence of mixture of macroporous and mesoporous properties in the samples [11]. Hysteresis loop is of Type B which indicate the presence of slit pore shaped [11-12]. Mostly the adsorption was interrupted by the present surface molecules such as surface hydroxyl ($^-$OH) and nitrate (NO_3^-) from the preparation process especially at calcination temperature $\leq 300^oC$.

In this work , Co(II)-doped MnO (0.05:1) material calcined at 300^oC has higher specific surface area, A_{BET} = 41.135 m^2/g. After calcination at 400 and 600^oC, the material showed decreasing of A_{BET} value,12.680 and 9.957 m^2/g respectively. A pattern of the A_{BET} value for ratio (0.5:1) is different. At temperature 300^oC, the A_{BET} value is 39.118 m^2/g and increased to 56.875 m^2/g at 400^oC. However, as the temperature increase to 600^oC, the A_{BET} value of sample decrease drastically to 10.282 m^2/g. The increasing of A_{BET} values is probably due to the complete elimination of the surface molecules from the material.

Although the Co(II)-doped MnO (0.05:1) sample after calcination at 300^oC has a high specific surface area, A_{BET} 39.118 m^2/g, it is not giving a good catalytic activity. This may be explained due to the fact that at this temperature, not all the surface molecular water from the surface material has been eliminated. The decrease of A_{BET} value probably due to the occurrence of agglomeration process whereby the primary particle was transformed to secondary particle. This phenomenon will effect the growth of particle size. Generally, materials with higher A_{BET}, contributes more active sites for catalytic activities. Therefore in this research samples calcined at 400^oC showed the highest surface area, and are suitable to be used as catalyst for carbon monoxide and hydrocarbon gas treatment.

Furthermore, Table 4 show the significant changes of pore volume, V_p and pore diameter, d for Co(II)-doped MnO catalyst system. For Co(II)-doped MnO (0.05:1) system, as the calcination temperature is increased, the A_{BET} value, V_p and d values are also increases. Meanwhile, for Co(II)-doped MnO (0.5:1) system, the A_{BET} value is directly proportional with V_p but d value is increased with the increasing of calcination temperature.

Table 4: Data of N_2 adsorption analysis using the BET method

(i) Co(II) doped MnO(0.05:1)

Temperature (^oC)	V_m (cc/g)	A_{BET} (m^2/g)	C	V_p (cc/g)	d (nm)
300	9.449	41.135	102.319	0.115	12.119
400	2.913	12.680	85.821	0.029	10.404
600	2.287	9.957	80.865	0.017	7.694

(ii) Co(II) doped MnO(0.5:1)

Temperature (^oC)	V_m (cc/g)	A_{BET} (m^2/g)	C	V_p (cc/g)	d (nm)
300	8.986	39.118	84.377	0.072	7.966
400	13.065	56.875	92.234	0.139	10.491
600	2.362	10.282	73.400	0.027	13.431

V_m= mono layer volume, A_{BET} = surface area, C = BET constant, V_p= pore volume, d = pore diameter

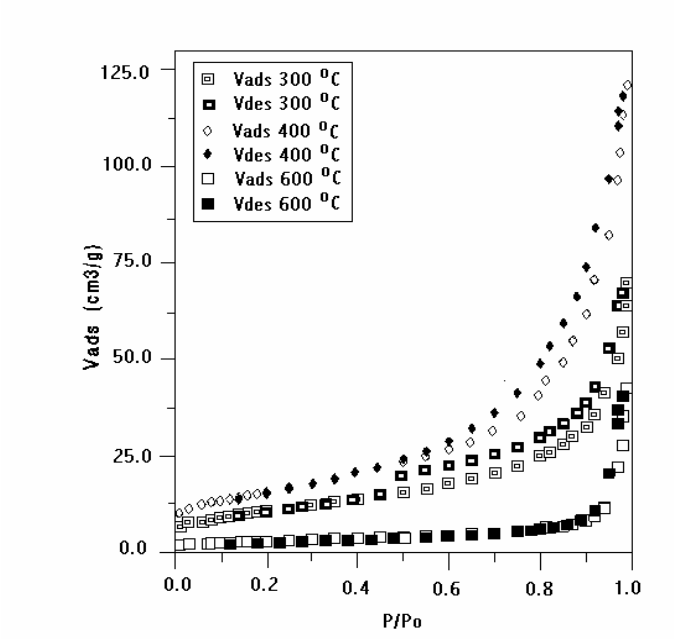

Figure 7 : Isotherms of the Co(II)-doped MnO (0.05:1) catalyst calcined at various temperatures

Photoelectron X-ray Spectroscopy (XPS) Analysis

XPS spectra of the Co(II)-doped MnO (0.05:1) catalyst is shown in Figure 8, 9 and 10, and the data is given in Table 5, 6 and 7. The deconvolution of Mn($2p_{3/2}$) region gives two different peaks. The fairly highest Mn($2p_{3/2}$) peak at binding energy of 641.4 eV, after calcination of sample at 400^{o}C, is assigned to Mn^{3+}. This result is consistent with the observation that Mn exists in the form of $Mn/Na_2WO_4/MgO$ or Mn/Na catalyst systems(13,14). Whereas, the other Mn($2p_{3/2}$) peak which occurred at 644.2 eV is assigned to Mn^{2+} which is similar to that obversed in the $Mn/Na_2WO_4/MgO$ and Mn/Cu catalyst system(13,15). When the calcination was further increased, similar pattern was displayed . However, the percentange concentration of Mn^{2+} surface species, was decreased, but the Mn^{3+} species was increased instead.

Table 5: Parameter dekonvolusi daripada spektrum XPS bagi Mn-2p dalam sampel Co(II)-dop MnO (0.05:1)

Sample Treatment (^{o}C)	**Binding Energy (eV)**		**ΔE_{SO} (eV)**	**$2p_{3/2}$ Area (counts)**	**$2p_{3/2}$ Area (%)**	**Assignment**
	$2p_{3/2}$	**$2p_{1/2}$**				
400	641.4	653.2	11.8	119	72	Mn^{3+}
	644.2	655.4	11.2	46	28	Mn^{2+}
600	640.8	652.5	11.7	277	80	Mn^{3+}
	644.1	655.2	11.1	108	20	Mn^{2+}

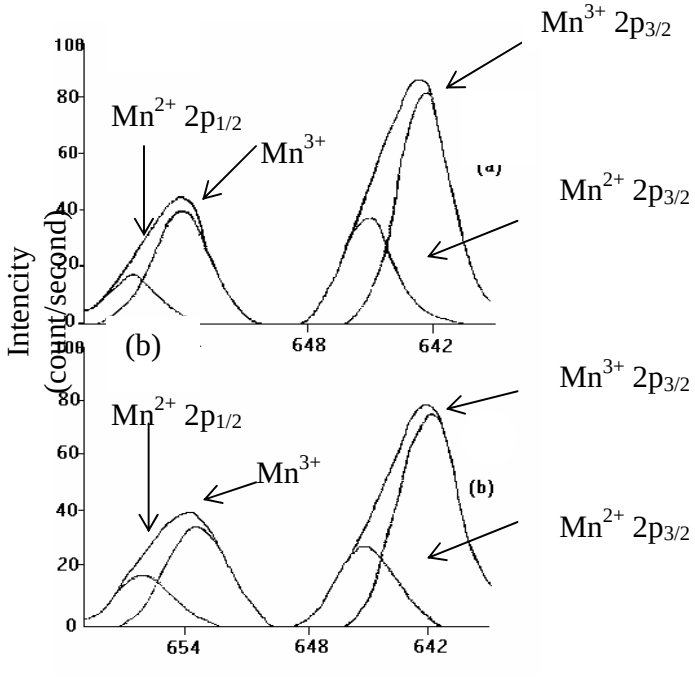

Figure 8: Parameter dekonvolusi XPS bagi Mn-2p dalam sampel Co(II)-dop MnO (0.05:1) yang dikalsinkan pada suhu (a) 400^{o}C dan (b) 600^{o}C

The XPS spectrum for sample calcined at 600^{o}C (Table 6, Figure 9), was only shown since the sample that was calcined at 400^{o}C was not resolved. The deconvolution of Co($2p_{3/2}$) and Co($2p_{1/2}$**)** regions, each gave a single peak at binding energy of 779.1 and 781.7 eV respectively. These binding energy are very much similar to that observed in the Co/SiO_2 and $Pd/Co/La/Al_2O_3$ (16,17) and was assigned to the present of Co^{2+} and Co^{3+}.

Table 9: Deconvolution Parameter from XPS spectrum for Co-2p in Co(II)-dop MnO (0.05:1) catalyst sample.

Calcination temperature (^{o}C)	**Binding energy (eV)**	**ΔE_{SO} (eV)**	**Peak area (count)**	**Peak area (%)**	**Deduction**

	$2p_{3/2}$	$2p_{1/2}$				
600	779.1	781.7	2.6	62.2	100	Co^{3+}/Co^{2+}

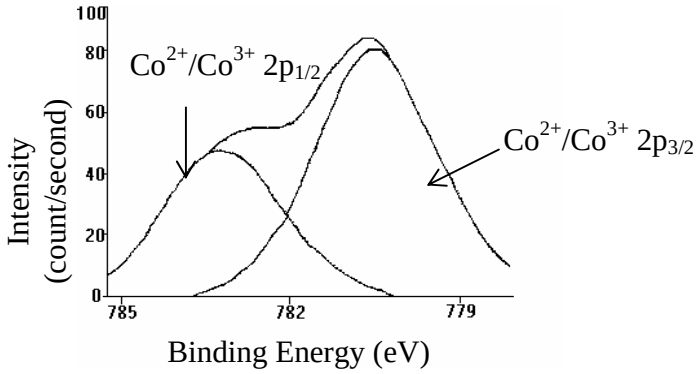

Figure 7: Deconvolution Parameter of XPS spectrum for Co-2p in Co(II)-dop MnO (0.05:1) catalyst sample calcined at 600^{o}C.

The deconvolution parameter from XPS for Co(II)-dop MnO (0.05:1) material in O(1s) region was given in Table 10 and the spectrum was displayed in Figure 8. At the calcination temperature of 400^{o}C, three peaks were observed at binding energy of 529.3, 531.4 and 533.2 eV and was assigned to Mn^{3+}-O, O-H and Co-O species respectively. These results are in consistent with those observed in Mn-K(14) or $Mn/Na_2WO_4/MgO$(13), MgO/CoO(18) and Co/SiO_2(16) materials respectively. However, after calcination at 600^{o}C, four peaks were observed at binding energy of 528.9, 530.5, 531.5 and 533.0 eV which was assgned to Mn^{2+}-O, Mn^{3+}-O, O-H and Co-O respectively. At this condition, the peaks due to two different oxidation states of Mn is well resolved.

Table 10: Deconvolution parameter from XPS spectrum for O-1s region in Co(II)-dop MnO (0.05:1) catalyst material.

Calcination temperature	**Binding energy**	**Peak area (count)**	**Peak area (%)**	**Deduction**

(°C)	(eV))			
400	529.3	136	31	Mn^{3+}-O
	531.4	182	41	O-H
	533.2	123	28	Co-O
600	528.9	105	26	Mn^{2+}-O
	530.5	113	29	Mn^{3+}-O
	531.5	93	23	O-H
	533.0	90	22	Co-O

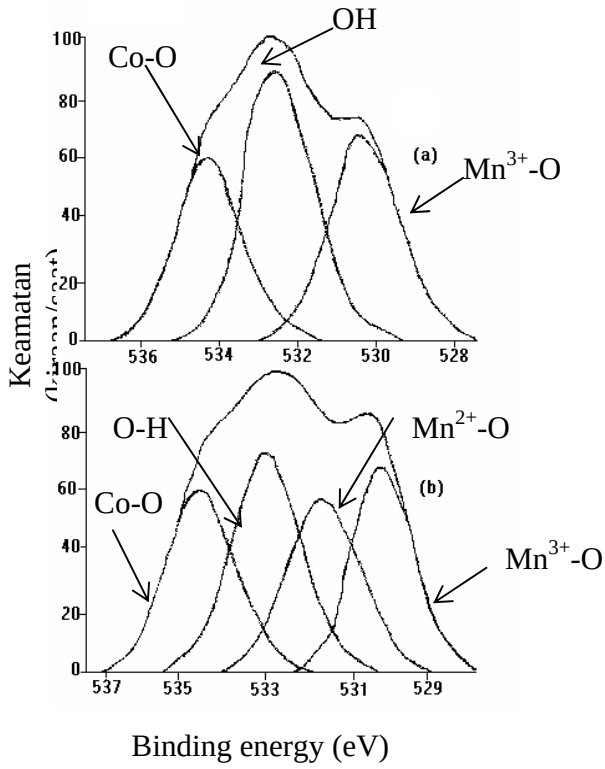

Figure 8: Deconvolution parameter from XPS spectrum for O-1s region in Co(II)-dop MnO (0.05:1) catalyst material calcined at (a) 400°C dan (b) 600°C

Conclusion

Samples calcined at 400^{o}C showed the optimum catalytic activity towards carbon monoxide and hydrocarbon conversion. The structural study of these materials show a high specific surface area which contribute more active sites and enhance the catalytic activity. In addition, XRD analysis for sample with atomic ratio of 0.05:1, showed the existence of MnO_2 phase with tetragonal structure. However, a further additional of dopant seems to transform the material into amorphous in nature, and thus deactivate the catalytic activity performance. The XPS analysis reveal that at this optimum conditions, the surface active site of the catalyst material is comprises of mixed valence cation of Mn^{3+}/Mn^{2+} and Co^{3+}/Co^{2+}.

Acknowledgements

We thank the Research and Development Unit of UTM, (UPP Vot no. 71051 and 71160), Ministry of Science and Environment, Malaysia (IRPA Vot no. 72008) and UTM Scholarship to support NS study.

References

10. Y.J. Mergler, A.Van Aaslt, J.Van Delft and B.E.Nieuwenhugs, 1996, *J. of Catal*, **161**, 310-318.
11. W.A.W.A. Bakar, P.G.Harrison and N.A.Buang, "Investigation of Oxidation States and Catalytic Activity of Cu(II) dan Cr(VI)-doped ZrO_2 Environmental Catalysts" , Proceeding of Malaysian Chemical Congress, Nov 97.
12. G.F.Liptrort, 1975, Inorganic Chemistry Throught Experiment , Mills and Boon Ltd: London, pg. 158-159.
13. I. Baba, 1994. Kimia Tak Organik: Konsep dan Struktur, Dewan Bahasa dan Pustaka : Kuala Lumpur, pg. 228.
14. W.A.W.A.Bakar, 1995, *"Non-noble Metal Environmental Catalysts: Synthesis, Characterisation dan Catalytic Activity"*, P.*h*.D Thesis, University of Nottingham, United Kingdom.
15. N.A.Buang, W.A.W. A.Bakar and P.G.Harrison, 1998, *J. of Malaysian Anal. Sci*., in press.
16. P.Porta, G.Moretti, M.Musicanti and A. Nardella, 1991, "Characterization of Copper-Manganese Mixed Oxide", *Catalysis Today*, **9**, 211-218.
17. Tatsuji Yamashita and Albert Vannice, 1996, *J. of Catalysis*, **161**, 254-262.

18. Power Diffraction File, 1991, Inorganic Phases, International Centre for Diffraction Data, American Society of Testing Material.
19. K. Matan, D. Zhao, D. Goldfard, W. Azelee, D. Daniell, and P.G. Harrison, 1995, *J.Phys. Chem*., **99**, 9966.
11. S.J.Gregg and K.W.Sing,1982. Adsorption , surface Area dan Porosity, 2nd Ed., Academic Press : London, pg. 248-249.
12. G.C.Bond, 1972. Principle of Catalysis, 1st Ed., Chemistry Society, London, pg. 60-61.
13. Kou, Y., Zhang, B., Niu, J.Z., Li, S., Wang, H., Tanaka, H. dan Yoshida, S., (1998), J.Catal, Vol. 173, 399-408.
14. Wang, D., Rosynek, M.A. dan Lunsford, J.H., (1995), J.Catal, Vol. 155, 390-402.
15. Wöllner, A. and Lange, F., (1993), App. Catal. A : General, Vol. 94, 181-203.
16. Ming, H. and Baker, B.G., (1995), App. Catal. A : General, Vol. 123, 23-36.
17. Skoglundh, M., Johansson, H., Löwendahl, L., Jansson, K., Dahl, L. dan Hirschauer, B., (1996), App. Catal. B: Environmental., Vo1. 7, 299-319.
18. Russell, S.D., Jurczyk, K. and Kob, N., (1997), App. Catal. B: Environmental., Vo1.13, 69-79.

CHAPTER 6

Catalytic, Surface and Structural Evaluation of Co(II)-Doped MnO Catalysts For Environmental Pollution Control

Wan Azelee Wan Abu Bakar *, Mohd.Yusuf Othman and Norazila Saat
Department of Chemistry, Faculty of Science
Universiti Teknologi Malaysia
Locked Bag 791, 80990 Johor Bahru
Johor, Malaysia

Keywords: X-Ray Diffraction(XRD), X-Ray Photoelectron Spectroscopy(XPS), Gas Adsorption, Catalytic Activity

Abstract

Studies on catalytic activity of Co(II)-doped MnO catalyst at various ratios and temperatures illustrated that the samples with atomic ratio of (0.05:1) and calcined at 400^{o}C gave better conversion of toxic gases, CO and C_3H_8, compared to other atomic ratio compositions and calcination temperatures. Pore texture analysis of these samples displayed the isotherm of Type III with hysteresis loop suggesting the present of mixture porosity of macropore and mesopore. Furthermore, XRD analysis revealed that after calcination above 400^{o}C, the peak due to cobalt oxide phase was observed suggesting some incorporation of cobalt oxide particles in the lattice structure of MnO. Meanwhile, the XPS analysis conclude the existence of active surface species of Mn^{2+} and/or Mn^{3+}, and Co^{2+} and/or Co^{3+} which contribute to the enhancement of the catalytic performance of the catalyst sample.

Introduction

Among the major pollutants originating from automotive and industrial activities are gases such as CO, hydrocarbons and NO_x. By using catalytic converter these components can be treated to non toxic gases such as CO_2, H_2O and N_2 [1]. The current catalytic converter consists of the noble metals that are very expensive and nearly exhausted. The viable usage of non noble metal oxides as catalyst in catalytic converter has attracted researchers to explore in this area due to low price, high availability and strategic importance. The catalytic converter usually consists of the transition metals whereby they are noted for their redox behaviour and in most cases their ability to exist in more than one stable oxidation state[2-4]. The

studies of catalyst materials such as tin (IV) oxide, cerium (IV) oxide and zirconium (IV) oxide had been progressively conducted and showed a promising catalytic behaviour[5-6]. In addition, manganese oxide based catalyst also showed a good catalytic activity. Copper-manganese mixed oxides and in particular, amorphous hopcalite "$CuMn_2O_4$", are powerful oxidation catalyst. It is known that these materials can catalyze the oxidation of CO to CO_2 at 65^oC and at higher temperature 300-500^oC promoted the combustion of several organic compounds including hydrocarbons, halide and nitrogen containing compounds [7]. Manganese oxides such as Mn_2O_3, Mn_3O_4 and MnO_2 can decomposed N_2O but Mn_2O_3 is better for catalytic NO decomposition [8]. As such detail studies has to be carried out to investigate what's contribute to the enhancement towards CO, hydrocarbon oxidation and NOx reduction in manganese based oxide catalyst system. In this paper the discussion was limited to metal oxide catalysts which consist of Co(II) oxide doped MnO as based material to elucidate it's surface, structure and catalytic activity properties.

Experimental

Preparation of Sample

Catalyst was prepared by impregnation method. The appropriate quantities of $Mn(NO_3)_2.6H_2O$ was stirred for 30 minutes with a minimum amount of triply distilled water (t.d.w). The specific quantities of $Co(CH_3OO)_2.6H_2O$ was dissolved in minimum amount of t.d.w. This solution was added slowly into the $Mn(NO_3)_2.6H_2O$ solution and left stirred for another 30 minutes. The resulting reddish purple solution was poured into an evaporating dish and left dry at 60^oC for 24 hours. Then the sample was calcined at 300, 400, 600, 800 and 1000^oC in muffle furnace for 17 hours at a slow heat ramp of 10^oC/min. The calcined samples were ground into fine powder using a mortar and characterised with, nitrogen gas adsorption, X-Ray Diffraction and photoelectron X-ray spectroscopy techniques.

Gas Adsorption Analysis

The specific surface area and porosity measurements were carried out on a micromeritic ASAP 2010 instrument using the N_2 gas adsorption technique. Samples were vacuumed at 120^oC to eliminate all the gases and moistures.

X-Ray Diffraction (XRD) Analysis

Samples were analysed by the XRD spectrometer which was performed on Philip PW 1730/10 using Cu-Kα radiation. The 2θ angular region from 10-70 ^{o} was scanned. The XRD diffractogram pattern of the samples were interpreted using the Powder Diffraction File (PDF)[9].

Photoelectron X-ray Specroscopy Analysis

The XPS studies were performed using a Kratos Instrument type XSAM HS surface analysis spectrometer with MgKα X-ray source(1253.6eV) and a spectrum was taken at 10mA current and 14 kV energy source. The spectrometer was calibrated using clean Ag plate assuming binding energy of the Ag ($3d_{5/2}$) line to be at 368.25 eV. The C (1s) peak of carbon at 284.5 eV was used as a second reference. The samples were mounted onto a standard holder stub by using double sided adhesive tape. Survey scan in the range of 10 to 1100 eV were recorded at a pass energy of 160 eV with a step size of 1 eV $step^{-1}$ and a sweep time at 300 second $sweep^{-1}$. Narrow scan (20 eV pass energy, 0.1 eV $step^{-1}$ and sweep time at 59.898 second $sweep^{-1}$) was obtained for the elemental analysis regions. The pressure in the sample analysis chamber (SAC) during the scan was approximately 5 x 10^{-9} or less. All core-level spectra were deconvoluted into Gaussian component peaks using soft-ware called Vision, provided by Kratos Instruments.

Catalytic Activity Studies

The catalytic studies were perfomed using a fixed bed microreactor. The sample (0.5 g) was packed in a pyrex glass tube and located in the reactor furnace. Sample was activated by in-situ heat treating in the microreactor furnace at 300^{o}C for 2 hours under a flow of air (21 % O_2 + 79 % N_2). The sample was allowed to cool to room temperature under the flow of air. Propane gas was flowed to observe the conversion of C_3H_8 to CO_2 and H_2O, and CO gas was flowed to observe the conversion of CO to CO_2 . A stretching mode of C_3H_8, CO and CO_2 were monitored by FTIR at regions of 3040-2840, 2244-2044 and 2379-2259 cm^{-1} respectively. The samples were tested with both 3 % of C_3H_8 (3 % C_3H_8, 20.32 % O_2 and 76.48 % N_2) and 5 % CO (5 % CO, 20.00 % O_2 and 75.00 % N_2) under the rich condition with a flow rate of 97 and 100 mL/min respectively. The results of conversion of C_3H_8 and CO were compared with the commercial catalysts, Pt/Al_2O_3 and $CuMn_2O_4$ (hopcalite) with 100 % conversion, $T_{100}(C_3H_8)$= 380^{o}C and 420^{o}C and T_{100}(CO)= 200^{o}C and 65^{o}C respectively.

Results and Discussion

Catalytic Activity Study

Both samples with atomic ratio of 0.05:1 and 0.5:1 after calcination at 400^{o}C showed a good catalytic activity compared to 300 and 600^{o}C (Table 1, Figure1-4). The Co(II)-doped MnO (0.05:1) catalyst material calcined at 300 and 600^{o}C both gave 100 % conversion of propane, T_{100}= 470 and 420^{o}C with both light-off temperature, T_{Lo} >100^{o}C. Meanwhile calcination at 400^{o}C, $T_{100}(C_3H_8)$= 280^{o}C showed an excellent catalytic activity compared to both commercial catalysts with T_{Lo} < 100^{o}C (Figure 1). Further increased of dopant to 0.5 and calcined at temperature 300 and 400^{o}C, gave T_{Lo} ~ 100^{o}C with $T_{100}(C_3H_8)$= 420 and

380^{o}C respectively. Hence, samples that were calcined at 400^{o}C gave a better catalytic activity compared to commercial catalysts. Furthermore, samples calcined at 600^{o}C illustrated the deactivation in catalytic activity eventhough the T_{Lo} occur at much lower temperature (Figure 2).

Meanwhile, for the catalytic oxidation of CO, the Co(II)-doped MnO (0.05:1) catalyst material calcined at 300 and 600^{o}C both gave T_{100}= 240 and 200^{o}C with both light-off temperature, T_{Lo} >100 ^{o}C. However, sample calcined at 400^{o}C gave much better catalytic activity compared to commercial catalyst, Pt/Al_2O_3 with T_{100}= 90^{o}C and the T_{Lo} occur at room temperature (Figure 3). Further increased of dopant to 0.5, decreased the catalytic activity whereby deactivation took place in all calcination temperatures. The calcination at 400^{o}C gave T_{100}= 130^{o}C with T_{Lo} at room temperature. Calcined samples at 300 and 600^{o}C gave T_{100}(CO) = 260 and 200^{o}C respectively with both light-off temperature, T_{Lo} > 100^{o}C.

Table 1: The catalytic activity data for propane conversion over Co(II) doped MnO catalyst material.

Sample	**T_{100} (C_3H_8) (^{o}C)**	**T_{100} (CO)(^{o}C)**
Commercial catalysts		
Pt/Al_2O_3	380	200
$CuMn_2O_4$(hopcalite)	420	65
Co(II) doped MnO (0.05:1)		
300 ^{o}C	470	240
400 ^{o}C	280	90
600 ^{o}C	420	200
Co(II) doped MnO (0.5:1)		
300 ^{o}C	420	260
400 ^{o}C	380	130
600 ^{o}C	420	200

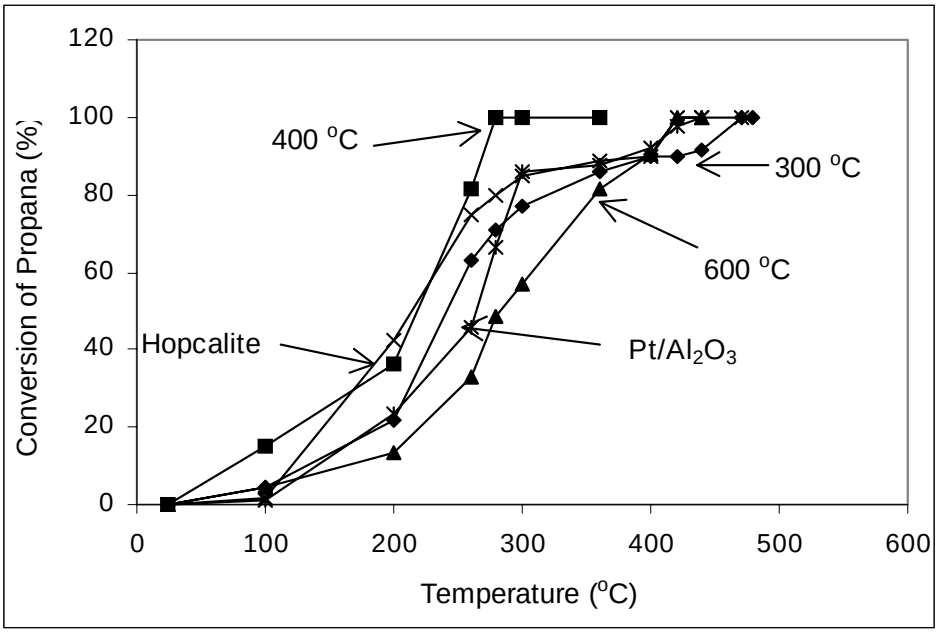

Figure 1: Conversion of propane by Co(II)-doped MnO (0.05:1) at various temperatures

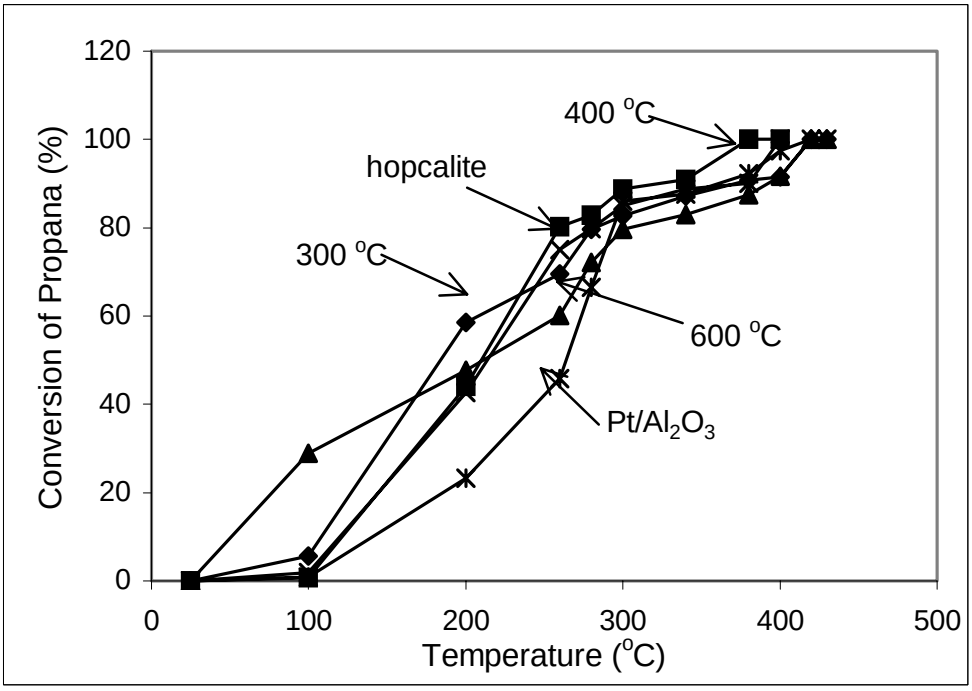

Figure 2 : Conversion of propane by Co(II)-doped MnO (0.5:1) at various temperatures

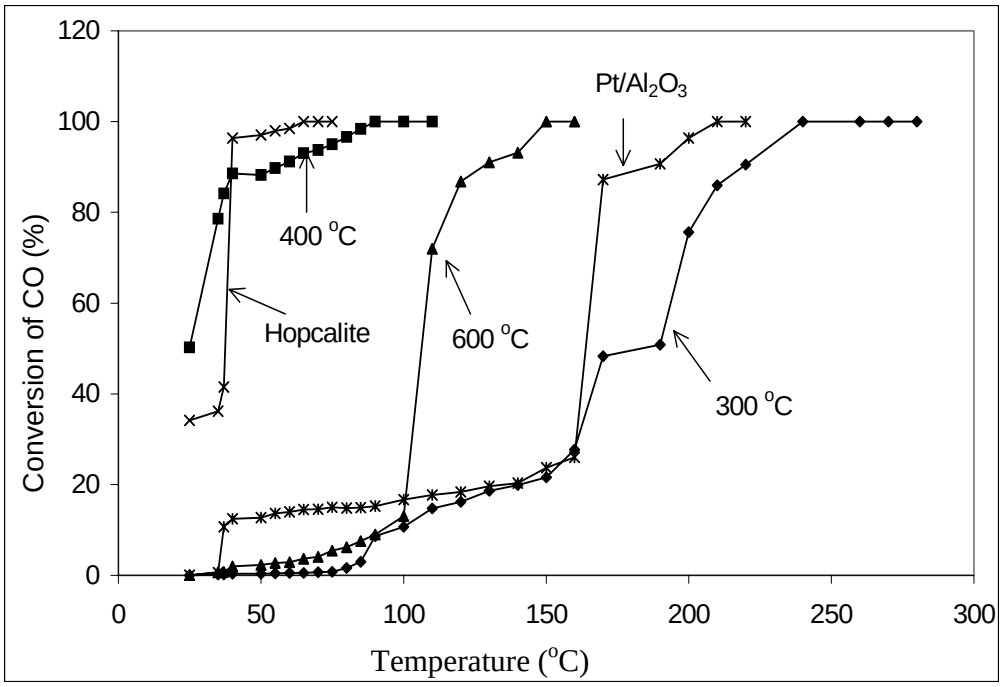

Figure 3: Conversion of CO by Co(II)-doped MnO (0.05:1) at various temperatures

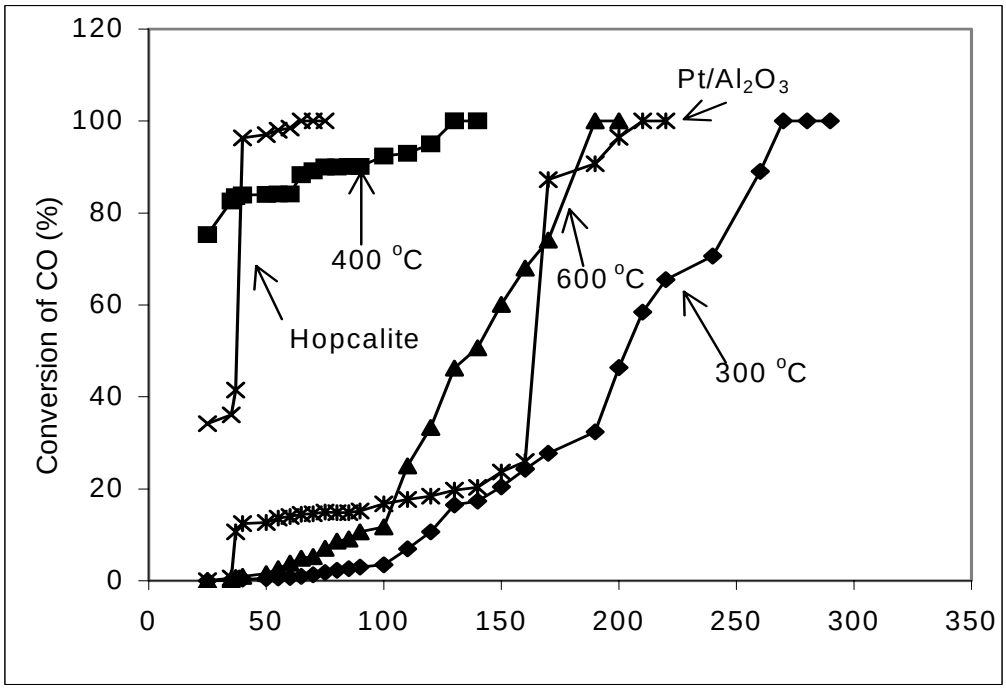

Figure 4: Conversion of CO by Co(II)-doped MnO (0.5:1) at various temperatures

XRD analysis

The diffractogram data obtained from the XRD analysis were tabulated in Table 2 and 3. The phase changes for Co(II) doped MnO catalysts with ratios 0.05:1 and 0.5:1 at various calcination temperatures were obtained by comparing the 2θ value of materials studied with the 2θ value of phases from the Powder Diffractogram File.

For the Co(II) doped MnO (0.05:1) catalyst calcined at 400^{o}C, the phase was due to based materials, MnO with orthorhombic in structure at the highest peak of 2θ value = 36.33^{o} or at d value = 2.45 Å [PDF[9] d value = 1.47 Å]. In addition, two other peaks at 2θ value = 36.09 and 63.65^{o} or at d value = 2.48 and 1.46 Å were assigned to Mn_2O_3 in cubic structure [PDF[9] d value = 2.42 and 1.46 Å]. On calcination at 600^{o}C, the peaks due to Mn_2O_3 were observed at 2θ value = 33.21 and 63.65^{o} or at d value = 2.69 and 1.46 Å [PDF[9] d value = 2.67 and 1.47 Å], the peaks of $MnCo_2O_4$ were obtained at at 2θ value = 30.63, 35.55 and 57.98^{o} or at d value = 2.91, 2.62 and 1.58 Å [PDF[9] d value = 2.95, 2.62 and 1.60 Å] and a peak due to MnO was observed at 2θ value of 36.08^{o}. Further increased of temperatures at 800^{o}C revealed no profound phase changes for both metals oxide except two additional peaks due to $MnCo_2O_4$ occurred at 2θ value = 38.46 and 57.95^{o} or at d value = 2.33 and 1.59 Å [PDF[9] d value = 2.32 and 1.60 Å]. The calcination at 1000^{o}C showed the existence of MnO phase with cubic structure at 2θ value = 30.62, 32.81 and 36.08^{o} or at d value = 2.91, 2.73 and 2.49 Å [PDF[9] d value = 3.01, 2.69 and 2.43 Å](Table 2), beside the peaks due to $MnCo_2O_4$ phase in cubic form.

For the Co(II)-doped MnO (0.5:1) catalyst, phase changes occurred at 600^{o}C whereby the peaks were identified as MnO with orthorhombic structure at 2θ value = 33.18, 36.33 and 60.90^{o} or at d value = 2.69, 2.45 and 1.58 Å [PDF[9] d value = 2.64, 2.40 and 1.60 Å]. Meanwhile, for the peaks at 2θ value = 29.52, 48.05 and 65.50^{o} or at d value = 3.02, 1.89 and 1.42 Å was assigned to Co_3O_4 phase [PDF[9] d value = 2.95, 1.87 and 1.43 Å]. Further increased of temperatures at 800^{o}C, new phase was observed at 2θ value = 33.13, 36.60 and 60.89^{o} or at d value = 2.70, 2.45 and 1.52 Å due to Mn_2O_3 phase with orthorhombic structure [PDF[9] d value = 2.64, 2.40 and 1.50 Å], beside the peaks due to Co_3O_4 phase. A profound changes of phases was observed after calcination temperature of 1000 ^{o}C due to cubic phase of CoO at 2θ value = 29.52, 39.33 and 69.27^{o} or at d value = 3.02, 2.28 and 1.35 Å [PDF[9] d value = 2.99, 2.25 and 1.37 Å] and orthorhombic phase of MnO_2 phase with orthorhombic structure was observed at 2θ value = 33.18, 36.33 and 39.08^{o} or at d value = 2.69, 2.45 and 2.30 Å [PDF[9] d value = 2.65, 2.45 and 2.34 Å](Table 3).

In principle, XRD analysis give an information of phase changes and structure transformation of the sample. Furthermore at high calcination temperature, the diffractograms pattern of each materials showed narrow peaks with higher intensity which indicate the increase of crystalline properties in the materials[10]. The catalytic activity was reduced when the cobalt oxide peaks were observed in the diffractogram. This

phenomenon was probably due to the incorporation of cobalt particle in the bulk lattice structure of MnO and thus reduced the efficiency of gas adsorption on the catalyst surface. Consequently, the active site will reduce and caused the deactivation of catalytic activity. The Cu(II)-doped SnO_2 and Cr(VI)-doped SnO_2 catalysts[5] showed similar result which exhibited the deactivation of activity when the formation of CuO and Cr_2O_3 were clearly observed in XRD diffractogram. The EPR and ESEEM analyses revealed the incorporation of Cu atom in SnO_2 lattice [10].

Table 2: Peaks position (2θ) in the XRD pattern of Co(II) doped MnO (0.05:1) catalyst system.

Temperature (^oC)	2θ (^{o})	Assignment
400	36.08	MnO(o)
	36.15	Mn_2O_3(c)
	63.72	Mn_2O_3(c)
600	30.63	$MnCo_2O_4$(c)
	33.21	Mn_2O_3(c)
	35.55	$MnCo_2O_4$(c)
	36.08	MnO(o)
	57.98	$MnCo_2O_4$(c)
	63.63	Mn_2O_3(c)
800	30.67	$MnCo_2O_4$(c)
	33.15	Mn_2O_3(c)
	36.15	Mn_2O_3(c)
	38.46	$MnCo_2O_4$(c)
	57.95	$MnCo_2O_4$(c)
	63.70	Mn_2O_3(c)
1000	30.62	MnO(c)
	32.81	MnO(c)
	36.08	MnO(c)
	57.86	$MnCo_2O_4$(c)
	63.77	$MnCo_2O_4$(c)

o: orthorhombic, c: cubic

Table 3: Peaks position (2θ) in the XRD pattern of Co(II) doped MnO (0.5:1) catalyst system.

Temperature(^{o}C)	2θ(^{o})	Assignment
600	29.52	Co_3O_4(c)
	33.18	MnO(o)
	36.33	MnO(o)
	48.05	Co_3O_4(c)
	60.90	MnO(o)
	65.50	Co_3O_4(c)
800	29.57	Co_3O_4(c)
	33.18	Mn_2O_3(o)
	36.60	Mn_2O_3(o)
	60.89	Mn_2O_3(o)
	65.43	Co_3O_4(c)
1000	29.52	CoO(c)
	38.18	MnO_2(o)
	36.63	MnO_2(o)
	39.08	MnO_2(o)
	39.33	CoO(c)
	69.27	CoO(c)

o: orthorhombic, c: cubic

Gas adsorption

A non porous silica, TK-800 was used as a reference for the BET and α_s method. The results obtained was given in Table 4. All isotherms showed similar characteristic features of adsorption of Type III isotherm with hysteresis loop (Figure 7). This is assigned to the existence of mixture of macroporous and mesoporous properties in the samples [11]. Hysteresis loop is of Type B which indicate the presence of slit pore shaped [11-12]. Mostly the adsorption was interrupted by the present surface molecules such as surface hydroxyl ($^-$OH) and nitrate (NO_3^-) from the preparation process especially at calcination temperature $\leq 300^oC$.

In this work , Co(II)-doped MnO (0.05:1) material calcined at 300^{o}C has higher specific surface area, A_{BET} = 41.135 m^2/g. After calcination at 400 and 600^{o}C, the material showed decreasing of A_{BET} value,12.680 and 9.957 m^2/g respectively. A pattern of the A_{BET} value for ratio (0.5:1) is different. At temperature 300^{o}C, the A_{BET} value is 39.118 m^2/g and increased to 56.875 m^2/g at 400^{o}C. However, as the

temperature increase to 600°C, the A_{BET} value of sample decrease drastically to 10.282 m^2/g. The increasing of A_{BET} values is probably due to the complete elimination of the surface molecules from the material.

Although the Co(II)-doped MnO (0.05:1) sample after calcination at 300°C has a high specific surface area, A_{BET} 39.118 m^2/g, it is not giving a good catalytic activity. This may be explained due to the fact that at this temperature, not all the surface molecular water from the surface material has been eliminated. The decrease of A_{BET} value probably due to the occurrence of agglomeration process whereby the primary particle was transformed to secondary particle. This phenomenon will effect the growth of particle size. Generally, materials with higher A_{BET}, contributes more active sites for catalytic activities. Therefore in this research samples calcined at 400°C showed the highest surface area, and are suitable to be used as catalyst for carbon monoxide and hydrocarbon gas treatment.

Furthermore, Table 4 show the significant changes of pore volume, V_p and pore diameter, d for Co(II)-doped MnO catalyst system. For Co(II)-doped MnO (0.05:1) system, as the calcination temperature is increased, the A_{BET} value, V_p and d values are also increases. Meanwhile, for Co(II)-doped MnO (0.5:1) system, the A_{BET} value is directly proportional with V_p but d value is increased with the increasing of calcination temperature.

Table 4: Data of N_2 adsorption analysis using the BET method

(i) Co(II) doped MnO(0.05:1)

Temperature (°C)	V_m (cc/g)	A_{BET} (m^2/g)	C	V_p (cc/g)	d (nm)
300	9.449	41.135	102.319	0.115	12.119
400	2.913	12.680	85.821	0.029	10.404
600	2.287	9.957	80.865	0.017	7.694

(ii) Co(II) doped MnO(0.5:1)

Temperature (°C)	V_m (cc/g)	A_{BET} (m^2/g)	C	V_p (cc/g)	d (nm)
300	8.986	39.118	84.377	0.072	7.966
400	13.065	56.875	92.234	0.139	10.491
600	2.362	10.282	73.400	0.027	13.431

V_m= mono layer volume, A_{BET} = surface area, C = BET constant, V_p= pore volume, d = pore diameter

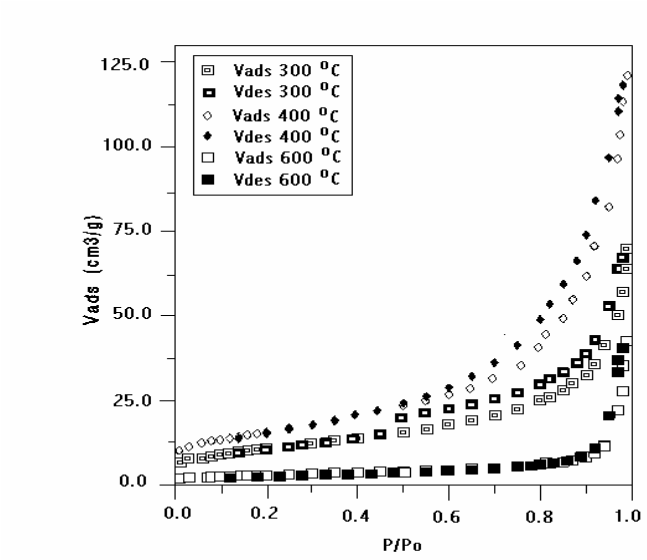

Figure 7 : Isotherms of the Co(II)-doped MnO (0.05:1) catalyst calcined at various temperatures

Photoelectron X-ray Spectroscopy (XPS) Analysis

XPS spectra of the Co(II)-doped MnO (0.05:1) catalyst is shown in Figure 8, 9 and 10, and the data is given in Table 5, 6 and 7. The deconvolution of Mn($2p_{3/2}$) region gives two different peaks. The fairly highest Mn($2p_{3/2}$) peak at binding energy of 641.4 eV, after calcination of sample at 400°C, is assigned to Mn^{3+}. This result is consistent with the observation that Mn exists in the form of Mn/Na_2WO_4/MgO or Mn/Na catalyst systems(13,14). Whereas, the other Mn($2p_{3/2}$) peak which occurred at 644.2 eV is assigned to Mn^{2+} which is similar to that obversed in the Mn/Na_2WO_4/MgO and Mn/Cu catalyst system(13,15). When the calcination was further increased, similar pattern was displayed . However, the percentange concentration of Mn^{2+} surface species, was decreased, but the Mn^{3+} species was increased instead.

Table 5: Parameter dekonvolusi daripada spektrum XPS bagi Mn-2p dalam sampel Co(II)-dop MnO (0.05:1)

Sample Treatment (°C)	**Binding Energy (eV)**		**ΔE_{SO} (eV)**	**$2p_{3/2}$ Area (counts)**	**$2p_{3/2}$ Area (%)**	**Assignment**
	$2p_{3/2}$	**$2p_{1/2}$**				
400	641.4	653.2	11.8	119	72	Mn^{3+}
	644.2	655.4	11.2	46	28	Mn^{2+}
600	640.8	652.5	11.7	277	80	Mn^{3+}
	644.1	655.2	11.1	108	20	Mn^{2+}

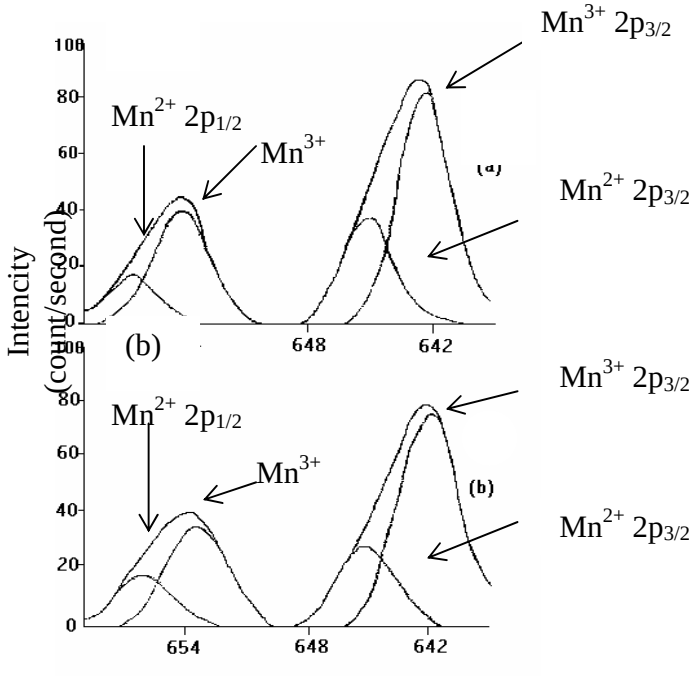

Figure 8: Parameter dekonvolusi XPS bagi Mn-2p dalam sampel Co(II)-dop MnO (0.05:1) yang dikalsinkan pada suhu (a) 400^{o}C dan (b) 600^{o}C

The XPS spectrum for sample calcined at 600^{o}C (Table 6, Figure 9), was only shown since the sample that was calcined at 400^{o}C was not resolved. The deconvolution of Co($2p_{3/2}$) and Co($2p_{1/2}$**)** regions, each gave a single peak at binding energy of 779.1 and 781.7 eV respectively. These binding energy are very much similar to that observed in the Co/SiO_2 and $Pd/Co/La/Al_2O_3$ (16,17) and was assigned to the present of Co^{2+} and Co^{3+}.

Table 9: Deconvolution Parameter from XPS spectrum for Co-2p in Co(II)-dop MnO (0.05:1) catalyst sample.

Calcination temperature (^{o}C)	**Binding energy (eV)**		**ΔE_{SO} (eV)**	**Peak area (count)**	**Peak area (%)**	**Deduction**
	$2p_{3/2}$	**$2p_{1/2}$**				
600	779.1	781.7	2.6	62.2	100	Co^{3+}/Co^{2+}

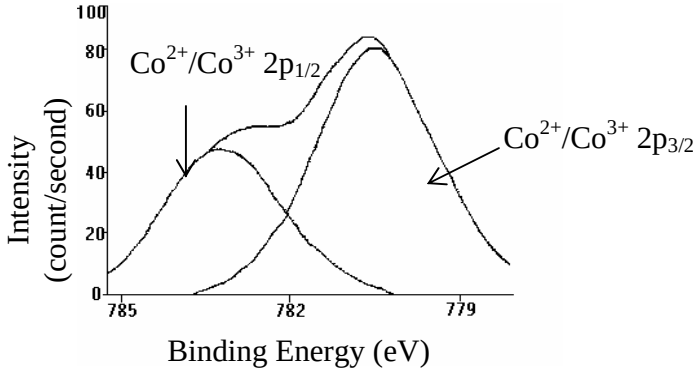

Figure 7: Deconvolution Parameter of XPS spectrum for Co-2p in Co(II)-dop MnO (0.05:1) catalyst sample calcined at 600^{o}C.

The deconvolution parameter from XPS for Co(II)-dop MnO (0.05:1) material in O(1s) region was given in Table 10 and the spectrum was displayed in Figure 8. At the calcination temperature of 400^{o}C, three peaks were observed at binding energy of 529.3, 531.4 and 533.2 eV and was assigned to Mn^{3+}-O, O-H and Co-O species respectively. These results are in consistent with those observed in Mn-K(14) or $Mn/Na_2WO_4/MgO$(13), MgO/CoO(18) and Co/SiO_2(16) materials respectively. However, after calcination at 600^{o}C, four peaks were observed at binding energy of 528.9, 530.5, 531.5 and 533.0 eV which was assgned to Mn^{2+}-O, Mn^{3+}-O, O-H and Co-O respectively. At this condition, the peaks due to two different oxidation states of Mn is well resolved.

Table 10: Deconvolution parameter from XPS spectrum for O-1s region in Co(II)-dop MnO (0.05:1) catalyst material.

Calcination temperature (^{o}C)	**Binding energy (eV))**	**Peak area (count)**	**Peak area (%)**	**Deduction**
400	529.3	136	31	Mn^{3+}-O
	531.4	182	41	O-H
	533.2	123	28	Co-O

600	528.9	105	26	Mn^{2+}-O
	530.5	113	29	Mn^{3+}-O
	531.5	93	23	O-H
	533.0	90	22	Co-O

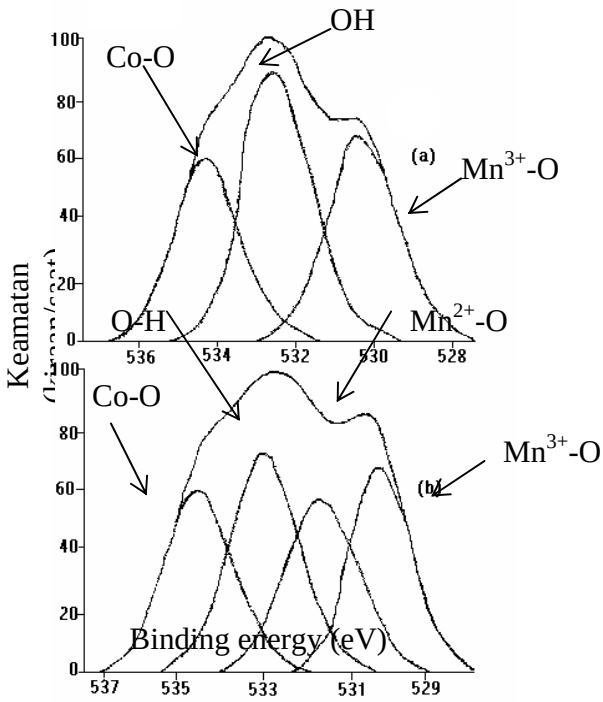

Figure 8: Deconvolution parameter from XPS spectrum for O-1s region in Co(II)-dop MnO (0.05:1) catalyst material calcined at (a) 400^{o}C dan (b) 600^{o}C

Conclusion

Samples calcined at 400^{o}C showed the optimum catalytic activity towards carbon monoxide and hydrocarbon conversion. The structural study of these materials show a high specific surface area which contribute more active sites and enhance the catalytic activity. In addition, XRD analysis for sample with atomic ratio of 0.05:1, showed the existence of MnO_2 phase with tetragonal structure. However, a further additional of dopant seems to transform the material into amorphous in nature, and thus deactivate the

catalytic activity performance. The XPS analysis reveal that at this optimum conditions, the surface active site of the catalyst material is comprises of mixed valence cation of Mn^{3+}/Mn^{2+} and Co^{3+}/Co^{2+}.

Acknowledgements

We thank the Research and Development Unit of UTM, (UPP Vot no. 71051 and 71160), Ministry of Science and Environment, Malaysia (IRPA Vot no. 72008) and UTM Scholarship to support NS study.

References

1. Y.J. Mergler, A.Van Aaslt, J.Van Delft and B.E.Nieuwenhugs, 1996, "Promoted Pt Catalysts for automotive Pollution Control: Characterisation of Pt/SiO_2, $Pt/CoO_x/SiO_2$, and $Pt/MnO_x/SiO_2$ Catalysts", *J. of Catal*, **161**, 310-318.
2. W.A.W.A. Bakar, P.G.Harrison and N.A.Buang, "Investigation of Oxidation States and Catalytic Activity of Cu(II) dan Cr(VI)-doped ZrO_2 Environmental Catalysts" , Proceeding of Malaysian Chemical Congress, Nov `97.
3. G.F.Liptrort, 1975, Inorganic Chemistry Throught Experiment , Mills and Boon Ltd: London, pg. 158-159.
4. I. Baba, 1994. Kimia Tak Organik: Konsep dan Struktur, Dewan Bahasa dan Pustaka : Kuala Lumpur, pg. 228.
5. W.A.W.A.Bakar, 1995, *"Non-noble Metal Environmental Catalysts: Synthesis, Characterisation dan Catalytic Activity"*, P.*h*.D Thesis, University of Nottingham, United Kingdom.
6. N.A.Buang, W.A.W. A.Bakar and P.G.Harrison, 1998, Investigation of Oxidation States of Cu(II) and Cr(VI)-doped ZrO_2 by X-ray Photoelectron Spectroscopy Technique.
   J. of Malaysian Anal. Sci., in communication.
7. P.Porta, G.Moretti, M.Musicanti and A. Nardella, 1991, "Characterization of Copper-Manganese Mixed Oxide", *Catalysis Today*, **9**, 211-218.
8. Tatsuji Yamashita and Albert Vannice, 1996, "N2O Decomposition over Manganese Oxides", *J. of Catalysis*, **161**, 254-262.
9. Power Diffraction File, 1991, Inorganic Phases, International Centre for Diffraction Data, American Society of Testing Material.
10. K. Matan, D. Zhao, D. Goldfard, W. Azelee, D. Daniell, and P.G. Harrison, 1995, " Characterisation of Cu^{2+} Sites in Cu/SnO^2 Catalysts by Electron Spin Echo Envelope Modulation Spectroscopy", *J.Phys. Chem*., **99**, 9966.

11. S.J.Gregg and K.W.Sing, 1982. “Adsorption , surface Area dan Porosity”, 2nd Ed., Academic Press : London, pg. 248-249.
12. G.C.Bond, 1972. “Principle of Catalysis”, 1st Ed., Chemistry Society, London, pg. 60-61.
13. Kou, Y., Zhang, B., Niu, J.Z., Li, S., Wang, H., Tanaka, H. dan Yoshida, S., 1998, “ Amorphous Features of Working Catalysts: XAFS and XPS Characterisation of $Mn/Na_2WO_4/SiO_2$ as Used for the Oxidative Coupling of Methane”, J.Catal, Vol. 173, 399-408.
14. Wang, D., Rosynek, M.A. dan Lunsford, J.H., 1995, “ Oxidative Coupling of Methane Over-Supported Sodium-Manganese Catalysts”, J.Catal, Vol. 155, 390-402.
15. Wöllner, A., Lange, F., Schmelz, H., and Knozinger, H., 1993, “ Characterisation of Mixed Copper-Manganese Oxides Supported on Titania Catalysts for Selective Oxidation of Ammonia”, App. Catal. A : General, Vol. 94, 181-203.
16. Ming, H. and Baker, B.G., 1995, “Characterisation of Cobalt Fischer-Tropsch Catalyst, I. Unpromoted Cobalt-Silica Gel Catalysts”, App. Catal. A : General, Vol. 123, 23-36.
17. Skoglundh, M., Johansson, H., Löwendahl, L., Jansson, K., Dahl, L. dan Hirschauer, B., 1996, “ Cobalt-Promoted Palladium as a Three-way Catalyst”, App. Catal. B: Environmental., Vo1. 7, 299-319.
18. Russell, S.D., Jurczyk, K. and Kob, N., 1997, “ Catalyzed Decomposition of N_2O on Metal Oxide Supports”, App. Catal. B: Environmental., Vo1.13, 69-79.

CHAPTER 7

Combustion of methane on CeO_2–ZrO_2 based catalysts

Wan Azelee Wan Abu Bakar *, Nor Aziah Buang and Mohd Tahir Ahmad
Department of Chemistry, Faculty of Science
Universiti Teknologi Malaysia
Locked Bag 791, 80990 Johor Bahru
Johor, Malaysia

Abstract

CeO_2–ZrO_2 solid solutions have been prepared by precipitation of the corresponding hydroxides. They were calcined and aged at various temperatures and characterised by X-ray diffraction measurements, BET and TPR measurements as well as by their activity in methane combustion. The $Ce_{0.67}Zr_{0.33}O_2$ solid exhibited the best thermal stability, the highest oxygen mobility and the best catalytic activity after ageing at 1000°C. It has been used to support active phases like platinum and manganese oxide. The fresh $Pt/Ce_{0.67}Zr_{0.33}O_2$ catalyst was much more active than the corresponding Pt/Al_2O_3 solid although a deactivation on stream was observed in the 200–500°C temperature range. Nevertheless, the promoting effect of the $Ce_{0.67}Zr_{0.33}$ support disappeared after ageing at 1000°C. In the case of MnO_x supported onto the $Ce_{0.67}Zr_{0.33}O_2$ solid solution the activity of the fresh solid is similar to that of the MnO_x/Al_2O_3 catalyst. After ageing at 1000°C, the solid solution is decomposed, the BET area dramatically decreased and the catalytic properties almost disappeared. As far as temperature applications exceeding 1000°C are concerned, the CeO_2–ZrO_2 solid solutions are not suitable supports for the catalytic combustion of methane.

1. Introduction

Catalytic combustion of methane and other hydrocarbons is a promising new technology for the production of energy without the formation of pollutants like nitrogen oxides [1,2]. For applications in gas turbines and boilers there is an urgent need for the development of new and thermostable catalysts for the combustion of natural gas. A new family of catalysts based on barium hexa-aluminates has recently received considerable attention for application in gas turbines [3–6].

In the case of three-way automotive catalysts, CeO_2 was widely used and its main function was to act as an oxygen storage component. Nevertheless its thermal stability seems to be not sufficient for temperatures exceeding 1000°C. Several attempts have been performed for the stabilisation of ceria against thermal sintering. Zr appears to be the best additive to increase the resistance of ceria to sintering [7–9]. In addition, the introduction of zirconia into ceria leads to the formation of solid solutions which exhibited to an improvement in the oxygen storage capacity as well as the oxygen mobility [10].

Because of their thermal stability as well as their oxygen mobility CeO_2–ZrO_2 solid solutions appear as promising candidates to be used as support (or active phases) in the catalytic combustion of hydrocarbons. Only a limited number of papers have been concerned by this objective [11–13].

In this paper, the stability of CeO_2–ZrO_2 solid solutions having various compositions is investigated, physicochemical characterisations were also performed at various stages of ageing. In a second step a solid solution was used as support for a noble metal (Pt) and for a transition metal oxide (MnO_x). The catalytic properties of such catalysts have been measured in fresh and aged states in relation with the physicochemical properties of the catalytic material.

2. Experimental

2.1. Synthesis of the solid solutions

The CeO_2–ZrO_2 mixed oxides have been prepared by coprecipitation with ammonia of an aqueous solution containing the corresponding nitrates $Ce(NO_3)_3$, $6H_2O$ and $ZrO(NO_3)_2$, $7H_2O$ according to the procedure used by Leitenburg et al. [11]. Pure ceria and zirconia have also been also prepared as reference supports using the same process. For this purpose an aqueous solution containing the Ce and Zr salts (0.2 M) was prepared and added dropwise to a large excess of ammonia in aqueous solution. The obtained hydroxides were washed and dried at 100_C for 12 h.

The mixture of the corresponding hydroxides was then calcined under flowing air for 6 h at 500, 700 and 900°C. The solids calcined at 700°C were called “fresh samples”. A simulation for the ageing of a combustion catalyst was performed by treating the “fresh” solid solutions under oxygen (5 vol.%)Cwater (10 vol.%) in nitrogen for 24 h at 1000°C and in some cases at

1200°C. Such a treatment is expected to appreciate the thermal stability of the various solid solutions and to determine the best support for high temperature applications. The solids treated at 1000°C under O_2CH_2O were called “aged samples”.

2.2. Elaboration of the catalysts

Pt supported catalyst. The selected solid solution, previously calcined at 700°C under air, was impregnated by an aqueous solution of the Pt precursor free of chloride ions in order to have a Pt content close to 2 wt.%. The $Pt(NH_3)_4(NO_3)_2$ complex was chosen as Pt precursor. Metallic platinum was formed in two steps (i) decomposition of the ammino complex by slow heating under oxygen at 400°C, (ii) reduction under flowing hydrogen at 300°C. Chemical analysis gave a platinum content of 1.6 wt.%. The “fresh catalyst” was obtained after hydrogen reduction at 300 _C whereas the “aged catalyst” was formed by ageing the fresh one under $N_2CO_2CH_2O$ at 1000_C for 24 h.

Mn supported catalyst. The same solid solution was also used for supporting Mn oxide. Mn impregnation was carried out by incipient wetness method using a solution of $Mn(NO_3)_2$, $4H_2O$. After an overnight drying at 100°C, manganese oxide was formed by calcination under air at 500°C for 6 h. The Mn content deduced from chemical analysis is equal to 7.05 wt.%. A calcination under air at 500°C led to the fresh catalyst, the treatment of the fresh sample under the ageing mixture at 1000°C for 24 h led to the “aged catalyst”.

2.3. Catalytic activity measurements

The activity of fresh and aged solid solutions and catalysts for methane combustion was measured on 500 mg of sample in a microreactor. Prior to any catalytic activity measurement, the samples were treated as follows:

1. the supports as well as the Mn supported catalyst were calcined under flowing oxygen at 400°C for 1 h
2. the Pt supported catalyst was reduced under hydrogen at 300°C for 1 h.

The samples were then cooled under nitrogen to 250–350°C and the feed of reactants was admitted onto the catalysts. It consists of 1 vol.% CH_4, 4 vol.% O_2 diluted in nitrogen with a flow rate of 6.4 l h^{-1}, the GHSV is close to 20 000 h^{-1}. The activity is measured for 3 h at a given temperature, the reaction temperature was increased by steps of 50°C.

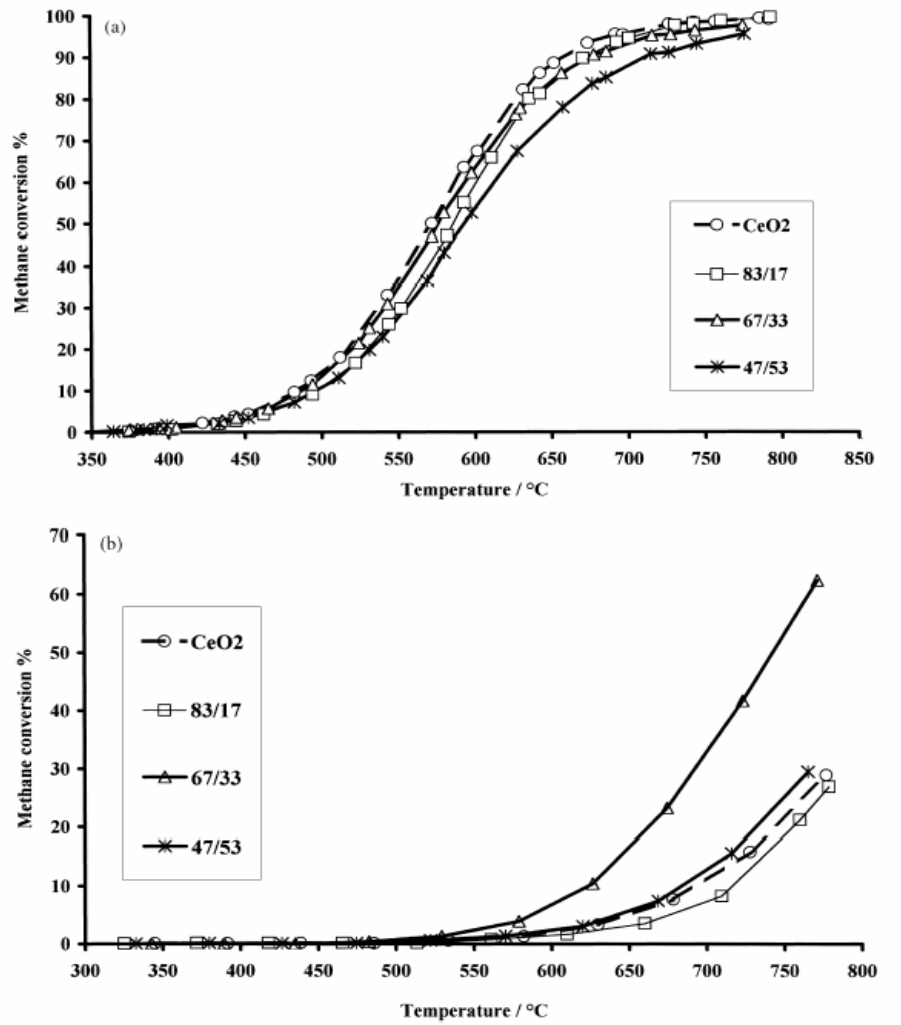

Fig. 1. Catalytic activity in the complete oxidation of methane over CeO_2 and the three CeO_2–ZrO_2 solid solutions: (a) fresh samples, calcination under air at 700°C, and (b) aged samples, calcination at 1000°C under O_2CH_2O in nitrogen.

3. Results and discussion

3.1. CeO_2–ZrO_2 solid solutions

Ceria, zirconia and three solid solutions have been prepared with the procedure described in the experimental part [11]. According to the chemical analysis, the solid solutions have the following compositions $Ce_{0:83}Zr_{0:17}O_2$ (called 83/17), $Ce_{0:67}Zr_{0:33}O_2$ (called 67/33) and $Ce_{0:47}Zr_{0:53}O_2$ (called 47/53).

The catalytic activity of the ceria as well as that of the CeO_2–ZrO_2 solid solutions was measured in the fresh and aged states. The results are shown in Fig. 1a and b. Fresh samples exhibit a non-negligible catalytic activity with a temperature of half conversion (T_{50}) varying from 572°C for CeO_2 to 593°C for the 47/73 sample. As previously observed for the catalytic oxidation of isobutane (10), the introduction of Zr_{4C} ions in the CeO_2 lattice does not markedly affect the catalytic activity. Ageing at 1000_C considerably decreased the catalytic activity, the T_{50} temperatures largely exceed 700°C.

In conclusion, the $Ce_{0:67}Zr_{0:33}O_2$ solid solution was chosen for supporting active phases in CH_4 combustion like metallic platinum and manganese oxides. This support was selected because of its specific properties after ageing at 1000°C: relatively high BET area, preservation of oxygen mobility and own catalytic properties in methane combustion.

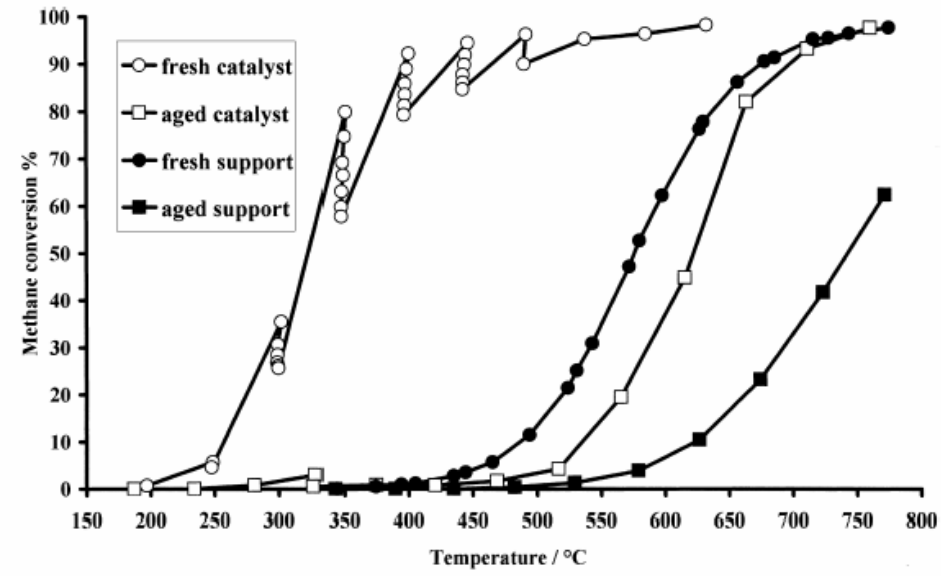

Fig. 2. Conversion of CH_4 into CO_2 as a function of the temperature for the $Pt/Ce_{0:67}Zr_{0:33}O_2$ catalyst as well as for the $Ce_{0:67}Zr_{0:33}O_2$ in fresh and aged states.

3.2. $Pt/Ce_{0:67}Zr_{0:33}O_2$ catalyst

The catalytic activity of the $Pt/Ce_{0:67}Zr_{0:33}O_2$ catalyst is given in Fig. 2 for the fresh and the aged states, for comparison purpose the activities of the support in the fresh and the aged states are also included. The activity of the fresh sample is strongly enhanced in comparison with the support alone, the T_{50} decreased from 576 to 335°C after Pt deposition. This catalyst is even more active than the corresponding one us- ing Al_2O_3 as support (T_{50}=470°C) [27] whereas its activity is comparable to that of a Pd/Al_2O_3 catalyst (T_{50}=320°C) [28,30]. Fig. 3 compares the activity of Pt/Al_2O_3 and $Pt/Ce_{0:67}Zr_{0:33}O_2$ catalysts as a function of the temperature. As far as the fresh states are concerned, it is quite clear that the solid solution leads
to an improvement of the catalytic activity. In accordance with our TPR results, the mobility of surface oxygen species of the support is enhanced by the presence of Pt particles leading to a large improvement of the catalytic performances.

In the 300–450°C range, the conversion decreases with the time on stream at a given temperature. This behaviour is illustrated by Fig. 4 in which the conversion of CH_4 into CO_2 at 350°C was plotted as a function of the reaction time. After a reaction time of 12 h a loss of conversion from 80 to 40% was observed. The activity was fully regenerated by treating the deactivated sample under hydrogen at 300°C for 1 h (Fig. 4). On the contrary, the deactivated catalyst did not recover its activity by treatment under nitrogen or oxygen at 350 or 500°C (Fig. 4). Such a behaviour is typical for Pt support on a CeO_2–ZrO_2 solid solution, the deactivation involved probably actives sites of the support. Different causes of deactivation may be considered:

- poisoning by water and/or CO_2, such a inhibiting effect of CO_2 and/or H_2O would be suppressed by a treatment at temperature high enough to decompose surface carbonates or to condense hydroxyl groups. Such an hypothesis was ruled out since a treatment under nitrogen at 500°C does not modify the deactivation whereas CO_3^{2-} and OH groups are eliminated.
- a sintering of the Pt particles could explain the loss of activity. Nevertheless the fraction of exposed platinum atoms in the deactivated state is close to that measured in the fresh state.

The deactivation is probably due to the progressive formation of some oxidised species bonded to the support or/and to the platinum particles, the identification of the species responsible for such a deactivation is still under study.

After ageing at 1000°C, the activity strongly decreased, the T_{50} temperature increased from 335 to ca. 620°C. The catalytic activity is close to that of Pt/Al_2O_3 aged in the same conditions (Fig. 6) [28–30]. Even if the right $Ce_{0:67}Zr_{0:33}O_2$ solid solution without

any demixion is still present and if the BET area value ($7 m^2 g^{-1}$) is not too low, the beneficial effect of the solid solution onto the catalytic properties of Pt in methane combustion is completely suppressed for the $Pt/Ce_{0:67}Zr_{0:33}O_2$ solid aged at 1000°C. An encapsulation of the metal particles has been considered, after ageing, in the case of rhodium and platinum deposited onto a CeO_2–ZrO_2 solid solution [27]. One important parameter in favour of the encapsulation would be the formation of a bulk oxide of the noble metal in the ageing conditions [26]. The formation of Pt bulk oxides which does not occur in similar conditions could be at the origin of the non-encapsulation of the Pt particles [26].

3.3. $MnO_x/Ce_{0:67}Zr_{0:33}O_2$ catalyst

The catalytic activity of the $MnO_x/Ce_{0:67}Zr_{0:33}O_2$ catalyst in the two states is shown in Fig. 5. A comparison with MnO_x/Al_2O_3 is given in Fig. 10 for the same type of ageing. In the fresh state the activity Mn oxide supported onto $Ce_{0:67}Zr_{0:33}O_2$ (T_{50}= 525°C) is slightly better than that of the support (T_{50}=576°C). Fig. 10 shows that at low conversion the $Ce_{0:67}Zr_{0:33}O_2$ solid solution has a slight positive effect on the catalytic activity in the fresh state. Nevertheless, over the full temperature range studied, the promoting effect of the $Ce_{0:67}Zr_{0:33}$ support onto the catalytic activity of manganese oxide is rather small. In addition, the catalytic activity is close to that of the $Ce_{0:67}Zr_{0:33}O_2$ support.

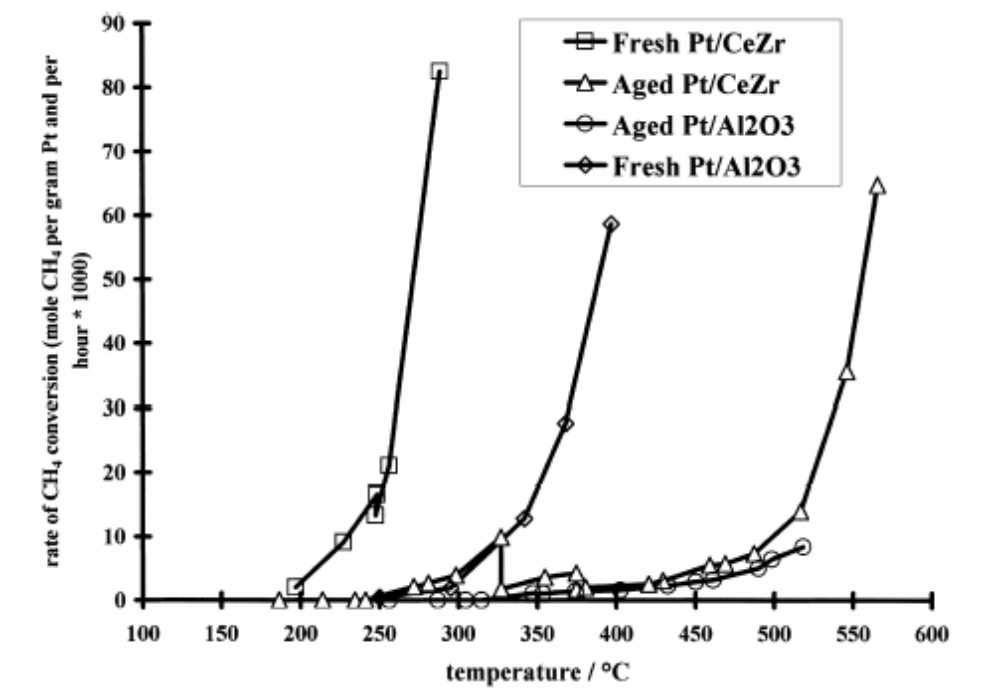

Fig. 3. Catalytic activity in methane combustion for platinum supported on alumina and on the $Ce_{0:67}Zr_{0:33}O_2$ solid solution in fresh and aged states.

After ageing the catalytic activity almost disappeared since the conversion at 800°C is ca. 10%, i.e. comparable to the activity due to the homogeneous reaction measured with a reactor filled with silica powder. Such an aged catalyst is largely less active than the corresponding MnO_x/Al_2O_3 solid (Fig. 10). Taking into account the BET areas of the $Ce_{0:67}Zr_{0:33}O_2$ support and of the $MnO_x/Ce_{0:67}Zr_{0:33}O_2$ catalyst, the intrinsic catalytic activity in CH_4 combustion has been calculated at 700°C: the intrinsic activity of the catalyst is equal to 1.7×10^{-4} mol CH_4 h^{-1} m^{-2}, whereas the corresponding value for the support is 2.0×10^{-4} mol CH_4 h^{-1} m^{-2}. The proximity of these two values strongly suggests that manganese oxide is no longer present at the surface of the support and is probably encapsulated or dissolved into the solid solution crystallites.

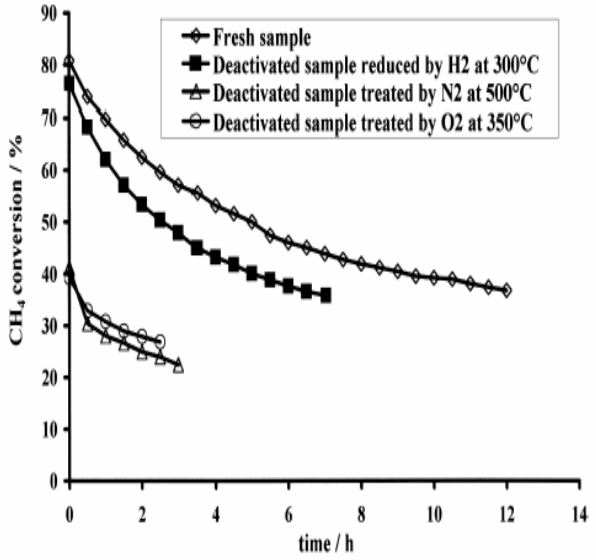

Fig. 4. Methane conversion into CO_2 on the fresh $Pt/Ce_{0:67}Zr_{0:33}O_2$ catalyst at 350_C as a function of the time on stream. Activity was measured on fresh catalyst as well as on deactivated catalysts subsequently treated, either under nitrogen, oxygen or hydrogen.

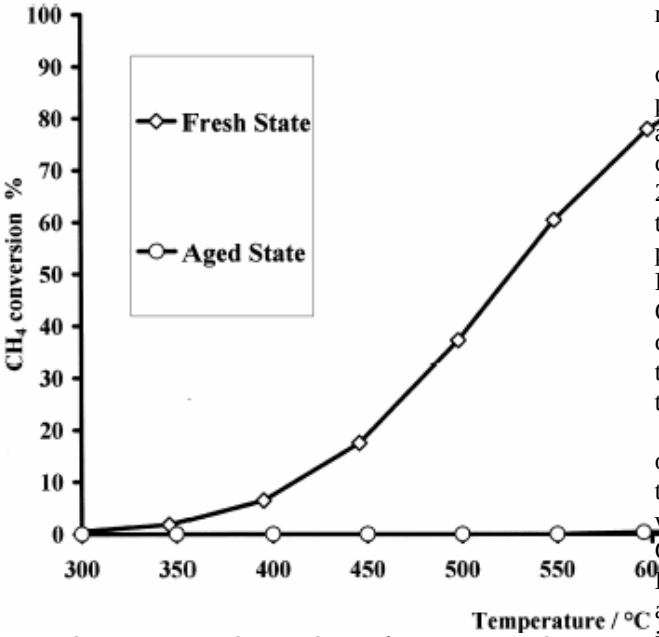

Fig. 5. Catalytic activity in methane combustion for MnO_x supported on the $Ce_{0:67}Zr_{0:33}O_2$ solid in fresh and aged states.

In the case of fresh Mn-doped ceria–zirconia solid solutions, Terribile et al. [13] have found a slight positive effect of Mn addition for the combustion of C1C alkanes. For instance, the T_{50} temperature for C_4H_{10} combustion decreased by ca. 60°C after introducing 5 mol% Mn in the $Ce_{0:8}Zr_{0:2}O_2$ mixed oxide. Such a promoting effect was strongly decreased in methane combustion, like in the present. The authors concluded that low temperature reaction conditions (combustion of C1C alkanes) might favour the reactivity of catalysts whose redox behaviour is promoted at low temperature.

In conclusion, the use of the $Ce_{0:67}Zr_{0:33}O_2$ solid solutions as support of Mn oxide has a limited beneficial effect on the catalytic activity in the fresh state. On the other hand, the aged solid has almost no catalytic activity. Such a behaviour is probably due to the loss of the thermal stability leading to the appearance of new solid solutions associated with a drastic loss of the surface area. In addition, it seems that manganese species are not accessible to the reactants. MnO_x seems to be responsible for the loss of the thermal stability of the solid solution.

4. Conclusion

The thermal stability of several solid solutions $Ce_{1-x}Zr_xO_2$ has been investigated in the range $0<x<0.53$. After ageing at 1000_C under oxygen and steam, the $Ce_{0:67}Zr_{0:33}O_2$ solid showed the best thermal stability and was selected as support for active phases. It was found that the various solid solutions have a non-negligible catalytic activity in methane combustion.

The $Pt/Ce_{0:67}Zr_{0:33}O_2$ catalyst was very active in CH_4 combustion, its activity was much higher than that of platinum deposited on alumina and comparable to that of a Pd/Al_2O_3 catalyst. Nevertheless, in isothermal conditions a deactivation on stream is observed in the 200–500°C temperature range. After ageing at 1000°C the thermal stability of the $Ce_{0:67}Zr_{0:33}$ solution is preserved, but the activity is similar to that of an aged Pt/Al_2O_3 catalyst : the positive effect of the $Ce_{0:67}Zr_{0:33}O_2$ support is no longer observed. The catalyst obtained by supporting manganese oxide onto the $Ce_{0:67}Zr_{0:33}O_2$ solid solution is slightly more active than the corresponding MnO_x/Al_2O_3 catalyst.

After ageing at 1000°C, the presence of manganese oxide leads to a complete loss of the thermal stability of the solid solution. A segregation of phases is observed with the formation of two new solid solutions, $Ce_{0:75}Zr_{0:25}O_2$ and $Ce_{0:16}Zr_{0:84}O_2$, at the same time the BET area dramatically decreases down to 0.4 $m^2\ g^{-1}$. The aged sample has no catalytic activity
in methane combustion below 700_C.

For the above results it can be concluded that the CeO_2–ZrO_2 solid solutions are not suitable supports for methane catalytic combustion as far as high temperatures applications are concerned.

Acknowledgements

We thank the Research and Development Unit of UTM, (UPP Vot no. 71051 and 71160), Ministry of Science

and Environment, Malaysia (IRPA Vot no. 72008) and UTM Scholarship to support MTA study.

References

[1] NO*x* : basic mechanisms of formation and destruction and their applications to emission control technologies, J.W. Patrick, K.M. Thomas (Eds.), Fuel 73 (1994) 1379.
[2] M.F.M. Zwinkels, S.G. Järås, P.G. Menon, T.A. Griffin, Catal. Rev.Sci. Eng. 35 (1990) 319.
[3] H. Inoue, K. Sekizawa, K. Eguchi, H. Aria, Catal. Today 47 (1999) 181.
[4] B.W.-L. Jang, R.M. Nelson, J.J. Spivey, M. Ocal, R. Oukaci, G. Marcellin, Catal. Today 47 (1999) 103.
[5] G. Groppi, C. Cristiani, P. Forzatti, J. Catal. 168 (1997) 95.
[6] D. Naoufal, J.M. Millet, E. Garbowski, Y. Brullé, M. Primet, Catal. Lett. 54 (1998) 141.
[7] M. Ozawa, M. Kimura, A. Isogai, J. Alloys Compounds 193 (1993) 73.
[8] J.P. Cuif, G. Blanchard, O. Touret, A. Seigneurin, M. Marczi, E. Quemere, SAE Paper 961906 (1996).
[9] P. Fornasiero, G. Balducci, J. Kašpar, S. Meriani, R. di Monte, M. Graiani, Catal. Today 29 (1996) 47–52.
[10] C.E. Hori, H. Permana, R.Y. Simon Ng, A. Brenner, K. More, K.M. Rahmoeller, D. Belton, Appl. Catal. B 16 (1998) 105.
[11] C. de Leitenburg, A. Trovarelli, J. Llorca, F. Cavani, G. Bini, Appl. Catal. A 139 (1996) 161.
[12] E. Bekyarova, P. Fornasiero, J. Kašpar, M. Graziani, Catal. Today 45 (1998) 178.
[13] D. Terribile, A. Trovarelli, C. De Leitenburg, A. Primavera, G. Dolcetti, Catal. Today 47 (1999) 133.
[14] M.H. Yao, R.J. Baird, F.W. Kuntz, T.E. Hoost, J. Catal. 166 (1997) 67.
[15] J.G. Nunan, W.B. Williamson, H.J. Robota, SAE Paper 960798 (1996).
[16] F. Fajardie, Ph. D. Thesis, Paris VI, France, 1996.
[17] R.D. Shannon, C.T. Prewitt, Acta Crystallogr. B 25 (1969) 925.
[18] E. Tani, M. Yoshimura, S. Somiya, J. Am. Ceram. Soc. 66 (1983) 506.
[19] A.E. McHale, Phase Diagrams for Ceramists, Annual 1991, Vol. 20, 1991.
[20] H.C. Yao, Y.F. Yu Yao, J. Catal. 86 (1984) 254.
[21] P. Fornasiero, G. Balducci, R. di Monte, J. Kašpar, V. Sergo, G. Gubitosa, A. Ferrero, M. Graziani, J. Catal. 164 (1996) 173.
[22] V. Perrichon, A. Laachir, S. Abouardanasse, O. Touret, G. Blanchard, Appl. Catal. A 129 (1995) 69.
[23] P. Fornasiero, R. Di Monte, G. Ranga Rao, J. Kašpar, S. Meriani, A. Trovarelli, M. Graziani, J. Catal. 151 (1995) 168.
[24] G. Ranga Rao, J. Kašpar, S. Meriani, R. Di Monti, M. Graziani, Catal. Lett. 24 (1994) 107.
[25] S. Salasc, Ph.D. Thesis, Lyon, France, November 1998.
[26] G.W. Graham, H.-W. Jen, W. Chun, R.W. Mc Cabe, J. Catal. 182 (1999) 228.
[27] P. Fornasiero, J. Kašpar, V. Sergo, M. Graziani, J. Catal. 182 (1999) 56.
[28] P. Briot, A. Auroux, D. Jones, M. Primet, Appl. Catal. 59 (1990) 141.
[29] P. Briot, M. Primet, Appl. Catal. 68 (1991) 301.
[30] M. Primet, et al., unpublished results.

CHAPTER 8
Methane combustion on perovskites-based structured catalysts

Wan Azelee Wan Abu Bakar *, Nor Aziah Buang and Imran Mohd Syakir
Department of Chemistry, Faculty of Science
Universiti Teknologi Malaysia
Locked Bag 791, 80990 Johor Bahru
Johor, Malaysia

Abstract

$LaMnO_3$ perovskites supported on La stabilised g-Al_2O_3 and MgO have been prepared and characterised as methane combustion catalysts. XRD analysis, BET surface area results and H_2 TPR measurements have all revealed the presence of significant interaction between the perovskite and the alumina based support, which becomes very strong upon thermal treatment at 1100ºC. On the other hand, MgO supported samples undergo only sintering processes with reduction of surface area upon treatment at 1100ºC. Catalytic activity measurements in methane combustion have been performed both in fixed bed and in monolithic reactor. The results on powders have shown that the dispersion on both supports is effective to enhance the catalytic performances of the catalysts treated at 800ºC. A very strong deactivation is observed for the La/Al_2O_3 supported catalyst when pre-treated at 1100ºC, while $LaMnO_3$/MgO shows a promising high thermal stability. The chemical nature of the active sites changes by dispersing $LaMnO_3$ on both supports, even if to a different extent, as revealed by the estimated values of apparent activation energy and reaction orders for methane and oxygen. Structured combustion catalysts have been prepared following well established procedures towashcoat commercial cordierite monoliths with lanthanum stabilised alumina. The subsequent deposition of precursors on the coated monolith has been obtained by deposition precipitation method. Comparison between monolith and corresponding powder sample shows a higher catalytic activity of the former, likely to be attributed to the better dispersion obtained with repeated deposition cycles of active phase on the thin washcoat layer. Moreover, a lower deactivation has been observed on monolith after ageing under reaction at 1050ºC for 2 h, suggesting promising developments of this technique to produce catalytic combustion systems for high temperature applications.

1. Introduction

Catalytic combustion is an attractive way to produce thermal energy of high quality from the environmental point of view, since it allows efficient and complete fuel burning at temperatures lower than in the flame combustion and without yielding undesired by-products, such as UHC, CO, NO_x and particulate [1,2]. One of the most interesting potential applications of the catalytic combustion is in the natural gas fuelled burners for gas turbine power generation [3]. The very high temperatures in this process demands to the researchers very hard tasks, since an unavoidable contrast between activity and stability has to be taken into account in the choice of the material. PdO is active already at low temperature but cannot stand temperatures higher than 800_C [4] and must be therefore protected from overheating. Its use in high temperature applications should be restricted to the ignition section of the reactor, the complete combustion being homogeneously achieved in the gas phase or in more stable catalytic segments in the final section of the burner [5,6].

On the other hand, hexaaluminates are very stable at elevated temperatures but their activity is very low, making them interesting only in the last stages of a multimonolith configuration [6]. In recent years, a lot of research effort has been devoted to the study of perovskite-type oxides in catalytic combustion [7]. These materials have a general ABO_3 structure and show quite promising activity even at moderate temperatures and good heat resistance up to about 2000ºC [7,8]. The number of perovskites with potential interest in the oxidation reactions is very great, owing to the number of A and B cations being able to enter in this structure and the possibility to partially substitute either A and/or B position (general formula $A_xA'_{1-x}B_yB'_{1-y}O_3$). Up to now, the best catalytic performances in fossil fuel combustion are exhibited by La or La–Sr based perovskites (in A position) containing Co, Fe or Mn as B cation [8,9].

Nevertheless, the application of perovskite is still limited by their low surface area and strong tendency to sinter. Conventional preparation methods need both long time and high temperatures in order to achieve the ABO_3 structure, resulting in very low surface area. Recent studies on the preparation methods of perovskites have been focused to the production of higher surface area catalysts. Despite some very interesting results achieved with preparation at lower temperatures (in particular by means of citrates precursors, sol–gel and freeze-drying methods), the surface area of these catalysts decreases very strongly upon treatment at elevated temperatures (above 900ºC). A different approach to increase both surface area and mechanical strength of perovskites is their dispersion on a high surface area support [10–16].

Alumina is the most widely used support but tends to loose its high surface area under severe operating conditions typical of the combustion process. Transition

aluminas start to loose area even below 800°C due to elimination of micropores, but the critical loss occurs above 1000°C with the transition to thermodynamically stable a-phase [17]. As reviewed by Arai and Machida [18], kinetic inhibition of sintering processes can be achieved by several additives, La_2O_3 being the most effective. One of the first attempts in preparing perovskite supported catalysts for methane combustion was made by Zhang et al. [10]. They succeeded in supporting $La_{0:8}Sr_{0:2}MnO_3$C*x* perovskite prepared by citrates method on La_2O_3_19Al_2O_3 or Mn_2O_3 modified La_2O_3_19Al_2O_3. It must be noticed that thermal treatment at elevated temp rature causes a marked reduction of activity due to the loss of surface area of the support. Moreover results obtained with $LaCrO_3/Al_2O_3$ in methane combustion after ageing at 1340K [11] showed that the deactivation is even higher than what is expected only by the surface area decrease. Chemical interaction between support and active phase must be implied, as shown in [12], where the authors reported the formation of a mixed perovskite phase $LaCr_xAl_{1-x}O_3$ at 1100_C for the $LaCrO_3/Al_2O_3$ system and at 1200°C for $LaCrO_3/LaAl_{11}O_{18}$. Arnone et al. [16] evidenced a measurable interaction between the active phase and the support after a 3 h treatment at 1100_C in flowing air of $LaMnO_3$ supported on La_2O_3/Al_2O_3. High thermal stability has been reported by Marti et al. [13] for aluminate spinels MAl_2O_4 (MDMg, Ni and Co), used as supports for $La_{0:8}Sr_{0:2}MnO_3$C*x* active phase. In those support materials the alumina lattice was saturated with bivalent metal ions so that no further migration of Mn from the active phase is possible.

Magnesia has also been proposed as support for combustion catalysts for its thermal stability exceeding that of alumina [18–21]. Moreover, no negative interaction of perovskite with the support has been found by Saracco et al. [15], with a series of $LaCr_xMg_{1-x}O_3$ perovskites dispersed on MgO. In some applications of catalytic combustion, such as in gas turbine combustors, structured catalysts must be used since they allow to minimise pressure drops [22]. Monolithic reactors have been intensively studied in recent years for either DeNO*x* [23] and catalytic combustion processes [22,24,25], but very few examples of perovskite-based structured catalysts have been reported for catalytic combustion. Ciambelli et al. [14] have investigated the catalytic performances of a series of extruded monoliths made of perovskite powders (La–Ce or Dy–Y in A position and Ni, Fe and Mn in B position). The comparison with the corresponding powder catalysts showed similar values of apparent activation energy for methane combustion, although with a not complete selectivity to CO_2.

More conventional procedures are based on covering cordierite monoliths with perovskite containing active phase. Arai and Machida [18] reported that honeycomb coating with perovskite–water slurry resulted in lower stability with respect to monoliths made of manganese-substituted hexaaluminates $Ba_{0:8}K_{0:2}MnAl_{11}O_{19}$. Zwinkels et al. [12] supported $LaCrO_3$ on a g-Al_2O_3 washcoated cordierite monolith. The supported catalyst was characterised as powder, while the activity data were obtained only with the monolithic reactors, so no comparison could be drawn between the characteristics of monolith and the precursor $LaCrO_3/Al_2O_3$ and $LaCrO_3/LaAl_{11}O_{18}$ powder particles. However it is evident, following this second more classical approach to obtain perovskite-based monoliths, that the study of the dispersion of the active phase on a washcoat support is very necessary. In this work we have investigated the catalytic properties in methane combustion of $LaMnO_3$ perovskites, supported on La stabilised g-Al_2O_3 and MgO, in order to combine high activity at low temperature, related to the higher surface area, with wider range of thermal stability due to the dispersion on the supports. Catalytic systems have been prepared as powders in order to characterise their physico-chemical properties and assess the influence of support on the catalytic features in methane combustion. Moreover, catalysts have also been prepared in the form of monoliths to compare the catalytic properties with those of powder samples in terms of ignition behaviour, catalytic performances and thermal stability.

2. Experimental

2.1. Catalyst preparation

2.1.1. Alumina supported $LaMnO_3$

Commercial g-Al_2O_3 (CK 300 with 200m^2/g, Akzo Chemie) was stabilised with 5 wt.% La_2O_3 using the wet impregnation technique. The alumina powder was suspended in an aqueous solution of $La(NO_3)_3$_6H_2O (Fluka, >99%) and the excess water removed in a rotary evaporator at 55°C under reduced pressure. After drying at 120°C, the powder was calcined in flowing air (100Ncm^3/min) at 800°C for 3 h, in order to decompose the nitrate. $LaMnO_3$ was deposited on the stabilised alumina from nitrate and acetate precursors with the deposition precipitation (DP) method, previously reported for the preparation of metal oxides supported catalysts [26]. Stabilised g-Al_2O_3 powder was suspended in a solution of suitable amounts of lanthanum nitrate, manganese acetate ($C_4H_6MnO_4$_4H_2O, Sigma, >99%) and urea (CH_4N_2O, Fluka, >99.5%) (molar ratio urea/cationic species 9:1) heated to 90_C for 5 h under stirring. At this temperature urea slowly decomposes producing ammonia homogeneously in the suspension, thus causing the preferential co-precipitation of hydroxides inside the pores of the support. The $LaMnO_3$ nominal loading in the catalysts was 30 wt.%. After removing the excess water and drying at 120°C, the

powder was treated in flowing air at 800°C for 3 h. Part of this catalyst was further treated at 1100°C for 3 h.

2.1.2. Bulk $LaMnO_3$

A bulk perovskite sample was also prepared by co-precipitation, using urea as a base, as for the DP method. A solution of lanthanum nitrate, manganese acetate and urea (molar ratio urea/cationic species 9:1) was heated to 90°C for 5 h under continuous stirring. After removing the excess water, the resulting powder was dried at 120°C and calcined in flowing air at 800°C for 3 h.

2.1.3. MgO-dispersed $LaMnO_3$

Magnesium oxide was obtained by thermal decomposition of carbonate($(MgCO_3)_4$_$Mg(OH)_2$.$5H_2O$, Carlo Erba, >99%) at 800_C for 3 h. Suitable amounts of lanthanum nitrate and manganese acetate to obtain 20 wt.% loading of perovskite in the catalyst were dissolved in water and MgO powder added under stirring. Due to its basic nature, MgO partially dissolved and the pH increased to a constant value of 10.5, causing the precipitation of metal hydroxides. The excess water was removed in the rotary evaporator at 55°C under reduced pressure. After drying at 120°C, the powder was calcined in flowing air (100Ncm_3/min) at 800 or 1100°C for 3 h. Table 1 reports the nominal compositions and calcinations temperatures of powder catalysts.

2.1.4. Monolith catalysts

Cordierite monoliths (Corning) with a cell density of 400 cpsi were cut to obtain samples with 25 channels cross-section. Monoliths were washcoated with alumina by dipping samples in a slurry of finely grounded g-Al_2O_3 powder, diluted nitric acid solution and pseudobohemite (Disperal, Condea Chemie) [27]. The total amount of solids in the slurry was 20 wt.%. Several dips were needed to obtain the desired amount of washcoat loading (approximately 25% of the total weight). In each cycle the excess slurry was removed by blowing air through the channels, after which the samples were dried at 120°C and then calcined at 550°C for 3 h. La_2O_3 (5 wt.%) was added to the alumina washcoat by impregnation in a water solution of lanthanum nitrate, followed by drying at 120°C and calcination at 800°C for 3 h. The $LaMnO_3$ active phase was added to the monolith samples using the DP method already employed for the preparation of the powder catalyst. In this case the monolith sample was suspended in the solution continually stirred. Several cycles were needed to reach the target loading of 30 wt.% of perovskite. After each cycle, the monolithic samples were calcined at 800°C for 3 h.

2.1.5. Experimental apparatus for catalyst testing

Catalytic combustion experiments were carried out with a quartz down flow reactor electrically heated in a three zones tube furnace. The reactor had an annular cross-section in the case of powders in order to obtain a small equivalent diameter that enables to control catalyst temperature and to reduce the temperature gradients within the bed. Catalyst particles in the range of 180–250 mm were diluted with quartz powders of the same dimension to approach reactor isothermicity and placed on a porous quartz disk. The temperature of the catalytic bed was measured by a K-type thermocouple placed inside the inner quartz tube, and axial gradients were verified to be always <3°C. For monolithic catalysts the external and central channels were blocked at both ends with ceramic wool, leaving eight free channels on the cross-section. The central channel was used to measure the monolith temperature with a sliding thermocouple. The narrowing of the reactor section in pre- and post-catalytic zone and the presence of quartz pellets upside the catalytic bed limited the occurrence of homogeneous reactions. The gaseous flow rates were measured by Brooks 5850 mass flow controllers and mixed at atmospheric pressure to obtain variable inlet concentrations of reactants. The feed and product streams were analysed by on line HP 6890 gas cromatograph with thermal conductivity and flame ionisation detectors, equipped with Porapak Q and molecular sieve 5A columns. All catalysts were tested twice and for each test the methane conversion was calculated as the average of at least three measurements. Carbon balance was close to within <5% in all catalytic tests.

3. Results

3.1. Catalytic activity measurements

The catalytic activity in methane combustion was measured both on supported catalysts and on MgO and La-stabilised g-Al_2O_3 supports. Homogeneous reaction tests have also been carried out with the reactor filled with quartz powders in order to evaluate the onset temperature of gas phase reactions. In all experimental conditions investigated, the only reaction product detected on perovskite based catalysts was CO_2, while with both supports and quartz a significant amount of CO was found in the products. Fig. 2 shows the results of the activity tests carried out in order to compare the catalytic performances in methane oxidation of the powder catalysts prepared. In particular, measured values of methane conversion are reported as functions of the reaction temperature in Fig. 1(a) and (c), and corresponding Arrhenius plots are shown in Fig. 1(b) and (d). Experimental conditions in these measurements were chosen so as to justify the assumption of isothermal catalytic bed. Inlet methane and oxygen concentrations

were respectively 0.4 and 10 vol.% (the remaining gas being nitrogen); the contact time, defined as the ratio between the mass of catalyst loaded and the flow rate of the inlet gas mixture (W/F), was 0.09 g_s/N cm^3.

The conversion plot obtained with only quartz loaded in the reactor allows us to assume the contribution of the homogeneous reactions as negligible for all catalysts examined. Dispersion of $LaMnO_3$ perovskite on both La-stabilised alumina and magnesia is effective to enhance the catalytic performances of the samples treated at 800_C. As clearly shown by conversion plots and values of T_{10}, T_{50} and T_{90} in Table 4, both 3-Al-8 and 2-Mg-8 are more active than the corresponding bulk $LaMnO_3$. An increase in the reaction rate per unit mass (reported in Table 4) by a factor larger than 2 is obtained dispersing the active phase on both Al_2O_3 and MgO. No major differences in the overall activity are observed between these two samples, even if it must be noticed that the MgO supported catalyst has lower loading of

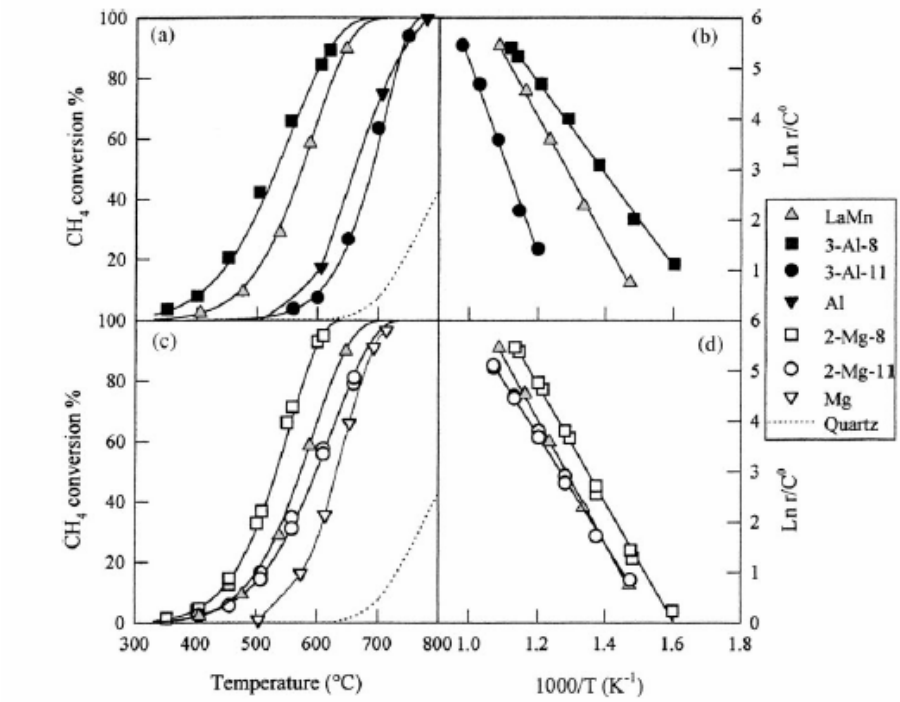

Fig. 1. Effect of temperature on methane combustion for powder catalysts and corresponding Arrhenius plots (0.4% CH_4, 10% O_2, W/FD0.09 g_s/N cm3). Continuous lines represent fittings with parameters obtained from kinetic analysis.

active phase and surface area. Very similar surface reaction rates (Table 4) and activation energies have been calculated for LaMn and 2-Mg-8 samples, suggesting that dispersion on MgO does not result in major modifications of chemical nature of active sites.

The slight reduction in the values of E_{act} for 2-Mg-8 could be related to a partial substitution of Mn^{3C} with Mg^{2C} in the perovskite structure, which is balanced by a higher fraction of Mn^{4C}, as shown by TPR analysis. On the other hand, lower values of both surface reaction rate and activation energy were measured for 3-Al-8. This reveals a significant influence of the alumina surface towards the formation of active sites, whose chemistry could be partially changed by the interaction with the support. The eventual formation of Mn_2O_3 and Mn_3O_4 micro-clusters should be also taken into account, since it has been reported that the activation energy in methane combustion on those manganese oxides is lower than on $LaMnO_3$ perovskite [16]. Thermal treatment at 1100°C reduces the activity of both g-Al_2O_3 and MgO supported catalysts, but the extent and the nature of this deactivation appear very different in the two cases. Indeed, 2-Mg-11 is only slightly less active than LaMn calcined at 800°C, while the comparison between the reaction rates per unit mass of 2-Mg-8 and 2-Mg-11 shows that the activity is reduced by a factor of about 2.5, even lower than what is expected from the total loss of surface area (reduced five times by the thermal treatment). As a consequence, surface reaction rate results increased.

Table 4
Catalytic performances in methane combustion of $LaMnO_3$ based catalysts

Catalyst ID	T_{10} (°C)	T_{50} (°C)	T_{90} (°C)	E_{act} (kcal/mol)	Reaction rate (500°C) (mmol/g h)	Surface reaction rate (500°C) (mmol/m^2 h)
LaMn	472	575	646	24.4	1.18	0.107
3-Al-8	413	532	622	18.2	2.75	0.031
2-Mg-8	440	533	598	23.3	2.32	0.093
3-Al-11	607	690	740	37.4	0.04	0.010
2-Mg-11	482	599	681	21.6	0.94	0.188
Monolith (46 000 h^{-1})	419	541	633	18.2	7.26	–

Moreover, the activation energy estimated on 2-Mg-11 was similar to that obtained on 2-Mg-8 and LaMn catalysts. On the other hand, 3-Al-11 sample undergoes a very strong deactivation due to the thermal treatment at 1100°C. Temperature for 90% conversion increases by 100°C when compared with that of LaMn and by 120°C with that of the corresponding 3-Al-8. The reduction in reaction rate is surely due to the considerable reduction of surface area to only 4m2/g, but also the value of activation energy (37 kcal/mol) is much higher than expected. Moreover XRD signals are very different and a much lower H_2 consumption is observed in TPR measurements. These evidences suggest that the chemistry of the catalyst is changed, as a result of a strong interaction between the active phase and alumina, enhanced by the high temperature pre-treatment. The DP method used to disperse the perovskite active phase does not appear to retard nor inhibit its chemical interaction with the support. A rough kinetics study has been performed for methane combustion on the five catalysts investigated. Several catalytic activity measurements have been carried out by varying both CH_4 and O_2 concentrations in the feed. Different temperature levels have been chosen in order to achieve similar conversions with all the catalysts. Resulting conversion data have been modelled by the power law rate equation:
$r = k\, p^{n}_{CH_4} p^{m}_{O_2}$, assuming isothermal plug flow conditions.

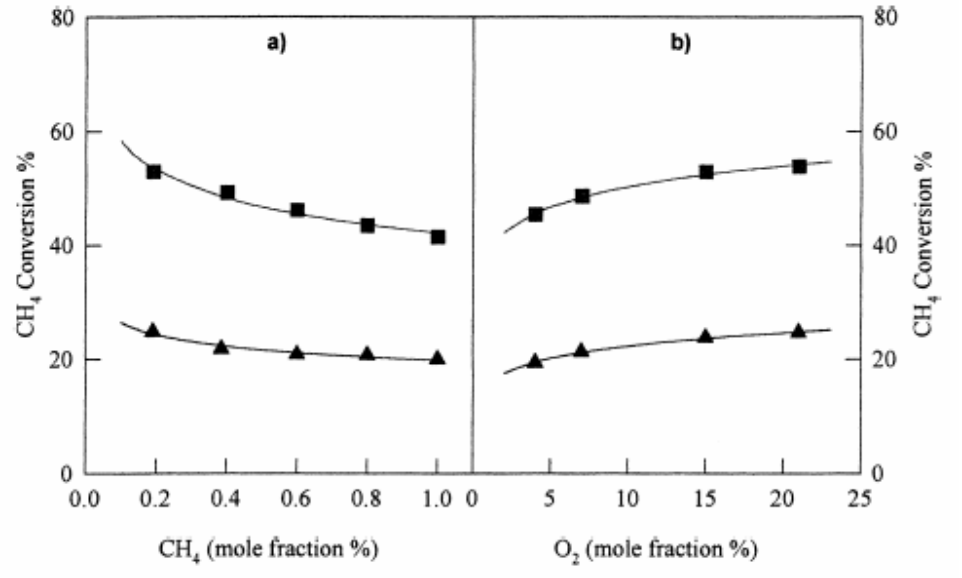

Fig. 2. Methane conversion as a function of the inlet CH_4 (a) and O_2 (b) concentration on LaMn catalyst. *T*D500_C (m) or 550_C (j). *W*/*F*D0.09 g_s/N cm^3. O_2 inlet concentration 10 vol.% in (a); CH_4 inlet concentration 0.4 vol.% in (b).

Fig. 2(a) and (b) reports the results obtained on the unsupported LaMn catalyst. A clear reduction of methane conversion to CO_2 is observed by increasing the inlet CH_4 concentration. Since it is possible to assume constant O_2 concentration throughout the reactor in these runs (oxygen being fed in large excess with respect to methane oxidation stoichioimetry), this behaviour is due to a less than linear dependence of the reaction kinetics on CH_4 concentration. The simplified kinetic model used to evaluate methane reaction order on LaMn catalyst: $r = k_0 p_{CH_4}^n$ gives n values weakly variable with temperature and around 0.84 (Table 5). This result is slightly different from the first order dependence reported by Arai et al. [8] for $La_{0.8}Sr_{0.2}MnO_3$ at higher CH_4 partial pressures. Better agreement could be found with the results reported in [8] about the effect of O_2 concentration on CH_4 conversion to CO_2. Fig. 3(b) shows that higher conversions are obtained by increasing oxygen inlet partial pressure over a range of values where it can be still considered to be in large excess. This effect, as modeled by the power law rate equation, reveals a reaction order for O_2 around 0.15, as reported in Table 5. The same investigation has been performed on supported perovskite samples too. The results are shown in Figs. 3 and 4, where the effect of inlet CH_4 and O_2 concentrations on methane conversion are presented, respectively. Also for supported samples a clear decrease in methane conversion to CO_2 occurs by increasing CH_4 inlet concentration, whereas a weak increase is obtained by increasing O_2 inlet concentration. Even if the general behaviour observed is the same, some clear differences should be pointed out. Table 5 shows that the reaction order of methane over supported catalysts is generally lower than the value found on unsupported LaMn sample (0.81–0.86). This should be related to the interaction with the support which modifies the active sites features.

Table 5
CH_4 and O_2 reaction orders in methane catalytic combustion estimated at several temperatures for all catalysts prepared

Catalyst ID	Temperature (°C)													
	450		500		550		575		600		620		650	
	n	*m*	*n*	*m*	*n*	*m*	*n*	*m*	*n*	*m*	*n*	*m*	*n*	*m*
LaMn			0.86	0.16	0.81	0.14								
2-Mg-8			0.69	0.17	0.72									
3-Al-8	0.77	0.19	0.77	0.19										
2-Mg-11					0.65	0.14	0.70	0.17	0.71	0.18	0.74	0.19		
3-Al-111													0.61	
Monolith		0.18[a]	0.80											

[a] T=420°C.

Moreover, on MgO supported catalysts, reaction orders remain quite constant upon treatment at 1100_C, since we estimated *n*D0.69–0.72 (variable with temperature), *m*D0.17 on 2-Mg-8 and *n*D0.65–0.74, *m*D0.14–0.19 on 2-Mg-11. A different behaviour was revealed by Al supported samples on which methane reaction order is 0.77 on 3-Al-8 and 0.61 on 3-Al-11, further confirming the change in chemical nature of the latter sample due to high temperature treatment that brings an irreversible deactivation. Saracco et al. [15] found first-order dependence on CH_4 concentration of methane oxidation rate over MgO supported $LaCr_xMg_{1-x}O_3$ catalysts and a general weak effect of oxygen concentration on the reaction kinetics. In particular, a zero order for O_2 was reported on the unsubstituted $LaCrO_3$ perovskite, supported or not, thus evidencing a significant difference
in methane oxidation kinetics with respect to our 2-Mg-8 and 2-Mg-11 samples. Future work should be devoted to further investigate the mechanism producing an apparent CH_4 reaction order lower than 1 for $LaMnO_3$ and its reduction after dispersion on high surface area supports.

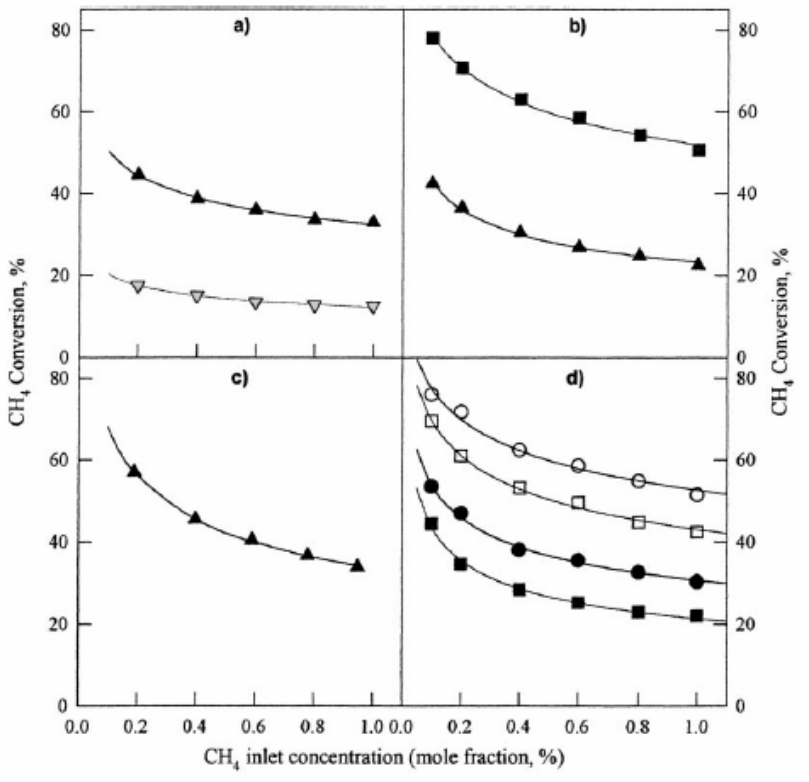

Fig. 3. Methane conversion as a function of the CH_4 inlet concentration over 3-Al-8 (a), 2-Mg-8 (b), 3-Al-11 (c) and 2-Mg-11 (d). Reaction temperature: 450 ( ), 500 (m), 550 (j), 575 (d), 600 (h), 620_C (s). *W*/*F*D0.09 g_s/N cm3, O_2 inlet concentrationD10 vol.%.

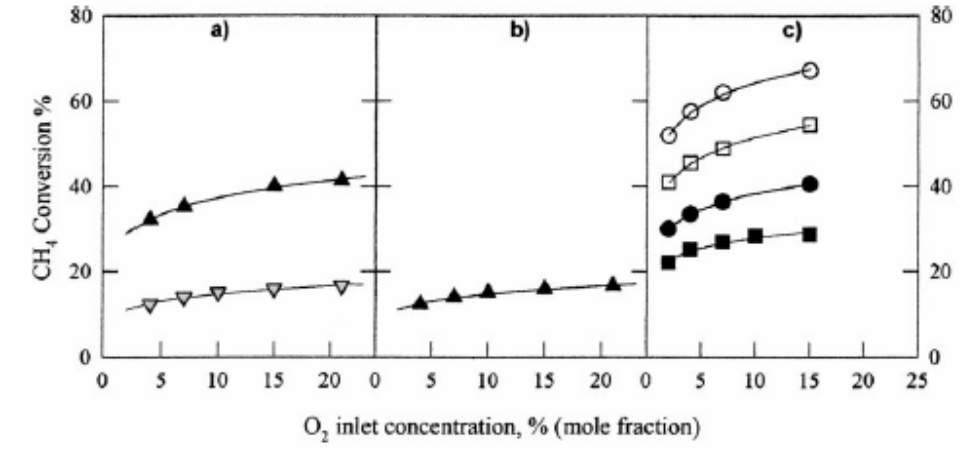

Fig. 5. Methane conversion as a function of the O_2 inlet concentration over 3-Al-8 (a), 2-Mg-8 (b) and 2-Mg-11 (d). TemperatureD450 ( ), 500 (m), 550 (j), 575 (d), 600 (h), 620°C (s). *W*/*F*D0.09 g_s/N cm3. CH_4 inlet concentration 0.4 vol.%.

3.4. Monolithic reactor

The catalytic properties of the monolithic system have been evaluated by carrying out activity tests for methane combustion in the same experimental conditions investigated on powders.

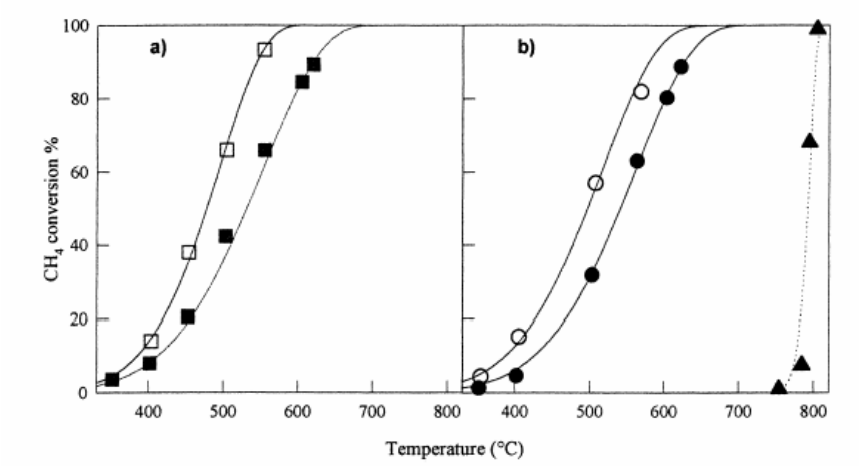

Fig. 6. Effect of temperature on methane combustion for monolith catalysts (0.4% CH_4, 10% O_2). (a) Comparison of monolith (h) and 3-Al-8 sample (j) at the same areal velocity; (b) comparison of fresh (s) and aged (d, 2 h under reaction at 1050_C) monolith with a cordierite sample (m) (W/FD0.055 g_s/N cm^3). Continuous lines represent fittings with parameters obtained from kinetic analysis.

Fig. 6(a) reports the conversion plots for the monolith as compared with the 3-Al-8 sample with the same chemical composition. Conversions over monolith catalyst are always higher than the corresponding ones over 3-Al-8 powders, either comparing them at the same value of space velocity (flow rate/reactor volume) or areal velocity (flow rate/catalyst wetted surface). Moreover, Table 4 reports the value of T_{10}, T_{50} and T_{90} measured with the same space velocity used by Zwinkels et al. [12] (46 000 h^{-1}). It appears that our monolithic catalyst exhibit an higher activity, probably related to the better performances in methane combustion of $LaMnO_3$ catalyst with respect to $LaCrO_3$ [8,9]. Fig. 6(b) reports the conversion plot for fresh monolithic catalyst compared with that of the same sample aged under reaction at 1050°C for 2 h, showing a surprising lower deactivation due to thermal treatment at elevated temperature with respect to the corresponding powder catalyst. Further investigation is needed on this phenomenon and will be required to future work. At the moment, a possible interpretation could be related to a better dispersion of active phase on support due to repeated cycles of deposition necessary to obtain the target loading. Fig. 6(b) also shows conversion data measured on a nude cordierite monolith, revealing no activity of cordierite in methane combustion, since CH_4 is converted to CO and CO_2 only at temperatures at which the homogeneous reactions take place. The Arrhenius plot obtained from the activity data gives the same value of activation energy of the corresponding powder catalysts 3-Al-8 (18.2 kcal/mol). This result suggests that the chemical nature of the active sites on monolithic and powder catalyst is unchanged. The activation energy obtained by Ciambelli et al. [14] on extruded $La_xCe_{1-x}MnO_3$ monolithic reactor is slightly higher (21.5 kcal/mol), although a not complete selectivity to CO_2 was found. After ageing at 1050°C the calculated activation energy for the monolith sample increases to 19.1 kcal/mol, a value much lower than that estimated for 3-Al-11, as a further confirmation of the reduced deactivation. The reaction kinetics exhibits a behaviour similar to that shown by 3-Al-8 powders. Fig. 7 shows that methane conversion is a decreasing function of CH_4 inlet concentration while it increases with increasing O_2 concentration, with estimated reaction orders very similar to those found for the supported powder catalyst, as reported in Table 5.

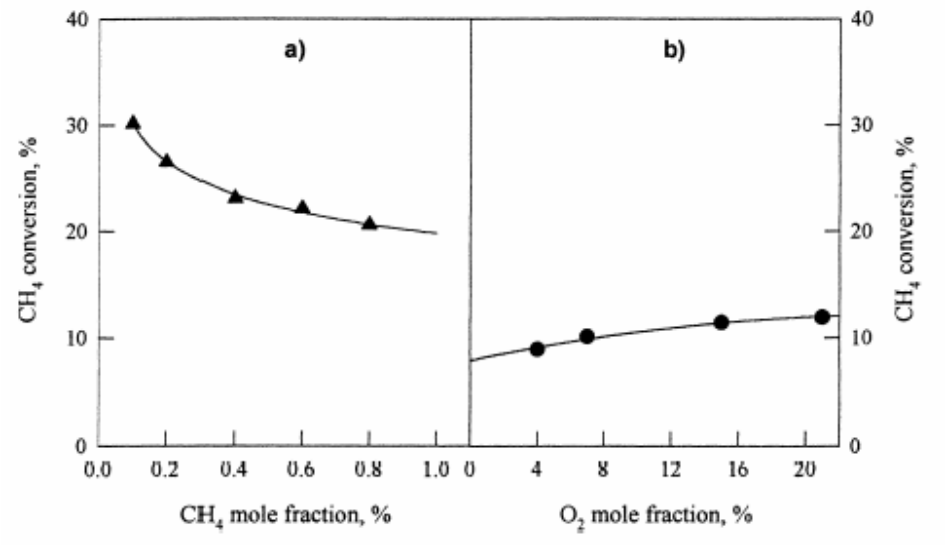

Fig. 7. Methane conversion as a function of the inlet CH_4 (a) and O_2 (b) concentration on monolith catalyst. *T*D500 (m) and 420_C (d). *W*/*F*D0.09 g_s/N cm3. O_2 inlet concentration 10 vol.% in (a); CH_4 inlet concentration 0.4 vol.% in (b).

4. Conclusions

$LaMnO_3$ perovskites supported on both lanthanum stabilised g-Al_2O_3 and MgO have shown high activity in methane combustion. The investigation on La/g-Al_2O_3 supported samples revealed a dramatic deactivation of the catalyst powders after ageing at 1100°C, due to a strong interaction between the active phase and the support. On the other hand, cordierite monoliths coated with the same $LaMnO_3$ supported on La/g-Al_2O_3 show higher activity and thermal stability than the corresponding powder catalyst. Promising results have also been obtained on MgO supported $LaMnO_3$ samples, whose high activity is associated with remarkable thermal stability. Further investigation is needed in order to set up novel preparation methods to coat monoliths with MgO supported perovskites.

Acknowledgements

We thank the Research and Development Unit of UTM, (UPP Vot no. 71051 and 71160), Ministry of Science and Environment, Malaysia (IRPA Vot no. 72008) and UTM Scholarship to support IMS study.

References

[1] M.F.M. Zwinkels, S.G. Jaras, P.G. Menon, in: A. Cybulski, J. Moulijn (Eds.), Structured Catalysts and Reactors, Marcel Dekker, New York, 1998, p. 149.
[2] Z.R. Ismagilov, M.A. Kerzhentsev, Catal. Rev. Sci. Eng. 32 (1990) 51.
[3] R. Dalla Betta, Catal. Today 35 (1997) 129.
[4] M.F.M. Zwinkels, S.G. Jaras, P.G. Menon, T.A. Griffin, Catal. Rev. Sci. Eng. 26 (1993) 319.
[5] R.A. Dalla Betta, J.C. Schlatter, D.K. Yee, D.G. Loffler, T. Soji, Catal. Today 26 (1995) 329.
[6] K. Eguchi, H. Arai, Catal. Today 29 (1996) 379.
[7] L.G. Tejuca, J.L.G. Fierro, J.M.D. Tascon, Adv. Catal. 36 (1989) 237.
[8] H. Arai, T. Yamada, K. Eguchi, T. Seyama, Appl. Catal. 26 (1986) 265.
[9] J.G. McCarty, H. Wise, Catal. Today 8 (1990) 231.
[10] H.M. Zhang, Y. Teraoka, N. Yamazoe, Appl. Catal. 41 (1988) 137.
[11] B. De Collongue, E. Garbowski, M. Primet, J. Chem. Soc., Faraday Trans. 87 (1991) 2493.
[12] M.F.M. Zwinkels, O. Haussener, P.G. Menon, S.G. Jaras, Catal. Today 47 (1999) 115.
[13] P.E. Marti, M. Maciejewski, A. Baiker, Appl. Catal. B 4 (1994) 225.
[14] P. Ciambelli, V. Palma, S.F. Tikhov, V.A. Sadykov, L.A. Isupova, L. Lisi, Catal. Today 47 (1999) 199.
[15] G. Saracco, G. Scibilia, A. Iannibello, G. Baldi, Appl. Catal. B 8 (1996) 229.
[16] S. Arnone, G. Busca, L. Lisi, F. Milella, G. Russo, M. Turco, Proceedings of the 27th Symposium on Combustion, The Combustion Institute, Boulder, 1998.
[17] J.S. Church, N.W. Cant, D.L. Trimm, Appl. Catal. A 101 (1993) 105.
[18] H. Arai, M. Machida, Appl. Catal. A 138 (1996) 161.
[19] I. Matsuura, Y. Hashimoto, E. Takahaysu, K. Nitta, Y. Yoshida, Appl. Catal. 74 (1991) 273.
[20] M. Berg, S.G. Jaras, Appl. Catal. A 114 (1994) 227.
[21] M. Berg, S.G. Jaras, Catal. Today 26 (1995) 223.
[22] S. Irandoust, B. Andersson, Catal. Rev. Sci. Eng. 30 (1988) 341.
[23] A. Cybulski, J.A. Moulijn, Catal. Rev. Sci. Eng. 36 (1994) 179.
[24] S.T. Kolaczkowski, Trans. Instn. Chem. Engrs 73 (1995) 168.
[25] J.W. Geus, J.C. van Giezen, Catal. Today 47 (1999) 169.
[26] X. Xu, J.A. Moulijn, in: A. Cybulski, J. Moulijn (Eds.), Structured Catalysts and Reactors, Marcel Dekker, New York, 1998, p. 599.
[27] M. Skoglundh, H. Johansson, L. Lowendhal, K. Jansson, L. Dhal, B. Hirschauer, Appl. Catal. B 7 (1996) 299.
[28] L. Lisi, G. Bagnasco, P. Ciambelli, S. De Rossi, P. Porta, G. Russo, M. Turco, J. Solid State Chem. 146 (1999) 176.

CHAPTER 9

Promotion of methane combustion activity of Pd catalyst by titania loading

Wan Azelee Wan Abu Bakar *, Nor Aziah Buang, and Yap Chui Peng
Department of Chemistry, Faculty of Science
Universiti Teknologi Malaysia
Locked Bag 791, 80990 Johor Bahru
Johor, Malaysia

Abstract

Methane combustion over Pd catalyst supported on KIT-1 mesoporous material was investigated. The catalytic activity of the Pd catalyst was considerably improved by titania loading. The stability of the Pd catalyst to the exposure at high temperature is also enhanced by titania loading. Titania which is chemically bonded with the skeletal of mesoporous material interacts with palladium co-loaded and suppresses the decomposition of palladium oxide; more active phase in the methane combustion compared to palladium metal, resulted in the improvement in the catalytic performance of the Pd catalyst.

1. Introduction

Catalytic combustion of fuel is carried out with no flame at low temperature, so it is safer than a conventional burning system and more friendly to the environment due to reduction of NO*x* and unburned hydrocarbon emissions [1,2]. As the burning temperature becomes lower, these advantages are more amplified. Therefore, highly active noble metals such as palladium and platinum are commonly used as active phases of combustion catalyst in order to achieve high activity even at low temperature [3,4]. Conventionally, alumina is used as a support due to its high thermal stability and strong interaction with metal, but in order to enhance activity and mass transfer, it is more efficient to use the support having a strong interaction with metal and large pores to achieve a high dispersion of metal and a negligible restriction to mass transfer. Since the combustion of fuel generates heat, the stability of a combustion catalyst to high temperature is very important. The catalytic activity may be reduced due to sintering of metal, change in the chemical state of active species or fouling of support. The strong interaction between metal and support is helpful to retain the active phase of the combustion catalyst during its exposure to high temperature [5]. Mesoporous material synthesized using detergent as a template has uniform mesopore with a diameter ranging from 25 to 100 nm [5,6]. The volume of reactant per catalyst bed is usually large in the catalytic combustion, so the low restriction to mass transfer at the mesopore is helpful to treat combustion stream of high space velocity, resulting in a good catalytic performance. Furthermore, the fact that metal can be dispersed on mesoporous material with a high dispersion by ion-exchange method as well as zeolite promises a high catalytic activity with a small amount of precious metal [7]. The low hydrothermal stability is considered to be a weak point for the application of mesoporous material as a catalyst support for the combustion, and the stability is considerably improved by inactivation of surface hydroxyl group by titania loading [8]. This paper is about the Pd catalyst supported on mesoporous material. The catalytic activity and stability of the Pd catalyst were considerably enhanced by titania loading as well as improvement of its hydrothermal stability. The impregnated state and promotion role of titania were discussed based on their characterization results and catalytic properties.

2. Experimental

Disordered mesoporous material (KIT-1) was synthesized from the gel of $6SiO_2$–1HTACl–$1.5Na_2O$– $4Na_4EDTA$–$0.15(NH_4)_2O$–0.75Al2O3–350H2O following Ryoo's procedure [9]. HTACl (25%, Aldrich) was used as templating material. Aluminum hydroxide (28%, Aldrich) was added to reactant gel to get KIT-1 mesoporous material having Si/Al ratio of 40. After synthesis at 98^{o}C for 2

days, pH of synthesizing solution was adjusted to 10.2. The pH adjustment was carried out twice. Mesoporous material was obtained after 4 days of hydrothermal synthesis and calcined at 550–C for 4 h in air flow of 50ml min-1. Cation was ion exchanged to ammonium ion by ammonium nitrate solution. Calcination at 550^{o}C produced proton-form mesoporous material. Palladium was impregnated on KIT-1 mesoporous material by incipient wetness method with Pd(NH3)4Cl2 (99%, Aldrich) solution. Pd catalyst was obtained after calcination at 550^{o}C for 4 h following by the reduction at 320^{o}C for 2 h in hydrogen flow of 30 ml min-1. Titania was loaded on Pd catalyst through a liquid-phase reaction between dehydrated mesoporous material and titanium *tert*-butoxide (99%, DuPont) in anhydrous ethanol solvent (99.5%, Duksan). After washing with anhydrous ethanol to remove non-reacted titanium *tert*-butoxide, the sample was calcined at 550^{o}C for 4 h in air to remove organic template and convert titanium alkoxide to titania. Methane combustion reaction was carried out at an atmospheric flow microreactor system. A quartz tube reactor (OD 1 2 in.) was charged with 0.26 g of the catalyst. A reactant comprising of methane and air with a volume ratio of 1:99 was supplied to the reactor and a WHSV was adjusted at 10 000 h^{-1}. Conversion was defined by the fraction of methane consumption. Combustion reaction was investigated from 200 to 800^{o}C in 50^{o}C intervals. A downward test to examine the thermal stability of the catalyst was followed by a reverse of the upward test. Reaction products were analyzed by using a gas chromatograph (HP 5890) equipped with a Porapak Q column.

3. Results and discussion

The combustion activities of KIT-1 mesoporous material and titania-only loaded catalysts are very low as shown in Fig. 4.

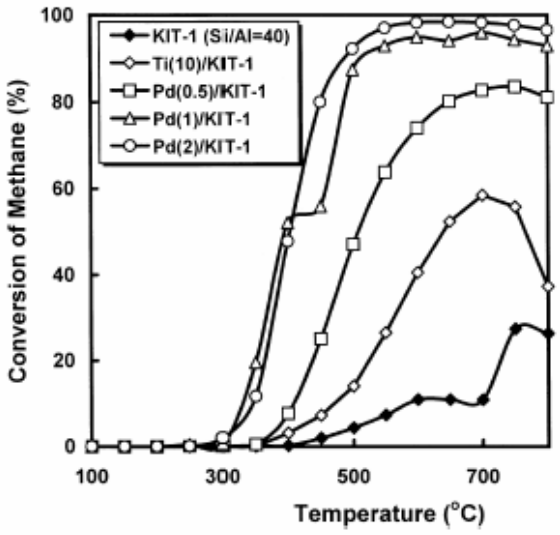

Fig. 1. Comparison of catalytic activity of KIT-1, Ti(10)/KIT-1, Pd(0.5)/KIT-1, Pd(1)/KIT-1 and Pd(2)/KIT-1 catalysts in the methane combustion.

The temperature for 50% conversion in the methane combustion was above 600^{o}C on the KIT-1 and Ti(10)/KIT-1 catalysts. Although titanium-loaded zeolite is known as an oxidation catalyst, the enhancement of the combustion activity by titania loading is negligible. However, the temperature for 50% conversion was lowered to about 500^{o}C with palladium loading of 0.5%. The temperature was gradually lowered by increasing the loading amount of palladium to 400^{o}C on the Pd(1.0)/KIT-1 catalyst. But further enhancement in the catalytic activity was not observed even by increasing the palladium loading to 2.0%. Although the increase in the activity with the loading amount of palladium is limited to 1.0%, it is certain that palladium is the active phase responsible for the catalytic combustion. The combustion activity of Pd/KIT-1 catalyst was considerably improved by titania loading. The temperature for 50% methane combustion was lowered to 300^{o}C on the Ti(5)–Pd(2)/KIT-1 catalyst as shown in Fig. 5. Since the intrinsic activity of titania on the combustion is negligible, the improvement in the combustion activity of the Pd catalyst by titania loading is caused by the interaction between palladium and titania, not by loaded titania itself.

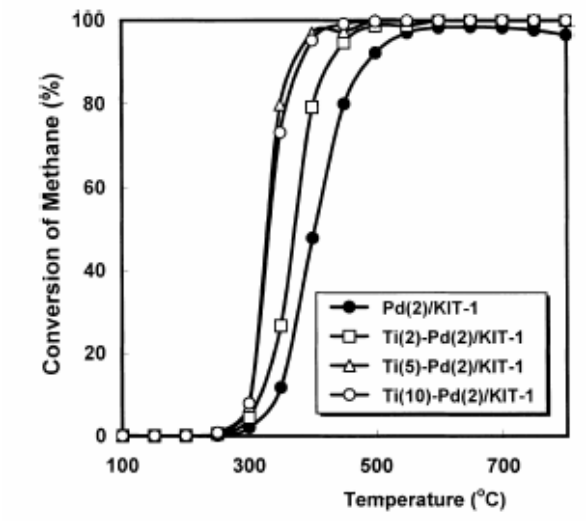

Fig. 2. Methane conversion on the Pd(2)/KIT-1 catalysts with different loadings of titania.

The combustion activity was gradually improved by titania loading within the loading amount of 5%, so the Ti(10)–Pd(2)/KIT-1 catalyst shows similar activity to the Ti(5)–Pd(2)/KIT-1 catalyst. The other essentially required property of a combustion catalyst, besides the high catalytic activity, is the stability in the catalyst performance to the variance in the combustion condition. The stability is usually examined at the upward and downward tests. Downward test reflects the degradation of the catalytic activity with the exposure to high temperature. A large difference between conversion profiles of upward and downward tests indicates a poor stability with the change in the reaction condition. The conversion profiles of the upward and downward tests on the Pd(2)/KIT-1 catalyst are not coincident as shown in Fig. 6.

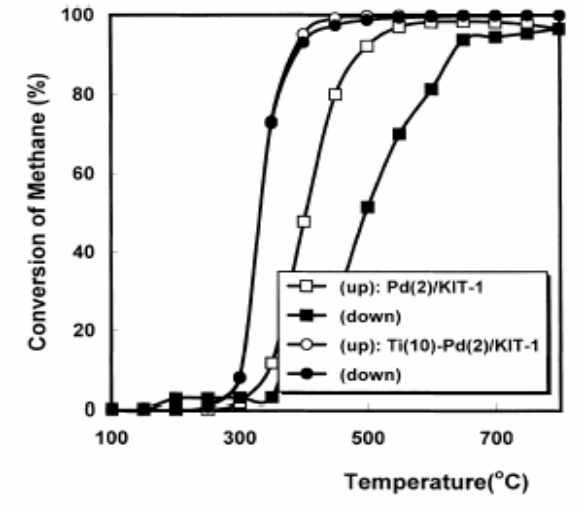

Fig. 3. Comparison of catalytic activity at the upward and downward test of Pd(2)/KIT-1 and Ti(10)–Pd(2)/KIT-1 catalysts in themethane combustion.

The conversion profile of the downward test shifted to high temperature compared to that of the upward test, indicating loss of activity due to the exposure to high temperature. However, an irreversible deactivation of the catalyst by sintering or fouling is not considered, because the repeated run of the upward test was followed the first run with a good accord. The possible cause for low activity at the downward test is ascribed to the reduction of palladium oxide due to decomposition at high temperature. This deduction is based on the fact that palladium oxide is more active than palladium metal in the methane combustion and is decomposed to palladium metal at high temperature [2]. On the other hand, both conversion profiles at the upward and downward tests on the Pd catalyst with titania loading [Ti(10)–Pd(2)/KIT-1] are nicely coincident. There is no decrease in the activity at downward test, indicating that thermal stability of the Pd catalyst is significantly improved by titania loading. The decomposition of palladium oxide is suppressed with the interaction between titania and palladium. The hydrogen uptake on Pd catalyst varies with the oxidation state of palladium. Additional hydrogen is required to remove surface oxygen of palladium oxide compared to palladium metal. The amount of hydrogen uptake of the Pd catalysts with titania loading and the dispersion of palladium obtained from hydrogen uptake are summarized in Table 1. The dispersion of palladium on the Pd catalyst increases with titania loading, indicating the retention of palladium oxide on the titania-loaded Pd catalyst. Titania inhibits the reduction of palladium, resulting in the improvement in the stability of palladium oxide. Titania loaded on mesoporous material by liquidphase reaction of titanium alkoxide is dispersed on pore wall amorphously, but has a tetrahedral coordination like silicon atoms which are composing the framework [12]. The improvement in the combustion activity and stability of the Pd catalyst by titania loading is ascribed by the interaction between palladium and titanium through oxygen. Highly stable titania suppresses the reduction of palladium oxide to metallic palladium. Since palladium oxide is more active than palladium metal in the methane combustion, maintenance of palladium oxide enhances the combustion activity. The interaction between palladium and titania suppresses the decomposition of palladium oxide even at high temperature, improving the stability of Pd catalyst with titania loading. Application of mesoporous material as a support for a combustion catalyst is a good example emphasizing the availability of its regular mesopore.

Furthermore, promotion of combustion activity and stability of the Pd catalyst by titania loading increases its applicability to combustor operating at medium temperature.

4. Conclusion

The catalytic activity and stability of Pd catalyst supported on KIT-1 mesoporous material were considerably enhanced by titania loading. This improvement is ascribed to the interaction between palladium and titania, suppressing the decomposition ofpalladium oxide at high temperature.

Acknowledgements

We thank the Research and Development Unit of UTM, (UPP Vot no. 71051 and 71160), Ministry of Science and Environment, Malaysia (IRPA Vot no. 72008) and UTM Scholarship to support YCP study.

References

[1] J.J. Chen, E. Ruckenstein, J. Phys. Chem. 85 (1981) 1606.
[2] T.R. Baldwin, R. Burch, Catal. Lett. 6 (1990) 131.
[3] A.K. Neyestanaki, N. Kumar, L.-E. Linfors, Fuel 74 (1995) 690.
[4] R. Burch, P.K. Loader, Appl. Catal. B 5 (1994) 149.
[5] J.S. Beck, R.F. Socha, D.S. Shihabi, J.C. Vartuli, US Patent 5 143 707 (1992).
[6] C.T. Kresge, M.E. Leonowicz, W.J. Roth, J.C. Vartuli, J.S. Beck, Nature 359 (1992) 710.
[7] J.-H. Lee, D.L. Trimm, Fuel Process. Technol. 42 (1995) 339.
[8] T.-G. Kang, J.-H. Kim, G. Seo, H.-C. Park, Hwahak Konghak 36 (1998) 364.
[9] J.M. Kim, J.H. Kwak, S. Jun, R. Ryoo, J. Phys. Chem. 99 (1995) 16742.
[10] J.M. Thomas, W.J. Thomas, Principles and Practice of Heterogeneous Catalysis, VCH, Weinheim, 1997, p. 267.
[11] D.J. Suh, T.-J. Park, S.-K. Iim, J. Catal. 149 (1994) 486.
[12] W.S. Ahn, D.H. Lee, T.J. Kim, J.-H. Kim, G. Seo, R. Ryoo, Appl Catal. A 181 (1999) 39.
[13] C.B. Dart, C.B. Khouw, H.-X. Li, M.E. Davis, Microporous Mater. 2 (1994) 425.

OVERALL CONCLUSIONS

From the catalytic activity studies of a series of transition metal oxide catalyst materials, it was possible to conclude that the efficency of the catalysts is greatly increased with the used of dopant with minimum loading of around 0.1 atom ratio. Further increased in the loading of dopant to 0.3 and 0.5 seem to deactivate activity towards the conversion of natural gas e.g. methane. Since these materials are good catalysts with high activity, an in depth investigation underlying their chemistry properties of the catalyst materials was carried out using various characterisation techniques.

XPS analysis revealed the formation of the cobalt oxide spinel system of Co_3O_4-CoO which is responsible to the enhancement of the catalytic activity performance towards methane oxidation. However, the formation of ternary compounds of $CuCrO_4$,and $CuCr_2O_4$ in the Cu(II)-doped ZrO_2 and Cr(VI)-doped ZrO_2 catalyst system inhibit the catalytic activity performance. XPS analysis also found out that the bridging oxo, $Zr< (O)_2 >Zr$ is the major species with more ionic in bonding character which further contributed to the catalytic activity performance.

Besides the formation of ternary compounds, spinel compounds and individual phases of dopants, the evolution of based materials phase structures were also observed from the the XRD analysis. The occurrence of this phenomenon with respect to the calcination temperatures explains the structural stabilization behaviour of the based materials used in the presence of dopants. The dopant cations may possibly have developed an O^{2-} ion vacancy during the stabilization process by doping. In this phenomenon the coordination number of the M^{4+} ion may undergo changes from 8 to 7 etc., depending on the O^{2-} ion vacancies. This means that an increase in the O^{2-} ion vacancies shifts the M^{4+} coordination number and at the same time causes changes in the based materials phase structure. The increased in the seven-coordinated M^{4+} ions made the bonding between based materials and oxygen more stronger, more covalent, and the structure is less conductive. Thus, producing a catalyst materials with poor catalytic activity performance, this was also demonstrated in this work, whereby all catalyst materials calcined at 800 and 1000 ^{o}C gave very poor catalytic activity performance towards methane oxidation due to the sole formation of monoclinic phase at the respective temperatures as described in the XRD phase structural analysis.

FUTURE WORKS

In catalysis it has been established that the catalytic reactions take place primarily on the surface of the catalyst material. The adsorbed atoms and molecules not only act as reactant but also modify the structure and the electronic state of the surface species during the course of chemical reactions. Hence, characterisation of these surface species by in situ EXAFS (Extended X-ray Absorption Fine Structure) would be beneficial. This technique will afford structural data, allowing the transformation of promoter metal ions from one environment to another to be closely monitored. Investigations on the behaviour of the surface species within the first few layers of the surface is best achieved by SEXAFS (Surface Extended X-ray Absorption Fine Structure). Here the behaviour of the surface species could be monitored without the influence of the bulk species causing an averaging effect of the spectrum over the whole sample.

Further characterisation of the surface species by EPR (Electron Paramagnetic Resonance) could be used to assess the presence of the paramagnetic metal ions species or oxygen atom in the form of superoxide (O_2^-) or other oxygen radical, on the surface of the catalyst material. Since a mixed metal oxides catalyst material is an orientationally disordered system, EPR spectra of paramagnetic transition metal cations suffer from low resolution due to inhomogeneous broadening. Hence, superhyperfine splittings due to nearby nuclear spin, which provide information regarding the close environment of the paramagnetic ion, are not resolved. Therefore, further studies by ESEEM (Electron Spin Echo Envelope Modulation) to measure the weak superhyperfirne interactions is possible. Results obtained from both EPR and ESEEM will then support assignments made in the XPS analysis for the presence of specific surface species expected to have a paramagnetic electron configuration at a specific binding energy. Considering all the complexities in these arguments it should be apparent that an extension of these studies using an EPR and EXAFS will provide more information on the electronic configuration of the metal ions species present on the surface of the catalyst material.